Progress in Upscaling Organic Photovoltaic Devices

Gabriel Bernardo, Tânia Lopes, David G. Lidzey, and Adélio Mendes*

Organic photovoltaic (OPV) cells have recently undergone a rapid increase in power conversion efficiency (PCE) under AM1.5G conditions, as certified by the National Renewable Energy Laboratory (NREL), which have jumped from 11.5% in October 2017 to 18.2% in December 2020. However, the NREL certified PCE of large area OPV modules is still lagging far behind (11.7% in July 2020). Additionally, there has been a rapidly growing interest in the use of OPVs for dim light indoor applications, with reported PCE of some large area (≥1 cm^2) devices, under 1000 lux, well above 20%. The transition of OPV from the lab to the market requires the development of effective manufacturing processes that can scale-up laboratory-scale devices into large area devices, without sacrificing performance and simultaneously minimizing associated manufacturing costs. This review article focuses on four important challenges that OPV technology has to face to achieve a reliable lab-to-fab transfer, namely: i) The upscaling of indium-tin-oxide (ITO)-based single cells and the interconnection of single cells into large area modules; ii) the development of alternatives to vacuum processing; iii) the development of alternatives to ITO-based substrates; and iv) strategies for improving the lifetime of large area OPV devices.

1. Introduction

Among the emerging solar cell technologies, organic photovoltaic cells (OPVs) have attracted great interest due to their promising performance and potential for low cost manufacture. OPVs can be manufactured over large areas, on lightweight plastic substrates with high flexibility, using high-throughput roll-to-roll (R2R) fabrication, which is compatible with solution processing technologies, potentially resulting in large reductions in fabrication costs and in the energy payback time (EPBT).

Research in OPVs started in the 1980's with the demonstration of a bilayer device, based on copper phthalocyanine and a perylene tetracarboxylic derivative, that exhibited a power conversion efficiency (PCE) of ≈1%, as described in the seminal work by Tang.[1] Later, in 1992, Sariciftci et al.[2] reported photo-induced electron transfer from a conducting polymer to fullerene. As a way to deal with the short exciton diffusion lengths in organic semiconductors, in 1995 Heeger et al.[3] introduced the concept of interpenetrating bicontinuous network of donor and acceptor materials, known as bulk-heterojunction (BHJ). OPVs were dominated by fullerene-based acceptors[4,5] for over two decades but, due to rapid developments in non-fullerene acceptors (NFA), fullerene acceptors have been outperformed in efficiency and progressively replaced by NFAs.[6–12] After a period of slow progress in the efficiency of small area (typically <10 mm^2) single junction OPV devices, observed between ≈2012 and 2018, OPVs have witnessed a rapid development in the last 2 years, with National Renewable Energy Laboratory (NREL) certified efficiencies under AM1.5G conditions jumping from 11.5% in October 2017 to 18.2% in December 2020.[13] These outstanding improvements were largely due to the development of new polymer donors[14–21] and new NFAs,[19–23] and have caused a surge of research activity in the OPV field.

In recent years, OPV devices have attracted growing interest as energy harvesters for indoor environments under artificial light sources, such as white light-emitting diodes (LEDs) and fluorescent lamps.[24–31] The cell requirements for indoor and outdoor light are crucially different, as the indoor light power is typically <1.0 mW·cm^{-2}, that is, 100–1000 times weaker than in AM1.5G (100 mW·cm^{-2}) and the spectrum of the indoor light is narrower and limited to the wavelength range 400–700 nm. Recent studies have demonstrated the high potential of OPVs for indoor applications, with reported PCE for small area devices of 28%[32] and more recently 31%.[33] OPVs are, therefore, currently envisaged as a future indoor energy harvester technology for powering low-power electronics and portable devices for the Internet of Things.[26]

Despite such progress, the potential advantages that OPV devices have to offer are still far from being a reality. Record OPV efficiencies are typically achieved with small active area devices (<1.0 cm^2), produced on rigid glass substrates under inert conditions, employing costly vacuum deposition steps and costly and scarce elements such as indium in the semitransparent front electrode. For example, the current maximum

Dr. G. Bernardo, Dr. T. Lopes, Prof. A. Mendes
LEPABE
Department of Chemical Engineering
University of Porto
Porto 4200-465, Portugal
E-mail: gbernardo@fe.up.pt
Prof. D. G. Lidzey
Department of Physics and Astronomy
The University of Sheffield
Sheffield S3 7RH, UK

The ORCID identification number(s) for the author(s) of this article can be found under https://doi.org/10.1002/aenm.202100342.

ADVANCED
SCIENCE NEWS
www.advancedsciencenews.com

ADVANCED
ENERGY
MATERIALS
www.advenergymat.de

NREL certified PCE of modules with an active area ranging 200–800 cm^2 is 11.7%;[34] a value much lower than 18.2% reported for small area devices.

There are several key challenges that OPV technology has to overcome to achieve a reliable lab-to-fab transfer.[35] One upscaling challenge is related to the optimization of the photo-active layer (PAL), including the choice of its deposition method. As a result of the limited exciton diffusion length (≈10 nm) and charge carrier mobility in organic semiconductors, the optimized thickness of the PAL in OPVs is typically less than 300 nm. Furthermore, the performance of large area OPV cells and modules is very sensitive to the presence of defects (which cause leakage currents) and thickness inhomogeneities in the active layer.[36,37] Therefore, one of the great challenges in the fabrication of high-efficiency large-area OPVs consists in the deposition of thin defect-free PAL with a homogeneous thickness over large areas. The upscaling of OPVs requires the use of large scale deposition methods such as inkjet printing,[38,39] spray coating,[40,41] doctor-blading/blade coating, slot-die coating, knife coating, gravure printing, flexographic printing, rotary screen printing, and flat-bed screen printing. All these printing and coating techniques have their own advantages and disadvantages and they have been extensively described in a number of review articles.[41–49] Other upscaling challenges relate to the use of green solvent formulations for PAL deposition, which replace the halogenated solvents typically used in small scale device development.[43,50–53] Other challenges concerns the development of new molecularly engineered donor and acceptor materials that can exhibit a high efficiency when formed into thick active layers (desirable for upscaling).[42,43,54,55] These challenges have been previously reviewed,[42,43,50,54,56] including some very recent reviews,[42,43,50,54] and will not be the subject of specific attention here.

As a benchmark for upscaling, this review mostly addresses the development of single cells and modules with an active area ≥1.0 cm^2, which has been considered as the minimum critical area for a scalability proof-of-principle,[54,57,58] and will focus on the following key issues:

i) Single Cells Versus Modules–Strategies are needed for upscaling individual cells and for upscaling modules of serially connected cells, minimizing performance losses. The efficiencies reported for large area cells are typically significantly lower than for small area cells, due to factors such as the limited conductivity of the transparent contact and the occurrence of film thickness heterogeneities in the PAL. A general technique to overcome the limited conductivity of the transparent contact is by connecting several smaller cells in series. This ensures that the photocurrent produced by the module is limited, while the voltage increases linearly with the number of cells. The production of these monolithically series-connected OPV cells requires patterning of each deposited layer to electrically connect them together. This technique, however, can also introduce large photocurrent and electrical fill factor losses which are mainly caused by the high electrical resistance of the interconnects.

ii) Indium-Tin-Oxide-Based Versus Indium-Tin-Oxide-Free Devices–Indium-tin-oxide (ITO) is commonly used as a transparent conductive electrode in OPV cells and modules, however indium is an expensive and rare metal. Furthermore, ITO only has a modest conductivity limiting the current extraction from large area devices. It also only has modest mechanical flexibility which makes it inappropriate for flexible device applications. For these reasons, several strategies explore replacing the ITO bottom electrode in large area devices.

iii) Vacuum-Based Versus Vacuum-Free Processing–Top (back) metal electrodes are usually deposited by thermal evaporation under vacuum. This vacuum-based process restricts the high throughput manufacture goal of OPVs and increases the associated costs. Solution-processed electrodes, to be used as alternative to the thermally evaporated electrodes, are therefore highly desirable as they could reduce significantly the EPBT.

iv) Improving the Stability of Large-Area Organic Photovoltaics– The operational lifetimes of large area devices are still significantly lower than the market requirements of ≥10 years. Strategies are needed to improve the stability of the devices including the development of new encapsulation strategies.

This review article is divided in three main parts: The first part (Section 2), addresses the upscaling of OPV devices based on ITO substrates and is divided in two sub-sections, which deal with the upscaling of single cells and the upscaling of modules consisting of connected cells. Inside each of these sub-sections, the upscaling using vacuum-based and vacuum-free processing are also considered separately. The second part (Section 3), addresses the upscaling of ITO-free cells and modules and separately considers the upscaling using different types of ITO-free bottom electrodes, such as, metal-based, carbon-based, and conducting polymer-based bottom electrodes. The third part (Section 4) then, addresses the testing and improvement of the operational lifetime stability of large area (≥1 cm^2) devices. Finally, Section 5 draws general conclusions regarding the future development of this very active research field.

2. Upscaling of Indium-Tin-Oxide-Based Devices

Indium tin oxide (In_2O_3:Sn, ITO) possesses a large number of highly mobile free carriers and an energy bandgap ≈3.8 eV. Due to these properties, ITO exhibits low electronic resistivity (≈10–20 Ω □$^{-1}$ on glass) and high optical transparency (>80% in the visible region), and is the most commonly used transparent bottom (front) electrode for OPVs.[59] ITO can be deposited on glass or plastic substrates by sputtering under ultra-high vacuum.

This section reviews the upscaling of OPV devices based on ITO bottom electrodes and is divided in two parts: Section 2.1 deals with upscaling of single cells and Section 2.2 deals with the upscaling of modules of serially connected cells.

2.1. Upscaling of Indium-Tin-Oxide-Based Single Cells

The most significant upscaling studies of ITO-based single cells are reviewed here and the performance of the most
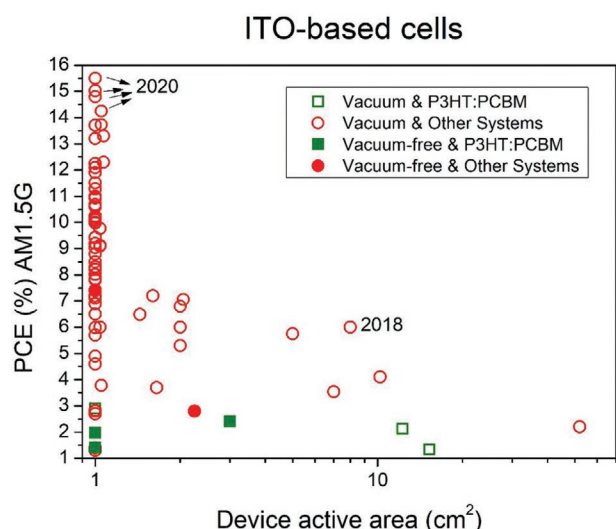
Figure 1. Performance of large area (≥1 cm²) ITO-based OPV single cells under AM1.5G conditions. The highest efficiency cells have been reported very recently, as indicated.

representative devices, processed either with or without metal evaporated top electrodes, are indicated in Table S1, Supporting Information, and are shown in **Figure 1**.

2.1.1. With Vacuum Conditions

The large majority of studies on the upscaling of ITO-based single cells have relied on the use of top electrodes evaporated under vacuum conditions and follow different strategies to achieve highly efficient devices with active areas ≥1.0 cm². Some studies have focused on optimizing large area coating and printing techniques; others have tested new donors, new acceptors and new ternary PALs; different devices architectures and cathode interfacial layers (CIL) have also been considered.

Among the scalable coating and printing techniques studied for large area OPVs are blade-coating,[60–64] slot-die coating,[64–69] spray-coating,[70–76] inkjet-printing,[77–79] maobi coating,[37] and wire-bar coating.[80]

Blade-coating of PALs, consisting of the donor:acceptor blend PBTA-TF:IT-M from non-halogenated solvent mixtures was used to produce cells with an active area of 1 cm² and a PCE of 10.6%.[60] Blade-coating was also explored by some authors[61–63] to deposit the PAL films by layer-by-layer (LbL) sequential processing, using non-orthogonal solvents. As compared to the common BHJ strategy, LbL presents several unique advantages including a much greater control of the D:A morphology over large areas, as well as better charge transport and extraction properties. Using this strategy, OPV cells based on bilayer donor:acceptor PALs were reported with an active area of 1.0 cm² and PCEs >10%, outperforming the corresponding standard donor:acceptor (BHJ) based devices.[61–63] The work by Sun et al.[63] is particularly impressive, wherein they used an LbL blade-coating strategy to produce cells with an average PCE of 15.03% compared to PCE of 14.01% for reference BHJ based devices. These cells had the structure ITO/PEDOT:PSS/PAL/PNDIT-F3N-Br/Ag, where the PAL consisted of the polymer

donor PM6 (also known as PBDB-TF) and the NFA Y6 (also known as BTP-4F).

An innovative deposition method was reported by Kim et al.[64] to simplify the fabrication of tandem OPVs. PAL materials (PTB7-Th:PC₇₁BM) were mixed with a non-conjugated polyelectrolyte [polyethyleneimine (PEI)] widely used as a cathode interfacial material. A blade or slot-die coating the PEI:PAL nanocomposite was used to create a bilayer with a PEI bottom layer and a PAL top layer via a spontaneous vertical phase separation of the materials driven by their surface energy differences. Cells with an active area of 1.0 cm² achieved a PCE of 9.1%.

Cells with area of 2 cm² and a PAL of PTB7:PC₇₁BM deposited using a slot-die R2R coating approach that combined additives and the use of an in-line drying oven, achieved an average PCE of 5.30%.[66] A sequential slot-die coating strategy, using a non-halogenated solvent, was used to deposit a ternary PAL, composed of PTB7-Th:PCBM: p-DTS(FBTTH₂)₂, forming flexible cells with areas of 1 and 2 cm², achieving PCEs of 7.11% and 6.8%, respectively.[67] A study of the effect of shear impulse during coating on the morphology of BHJs, reported 1.04 cm² cells based on two different slot-die coated PALs of PTB7-Th:PC₇₁BM and PBDB-T:ITIC, with maximum PCEs reported of 9.10% and 9.77% respectively.[68] Wu et al.[69] reported slot-die coated cells with 1.0 cm² active area and PCE of 11.19% based on the NFA system PBDB-T-SF:IT-4F.

Spray-coating has been explored as a scalable PAL deposition technique to produce large area OPV cells[70–76] and the corresponding mechanisms of film formation have been studied in detail.[74] Notably, Park et al.[70] created cells with size of 12.5 cm² and PCE of 1.68% from spray-coated P3HT:PCBM. Yang and coworkers[72] reported OPV cells with active areas of 1.0 and 10.2 cm² and PCEs of respectively 4.6% and 4.1% based on spray-coated PALs of PBDT-TFQ:PC₇₁BM. Later, the same authors[75] used spray-coating to deposit the PAL system PBTI3T:PC₇₁BM in single cells with an active area of 1 cm² that achieved an optimized PCE of 6.10%. These are amongst the highest efficiency large area cells based on spray-coated PALs reported so far in the literature.

Inkjet printing has also been studied to deposit the PAL of large area OPV cells.[77–79] Reference cells with 1 cm² active area, based on PV2000 PAL, inkjet printed using non-halogenated solvents, achieved a PCE of 4.9%.[78] Corzo et al.[79] reported 1.0 and 2.0 cm² active area cells with PCEs of ≈6%, based on an inkjet printed P3HT:O-IDTBR PAL, which are amongst the highest performances reported for inkjet printed large area cells. One of the main advantages of inkjet printing—freedom of design—was also exploited by fabricating a 2.2 cm² solar cell in the form of a marine turtle, as shown in **Figure 2**. This cell achieved a PCE of 4.76%, therefore demonstrating the versatility of digital inkjet printing for free-form manufacturing.

Maobi coating has been used to patch defects in the spin-coated PAL of large area cells, based on PBDB-T:ITIC.[37] Cells with areas of 1.6, 8, and 52 cm² achieved PCEs of respectively 7.2, 6.0 and 2.2%, where the larger cells contained a silver grid deposited on ITO to reduce the carrier collection path length.

Scalable techniques have also been investigated for the deposition of interfacial layers. Notably, Kang et al.[80] demonstrated cells with an active area of 1.0 cm² and PCE of 10.1%, with
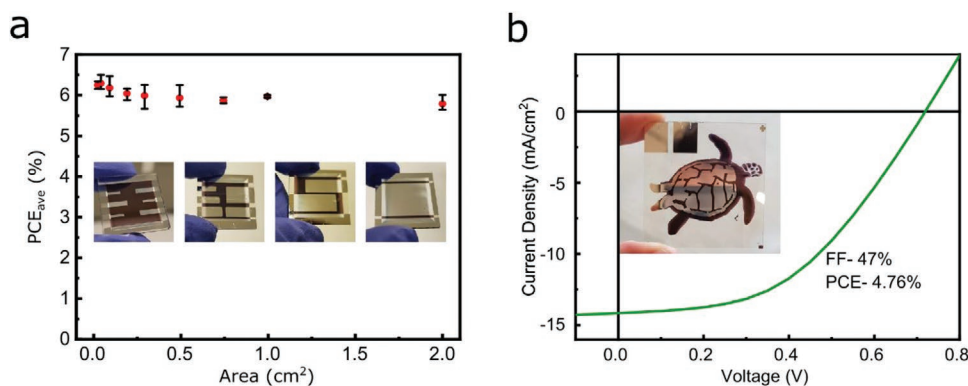
Figure 2. a) The performance of P3HT:O-IDTBR devices as a function of cell area and b) J–V of free-form inkjet-printed solar cell in the shape of a marine turtle on top of ITO glass. Reproduced with permission.[79] Copyright 2019, John Wiley & Sons.

structure glass/ITO/MoOx/PB3T:I-TM/PFN-Br/Al, where a very thin and highly uniform MoOx interfacial layer was wire-bar coated.

In the above studies of scalable processing techniques, the PAL was deposited either under ambient or inert conditions, however comparative studies of these two processing conditions are scarce. Dkhil et al.[81] reported 1.0 cm^2 cells based on PTB7-Th:PC$_{71}$BM achieving PCEs of 7.84% and 7.08% when processed under inert and air conditions, respectively.

Optimizing the molecular structures of organic photoactive materials has been the most successful method to increase the performance of the OPV devices and hence new NFAs,[82–85] polymer donors,[86–90] and small-molecule donors[91] have been tested with much success in large area cells.

In a seminal work, Zhao et al.[82] reported, in 2016, OPV cells with 1.0 cm^2 and structure ITO/ZnO/PBDB-T:ITIC/MoO$_3$/Al with a certified PCE of 10.78%; a value much higher than the PCE of 7.45% for a reference PBDB-T:PC$_{71}$MB based device, resulting from a much broader PAL absorption band and a more appropriate molecular energy level alignment. This was the first example of a NFA-based OPV cell exhibiting higher PCE than the corresponding fullerene-based OPV and paved the way for the outstanding improvements in PCE observed in the following years. More recently, Cui et al.[83,84] reported new NFAs with improved performances in OPV cells. First, the fluorine atoms on BTP-4F (Y6) were replaced with chlorine atoms originating BTP-4Cl, which has an extended optical absorption.[83] Single cells with an active area of 1 cm^2 (**Figure 3**) and inverted structure ITO/ZnO/PBDB-TF:BTP-4Cl/MoO$_3$/Al, achieved a PCE of 15.3% and improved V_{OC}, mainly due to reduced non-radiative energy losses, combined with a broader photo-response range. However, the BTP-4Cl has poor solubility and to improve the relationship between solubility and device efficiency, the alkyl chains in BTP-4Cl were later finely tuned creating the material BTP-eC9.[84] OPV cells with an active area 1 cm^2 and structure glass/ITO/PEDOT:PSS/PBDB-TF:BTP-ec9/PFN-Br/Al, where the PAL was blade-coated, achieved a very impressive maximum PCE of 16.2% (average 15.5%), which is among the top performances for single-junction OPV cells with an active area ≥1.0 cm^2, due to improved J_{SC} and FF.

Different novel polymeric donors have been tested in large area OPV cells including the random copolymers

PTAZDCB20[86] and PDT2fBTBT10,[87] the chlorinated polymer PBDB-T-2Cl,[88] P2F-EHp,[89] and the copolymer T1 (0.8 PBDB-TF + 0.2 PTO$_2$).[90] Replacement of the fluorine atoms in PBDB-T-2F with chlorine atoms originating PBDB-T-2Cl was shown to reduce the polymer HOMO and LUMO levels, contributing to an increase in V_{OC} and PCE of the corresponding devices.[88] Cells with the structure ITO/ZnO/PBDB-T-2Cl:IT-4F/MoO$_3$/Al and with an active area 1 cm^2, achieved a PCE of 11.51%. Fan et al.[89] synthesized new polymer donors (P2F-EH, P2F-EHp, P2F-EO) by fine-tuning modification of the side chains or end groups of existing high-performance polymers, and tested them in OPV devices. A certified PCE of 12.25% was achieved in single cells with an active area of 1 cm^2 based on the structure ITO/PEDOT:PSS/P2F-EHp:IT-2F/PFNDI-Br/Ag. Cui et al.[90] synthesized copolymers of PBDB-TF with PTO2 which, compared with PBDB-TF, show lower HOMO levels and broader optical absorption and are very soluble in most common solvents including non-halogenated solvents. OPV cells with 1 cm^2 and inverted structure ITO/ZnO/PAL/MoO$_3$/Al, where the PAL was blade-coated from non-halogenated solvents and consisted of a blend of copolymer T1 (0.8 PBDB-TF + 0.2 PTO$_2$) and the small molecule NFA IT-4F, achieved a PCE of 13.1%.
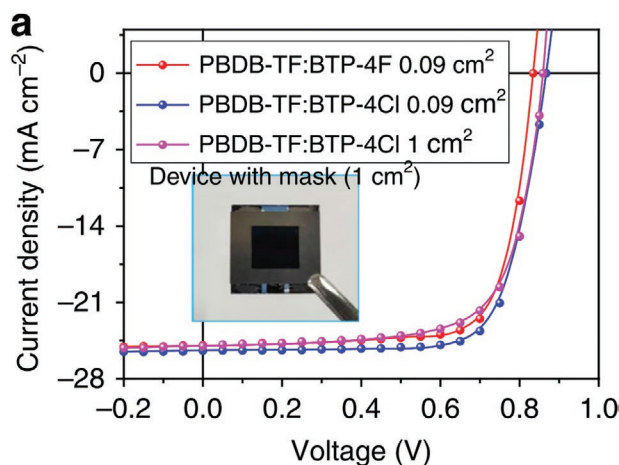

Figure 3. J–V curves of PBDB-TF:BTP-4Cl cell with active area of 1 cm^2. J–V curves for small area devices are shown for comparison. Reproduced with permission.[83] Copyright 2019, Springer Nature.

**ADVANCED
SCIENCE NEWS**

www.advancedsciencenews.com

**ADVANCED
ENERGY
MATERIALS**

www.advenergymat.de

Ternary blending of the PAL, either with two donors and one acceptor ($D_1:D_2:A$) or with one donor and two acceptors ($D:A_1:A_2$), has also proved and effective strategy to increase the PCE of devices compared to the corresponding devices based on binary blends.[92–95] The $D_1:D_2:A$ strategy was used by Zhang et al.[92] to produce cells with 5 cm^2 active area and PCE of 5.75% based on PTB7-Th:p-DTS(FBTTH$_2$)$_2$:PC$_{71}$BM. Liu et al.[93] reported 1.05 cm^2 active area OPV cells based on two different ternary blade-coated PAL structures: PM6/ICBA:IT-4F (named as PPHJ) and PM6:ICBA:IT-4F (BHJ), where ICBA is a minority component. Devices with PPHJ and BHJ structures achieved PCEs of 14.25% and 13.73%, respectively—both higher than similar devices without ICBA. Baran et al.[94] used a ternary blend $D:A_1:A_2$ strategy to produce 1 cm^2 active area cells with structure ITO/ZnO/P3HT:IDTBR:IDFBR/MoO$_3$/Ag, which achieved a PCE of 6.5%. The improved PCE, compared to the binary blend, was assigned to improved light harvesting in the visible region and to changes in microstructure that reduced charge recombination and increase the photo-voltage. All-polymer cells based on the ternary blend PBTA-Si:PTzBI-Si:N2200 were reported by Fan et al.[95] Cells with 1.0 cm^2 active area and structure custom-ITO/PEDOT:PSS/PAL/PFNDI-Br/Ag, achieved a PCE of 10.01%, where the custom-ITO, had a metal frame on its periphery.

A different strategy to optimize the performance of large area single cells has consisted in the study of different cell architectures[96] and different CIL.[97–99] Some authors[36,96] reported that multi-junction (tandem, triple, four) ITO-based cells suffer lower reductions in PCE on upscaling than the corresponding single junction cells, suggesting that multi-junction OPV cells can achieve higher efficiency and improved scalability. Kang et al.[97] studied the impact of different CILs on the performance of cells with structure ITO/PEDOT:PSS/PBDB-T-2F:IT-4F/CIL/Al. The best performances were obtained with a CIL consisting of naphthalene diimide (NDI)-based organic molecule (NDI-N), with cells having a 1.0 cm^2 active area achieved a PCE of 13.2%. Another study addressed the impact of the surface morphology of a ZnO CIL on the performance of inverted OPV cells.[98] Bai et al.[99] produced highly efficient (average PCE = 11.28%) semi-transparent cells with 1 cm^2 active area and structure ITO/Al(acac)$_3$/PM6:Y6/MoO$_3$/Ag (15 nm), where aluminum(III) acetylacetonate Al(acac)$_3$ was used as a novel CIL.

Large area ITO-based single cells, with top electrodes evaporated under vacuum, exhibiting promising PCE values (particularly considering they were fullerene-based), have also been reported, sometimes as reference cells.[100–103]

Large area ITO-based OPV single cells are also being investigated for indoor applications and the first report was made by Steim et al.[104] in 2011. Cells based on P3HT:PCBM and with an area of 1 cm^2, achieved a PCE of 2.7% under AM1.5G conditions (i.e., 100 000 lux) and achieved a PCE of ≈7%, corresponding to a power output of 19 µW·cm^{-2}, under a fluorescent lamp with 1000 lux. The requirements of shunt (R_p) and serial (R_s) resistances were observed to be different for indoor and outdoor cells, with indoor cells coping with higher R_s values ($R_s \leq 50$ Ω·cm^{-2}) than outdoor cells ($R_s \leq 3$ Ω·cm^{-2}) but requiring higher R_p values ($R_p \geq 85$ kΩ·cm^{-2}) than outdoor cells ($R_p \geq 1$ kΩ·cm^{-2}).

Quite recently, Cui et al.[85] synthesized a novel NFA (IO-4Cl) and blended it with PBDB-TF to obtain a PAL with an absorption spectrum that matches that of indoor light sources. Under AM1.5G conditions, 1 cm^2 cells with the acceptor IO-4Cl achieved a PCE of 9.80% which was lower than that reference cells with the acceptor IT-4F (PCE = 12.5%) having an identical size. By contrast, under light from a 2700 K LED lamp at 1000 lux, the same IO-4Cl-based cells achieved a PCE of 26.1%; a value that was much greater than the PCE of 21.2% obtained with the IT-4F-based cells. These results showed that the best blend compositions for AM1.5G and indoor conditions are not necessarily the same. The IO-4Cl-based cells were then upscaled to an active area of 4 cm^2 and the corresponding PCE at 1000 lux was determined as 23.9%. The authors observed that under indoor lighting, the parasitic R_s caused by the transparent electrodes was not a limiting factor to the PCE and therefore large-area OPV cells do not need to be made of thin strips. Additionally, under indoor lighting the performance of OPVs was observed to be less dependent on the PAL thickness than under 1 Sun AM1.5G conditions, meaning that thickness uniformity requirements over large areas are less stringent for indoor applications; a result that potentially facilitates upscaling using printing techniques.

In other work,[105] 1 cm^2 active area cells were studied with two additional PAL blends (PBDB-TF:ITCC and PBDB-TF:PC$_{71}$BM). Under AM1.5G conditions, ITCC and PC$_{71}$BM based cells achieved PCEs of 10.3% and 8.43%, respectively. Under 1000 lux (2700 K) LED illumination, the ITCC-based cell achieved a PCE of 22.0% with a V_{OC} of 0.962 V corresponding to an output power (P_{out}) of 66.5 µW.cm^{-2}, and the PC$_{71}$BM-based cell achieved a PCE of 18.1% with a V_{OC} of 0.784 V and a P_{out} of 54.7 µW.cm^{-2}. The performance of OPV cells for indoor applications was again observed to be less dependent on the PAL thickness.

2.1.2. With Vacuum-Free Conditions

Upscaling studies of ITO-based cells under vacuum-free conditions, that is, not relying on the use of thermal evaporated top electrodes, have been scarce and explore different vacuum-free processing strategies for depositing the top electrodes.

Eutectic metal alloys with low melting points (m.p.), such as Wood´s metal (m.p. ≈70 °C—50% Bi: 25% Pb: 12.5% Cd: 12.5% Sn) and Field's metal (m.p. of ≈62 °C—51% In: 32.5% Bi: 16.5% Sn), were coated at temperatures above melting point and tested as top electrodes in large area OPV cells,[106–108] but with very limited success (Table S1, Supporting Information). Using Field's metal cathode, the best PCEs reported were 2.4% in P3HT:PCBM cells with an active area of 3 cm^2[107] and 3.1% in PTB7:PC$_{71}$BM cells with an active area of 2.25 cm^2.[108]

Silver inks have also been deposited using inkjet or screen-print (under ambient conditions) and used as the top electrodes (either grids or full-layers) of large area OPV cells, however the reported results were quite modest[109,110] (Table S1, Supporting Information).

A more successful vacuum-free processing approach was reported by Czolk et al.[101] who produced reference ITO-based OPV cells, with 1.0 cm^2 active area and top electrodes consisting of Ag nanowires (AgNWs) intermixed with PEDOT:PSS. These cells had the structure

ADVANCED
SCIENCE NEWS
www.advancedsciencenews.com

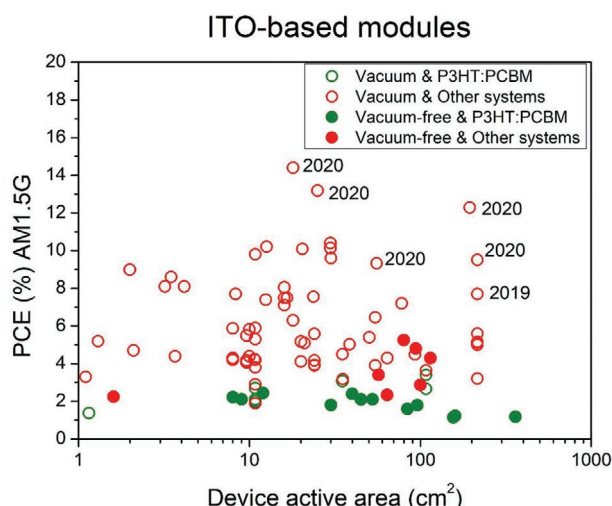ADVANCED
ENERGY
MATERIALS
www.advenergymat.de

Figure 4. Performance of large area (≥1 cm²) ITO-based OPV modules under AM1.5G conditions. As shown, the most efficient modules have been reported very recently.

glass/ITO/PEDOT:PSS/ZnO/PAL/AgNWs:PEDOT:PSS, where the PAL consisted of a ternary blend of PffBT4T-2OD:PC$_{61}$BM:PC$_{71}$BM, and achieved an impressive PCE of 7.4%

2.2. Upscaling of Indium-Tin-Oxide-Based Modules

In this section the most significant upscaling studies of ITO-based OPV modules are reviewed. The performances of the most representative ITO-based OPV large area modules, processed with and without top metal evaporated electrodes, are shown in Table S2, Supporting Information, and plotted in **Figure 4**.

Due to several technological issues, enlarging the area of single cells to increase the maximum output power is not always the best solution. Inhomogeneities in the active layer may degrade device performance, and these effects scale with the area of the cell. Furthermore, and more importantly, the limited conductivity of electrodes such as ITO makes it difficult to extract the large photocurrents generated in large area single cells. A common technique used to overcome the limited conductivity of the transparent front contact consists in connecting several narrow single cells in series. Assuming that in a module all the i cells connected in series behave identically, then the total photo-generated current J_{SC} (Module) equals the J_{SC} (i) of each individual cell, that is, J_{SC} (Module) = J_{SC} (i). On the other hand, V_{OC} (Module) = Σ V_{OC} (i). Therefore, this series connection strategy is typically preferred as it ensure that the photocurrent produced by the module remains limited (reducing resistive power losses), while the voltage increases linearly with the number of cells (**Figure 5**).

Although connection in series can be achieved by externally connecting cells that were produced separately (as is commonly done in the silicon photovoltaic industry), producing integrated monolithic OPV modules is far more attractive from a manufacturing perspective. In a monolithic connection, all the different layers are processed on one substrate and patterned in such a way that the different cells become interconnected in series, that is, the bottom electrode of one cell is directly connected to the top electrode of an adjacent cell. This is shown in **Figure 6**, where i) pattern P1 disconnects the individual bottom electrodes of all cells within the module from each other; ii) pattern P2 removes the material stack between the bottom and top electrodes allowing the formation of a low ohmic contact, and finally iii) pattern P3 divides the top electrodes between adjacent cells. The area between the P1 and P3 lines is the so-called "dead area" because it does not contribute to energy production. The ratio between the photoactive area and the total area of the module is referred to as the geometric fill factor (GFF). The smaller the dead area, the larger the GFF and the higher the module efficiency. Therefore, lines P1, P2, and P3 should be made as narrow as possible.
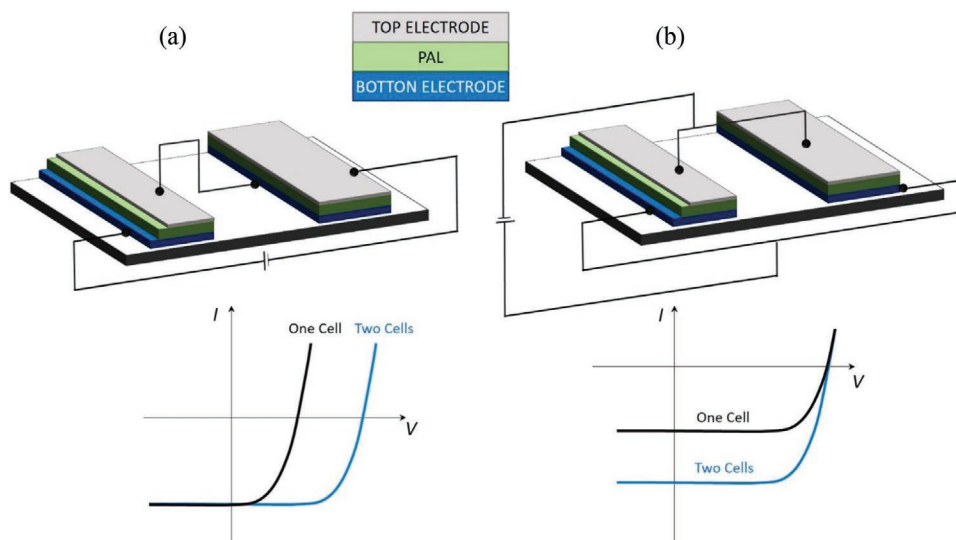

Figure 5. Schematic representation of the connection of two identical solar cells and the corresponding IV characteristic curves: a) Series connection; b) parallel connection.
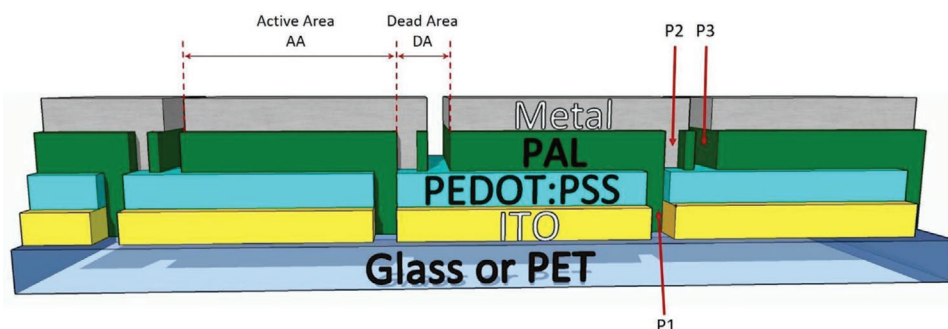
**ADVANCED
SCIENCE NEWS**
www.advancedsciencenews.com

**ADVANCED
ENERGY
MATERIALS**
www.advenergymat.de

Figure 6. Schematic illustration of an OPV module with lines P1, P2, and P3.

Common coating and printing techniques (like blade-coating, slot-die coating, screen printing, inkjet printing, gravure printing, and spray coating) can produce patterns making interconnections between single cells within a module by depositing the bottom electrode, the PAL, and the top electrode as one-dimensional stripes which are slightly offset with respect to each other. However, the relatively low resolution of these deposition techniques requires typical scribe widths ≥1 mm to prevent intermixing between inks applied to adjacent cells. This limits the achievable GFF to values typically below 85%. An alternative approach consists in creating lines P1–P3 by laser ablation which allows a much higher-precision (reproducible scribe width in the range 20–100 µm depending on the laser system), high-throughput and mask-free patterning process. Laser ablation employs a focused laser beam to selectively ablate materials from a surface.[111–114] When processing the different OPV layers, different wavelength and pulse duration are selected to reach different pulse energies which can melt and evaporate the processed layer without damaging the underlying layer. By minimizing the inactive areas used to interconnecting the individual solar cells in series within the module, a GFF of over 95% can be achieved.

For a module with a given total area, increasing the number of cells within the module leads to an increase in the number of interconnects (number of cells—1) which leads to a decrease in the GFF and a decrease in the overall module efficiency. On the other hand, decreasing the number of cells leads to an increase in cell width and in resistance losses due to the limited conductivity of the electrodes (especially ITO). Therefore, the optimum number of cells for a given area results from a balance of these two contradictory effects[115] and can be simulated as described by Lucera et al.[116]

2.2.1. With Vacuum Conditions

In 2007, Frederik Krebs at the Denmark Technical University (DTU)[117] published one of the earliest reports of an OPV module. This consisted of 91 individual cells, each with an active area of 2.4×3.0 cm^2, connected in series and parallel, making up a total active area of 655 cm^2 displaying, however, a very low PCE of 0.0002%.

Later, in 2009, Tipnis et al.[118] reported on the use of laser ablation to pattern OPV modules of connected cells and since then, the use of lasers for the patterning OPV modules has been the subject of intensive research.[119–125]

In 2013, Brabec and coworkers,[119] used an ultrafast fs-laser ablation system, with a pulse duration of <350 fs at repetition rates up to 960 kHz, to pattern OPV modules based on the structure ITO/Aluminium-doped ZnO (AZO)/P3HT:PCBM/PEDOT:PSS/Ag. Here a GFF > 90% was achieved with the module consisting of 10 monolithically interconnected stripe cells, each with width of 1.0 mm. The best modules with an active area of 1.15 cm^2, had a total interconnection width of 178 µm and a GFF of 83% and attained a PCE of 1.38%. The same laser system was later used by the group to; i) extend this concept to tandem P3HT-based modules with 10-cells and a device area of 1.1 cm^2 achieving a GFF of ≈85% and a PCE of 3.3%;[120] ii) produce P3HT-based modules consisting of 14 cells in series, with a total area of 35 cm^2 achieving a GFF > 95% and a PCE of 3.07%;[121] and iii) produce modules with GFF of 98.5% consisting of 14 cells connected in series with a total active area of 35 cm^2 and a total interconnection width below 100 µm. These were based on a PAL blend of PBTZT-stat-BDTT-8:PC$_{61}$BM and achieved maximum PCEs of 4.2% and 5.3%, respectively, on polyethylene-terephthalate/ITO-metal-ITO (PET/IMI) and on glass/fluorine-doped tin oxide (FTO) substrates.[122]

A ps-laser ablation system, with a pulse duration of 6 ps, was used by Röttinger et al.[124] to pattern ITO at repetition rates of 50 kHz and both metal and organic layers at 400 kHz. This produced modules consisting of six stripes with tandem cells that were based on the PAL blend HDR14:C$_{60}$. A GFF of 94% and a PCE of 4.3% were achieved for an aperture area of 64 cm^2.

Very recently, a ns-laser ablation system with a pulse duration of 20 ns was used by Distler et al.[125] to produce modules from the cell structure glass/ITO/ZnO/PM6:Y6:PC$_{61}$BM/MoOx/Ag having a GFF > 95%. By carefully tuning the laser ablation parameters combined with a modification of the standard patterning sequence (the P2 patterning was divided in two separate steps P2a and P2b) and an optimization of the active cell width (see **Figure 7**), the authors were able to produce; i) modules of 12 cells in series with total/active areas of 26.2/25.0 cm^2 and total area PCE of 12.6% and ii) larger modules of 33 cells with total/active areas of 204.0/194.8 cm^2 and total area PCE of 11.7%. These values currently represent world record energy efficiencies. The authors demonstrated that the required quality and reproducibility of laser patterning can be achieved with ns-lasers, rather than fs-lasers, thus reducing significantly the investment cost.

Alternative techniques for OPV patterning (i.e., not involving the use of lasers) have also been investigated. These included;
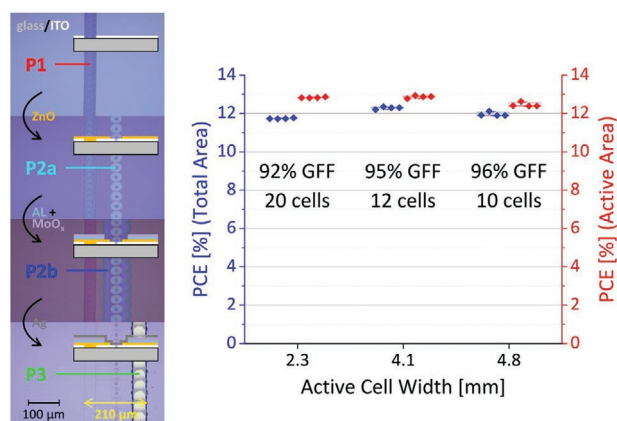
**ADVANCED
SCIENCE NEWS**

www.advancedsciencenews.com

**ADVANCED
ENERGY
MATERIALS**

www.advenergymat.de

Figure 7. a) Bright-field microscope images of all laser lines involved in the module production process, namely, P1, P2a, P2b, and P3, together with cross-section sketches of the layer stack after each laser patterning step. The black arrows indicate the different coating steps, that is, electron transport layer (ZnO), active layer (AL: PM6:Y6: PC60BM), hole transport layer (MoOx), and top electrode (Ag); b) Power conversion efficiencies (PCE) with respect to the total area (blue data, left y-axis) and the active area (red data, right axis) of modules comprising three different layouts (four modules each layout). The layout variation consists in different cell widths (see x-axis), a different number of cells connected in series, and different geometric fill factors (GFF). The total area of all modules is 26.2 cm². Reproduced with permission.[125] Copyright 2020, John Wiley & Sons.

i) a chemical-based patterning process achieved by printing thin lines of a fluoro-surfactant to repel the subsequently deposited PAL layer[126,127] and ii) a mechanical scribing process.[127,128] However, the GFF demonstrated was low.

Different module architectures and interfacial layers have also been explored in an attempt to increase the overall efficiencies.[96,129–131] Lee et al.[129] proposed a new architecture that avoids P2 patterning during the module production. In this architecture, the cells are connected in series with alternating conventional and inverted configurations using self-aligned dual charge-selecting interfacial layers. A module based on PCDTBT:PC$_{71}$BM was demonstrated having an active area of 10.68 cm², a high GFF of 96% and a PCE of 4.24%.

To reduce the resistive contribution from ITO, Xiao et al.[96] used a metal bus bar sub-electrode around 95% of the cell perimeter for each cell, which had an active area of 1 cm². Cells were then connected in series to form columns of 5 cells, while 5 columns were connected in parallel to form a module with a total active area of 25 cm² and an average PCE of 6.5%.

Hong et al.[130] demonstrated a new module architecture without patterning the electron transport layer (ETL) and hole transport layer (HTL). The inverted structure device ITO/ZnO/PAL/MoO$_3$/Ag consisted of patterned ITO, a stripe-patterned PAL (PTB7-Th:PC$_{71}$BM) and single-layers of ZnO and MoO$_3$ without any patterning. A module PCE of 7.5% was demonstrated with area of 4.15 cm² and a GFF of 90%.

Dong et al.[131] doped a ZnO CIL with the naphthalene-diimide based derivative NDI-PFNBr, which improved the PCE of the corresponding devices. Modules with active areas of 16 cm² (4 cells) and 93 cm² (13 cells), based on the structure glass/ITO/NDI-PFNBr@ZnO/PTB7-Th:PC$_{71}$BM/MoO$_3$/Ag achieved PCEs of 8.05% and 4.49%, respectively. Reference

modules with a ZnO CIL had an active area of 16 cm² and achieved a PCE of 7.11%.

Research of scalable deposition techniques to produce large area modules has also been the focus of much interest. The techniques that have been considered include blade-coating,[132–141] slot-die coating,[65,66,69,142–146] spray-coating,[75] reverse gravure coating,[147] Maobi coating,[37,148] and water transfer printing.[149]

Blade coating of large area modules has received special attention by Meng and coworkers.[132–137] Blade coating with uniform blade acceleration, instead of uniform blade speed, was used to create a more homogeneous film morphology and uniform film thickness.[132] The active layers were patterned manually using a knife edge and a metal interconnection mask as overlay. Modules with a total active area of 108 cm² composed of 10 cells connected in series achieved PCEs of 2.66% and 3.64%, respectively for PALs consisting of P3HT:PC$_{61}$BM and POD2TDTBT:PC$_{71}$BM blends. Rapid-drying blade-coating was later used by the same group to optimize the PAL morphology.[133] Blade-coating was explored to produce opaque and semi-transparent modules based on four different PAL blends.[134] The most efficient modules, with an active area of 10.8 cm², were obtained with PTB7-Th:PC$_{71}$BM and achieved PCEs of 5.9% for opaque and 5.3% for semi-transparent modules.[134] Blade coating was also used to deposit modules using the PAL (PTB7-Th:PC$_{71}$BM) and a CIL of MSAPBS with high uniformity and an impressive active area of 216 cm² demonstrated.[135] Accelerated blade motion was used as before[132] to accurately control the PAL film uniformity over large area and PCEs of 5.63% and 4.50% were reported for opaque and semitransparent modules, respectively. Notably, more recently, the same deposition technique was used to produce modules having an active area of 216 cm² for devices based on a donor:acceptor blend of NF3000-P:NF3000-N and using a CIL of TASiW-12, with a very impressive PCE of 9.50% demonstrated.[136] These values are among the highest PCE ever reported for OPVs with an active area > 100 cm².[136] In similar work by the same group, non-halogenated solvents were used to blade-coat PTB7-Th:PC$_{71}$BM PAL films to produce modules with a total active area of 216 cm² (16 cells) and an average PCE of 5.12%.[137] Non-halogenated solvents were also explored by other groups to blade-coat large area OPV modules.[138,139] For example Zhang et al.[138] produced 16 cm² modules based on a PTB7-Th:PC$_{71}$BM PAL, that reached a PCE of 7.5%. Zhao et al.[140] also demonstrated blade-coated modules with the PAL morphology optimized through a vacuum assisted annealing (VA) method. Modules with 3 cells, based on the PAL blend PBDB-TF:IT-4F, with a total active area of 12.6 cm², achieved an impressive PCE of 10.21%. Blade-coating has also been used in the production of tandem OPV modules[141] with active areas of 1.3 cm² (3 cells) and 2.1 cm² (5 cells) and with PCEs of 5.2% and 4.7%, respectively.

Slot-die coating has been studied for the upscaling of OPV devices.[65,66,69,142–146] In 2014, Hong et al.[65] prepared modules based on a P3HT:PCBM PAL, slot-die coated from CB:DCB mixtures, with an impressive total active area of 198 cm² and a PCE of 1.73% demonstrated. A mask was used for stripe patterning, and the modules consisted of 3 sub-modules connected in parallel; each sub-module was composed of

11 serially connected cells with 6 cm² active area per cell. Heo et al.[143,144] studied the use of slot-die coating to prepare modules based on blends of PC$_{71}$BM with the small molecule donors LGC-D023,[144] LGC-D073,[144] and BTR.[143] The most promising modules were based on LGC-D073:PC$_{71}$BM, had a total active area of 24 cm² and achieved a PCE of 5.50%.[144] Modules, with 5 serially connected cells (total active area of 23.7 cm², 4.74 cm² per cell) were prepared by Chang et al.,[145] where three different ETL/HTL combinations were tested, namely ZnO/MoO$_3$, PEI/MoO$_3$, and PEI/PEDOT:PSS. The ETL, PAL, and HTL were all deposited by slot-die coating under ambient conditions using a stainless steel meniscus guide for stripe patterning, with the Ag top electrode thermally evaporated through a stripe patterned shadow mask. The most promising modules were obtained using the PEI/PEDOT:PSS combination, and achieved a certified PCE of 7.56%. Lee et al.[146] prepared slot-die coated modules with a total active area of 30 cm², consisting of 5 cells connected in series, where the PAL consisted of a ternary blend of PTB7-Th:PC$_{71}$BM:COi8DFIC. Rigid modules including a slot-die-coated PAL achieved a PCE of 8.6%. Flexible R2R coated modules fabricated using a commercial machine achieved a PCE of 9.6%.

The use of spray-coating to produce large area OPV modules has been so far very limited. Zhang et al.[75] reported spray-coated modules based on the system PBTI3T:PC$_{71}$BM, with structures consisting of 6 series-connected single stripe cells (70 mm × 11 mm), each with an active area of 38.5 cm² and exhibiting a PCE of 5.27%.

Other less common scalable deposition techniques have also been tested in the production of large area OPV modules. R2R reverse gravure coating was used by Vak et al.[147] to produce P3HT:PCBM based modules (5 series-connected strip cells) with a total area of 45 cm² and a PCE of 2.1%. Inspired by an old Chinese calligraphy technique, Mao et al.[148] used a motor-driven, computer controlled Maobi coating system to deposit the PAL of large area solar modules (18 cm²) containing 14 cells connected in series. Modules based on a PAL of PBDB-T:ITIC achieved a PCE of 6.3%. Maobi coating was also used by the same authors to repair defects in blade-coated modules.[37] Modules based on the same PBDB-T:ITIC PAL system, consisting of 5 cells and a total area of 21 cm² (4.2 cm² per cell), achieved a PCE of 5.1%. Sun et al.[149] demonstrated the use of a water transfer printing method to produce a highly uniform PAL film on an OPV module with a total active area of 3.2 cm² and consisting of 4 cells. Modules with a PAL of PBDB-T-2F:IT-4F achieved a PCE of 8.1%.

The use of novel donors[150–152] and acceptors[153,154] and novel PAL blends,[92,155,156] has also been explored by some authors. Badgujar et al.[150] prepared modules with 11 serially connected cells and a total active area of 78.5 cm², where the PAL consisted of a blend of PC$_{71}$BM with newly synthesized oligomer donors based on benzodithiophene (BDT) units. The higher efficiency modules were made with the oligomer BDT2 and achieved a PCE of 7.45%, due to reduced charge recombination and a well-constructed 3D morphology. Novel synthesized donor polymers TPD-*n*, *n* = 1–3 and TPD-3F were used by Liao et al.[152] to fabricate OPV modules with 5 cells connected in series and with a total active area of 29.75 cm², corresponding to a GFF of ≈37%. The most efficient module (**Figure 8**) was

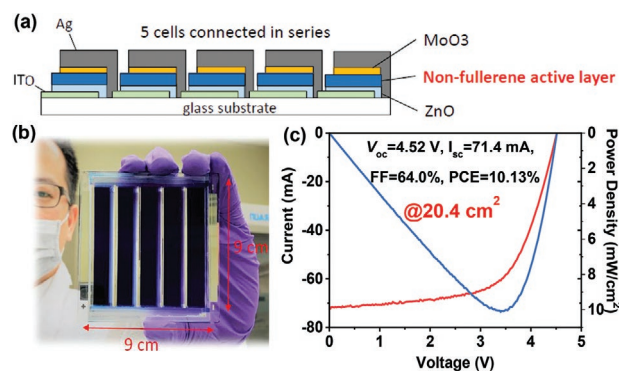**Figure 8.** a) Schematic of the TPD-3F-based OPV module structure. b) Photograph of a TPD-3F based OPV module. c) I–V characteristics of the TPD-3F-based OPV module. Reproduced with permission.[152] Copyright 2020, Elsevier.

based on TPD-3F:IT-4F and had a PCE of 10.13% (certified PCE of 10.08%) over an active area of 20.4 cm² as defined by an aperture mask; smaller cells (having an area of 0.04 cm²) had a PCE of ≈13%.

Lee et al.[153] synthesized a novel NFA T2-OEHRH, which was made of asymmetric side chains (octyl and 2-ethylhexyl) and an unfused bithiophene core and used it in OPV modules based on the D-bar-coated ternary PAL PTB7-Th:EH-IDTBR:T2-OEHRH. Modules consisting of 11 stripe cells connected in series, with a total aperture area of 55.5 cm² achieved a PCE of 9.32%.[153] Very recently, Dong et al.[154] synthesized a novel NFA (DTY6) by extending the branched alkyl chains of BTP-4F (also known as Y6) to improve the solvent processing ability and suppress excessive molecular aggregation due to the steric hindrance effect of the long-branched alkyl chains. Modules with a total active area of 18 cm² and consisting of 6 ITO/PEDOT:PSS/PM6:DTY6/PNDIT-F3NBr/Ag cells (each of 5 × 0.6 cm²) were monolithically connected in series and achieved an impressive PCE of 14.4% (certified PCE of 13.98%).[154] Ternary blends have also been used to increase the efficiency of OPV modules.[92,153,156] Huang et al.[156] prepared modules with 16 cell stripes connected in series (total active area of 216 cm²) with the structure glass/ITO/PEDOT:PSS/PAL/CIL/Al where the PAL consisted of a ternary blend of PBDB-T:ITIC:PC$_{71}$BM with different CIL used. Here, modules with a ZrOx CIL achieved an impressive (considering their large area) PCE of 7.7%.

ITO-based OPV modules have also been investigated for indoor applications,[157–161] as indicated in **Table 1**. Devices based on P3HT, PCDTBT, and PTB7 blended with PC$_{71}$BM were tested by Lee et al.[157] PCDTBT-based devices achieved the highest PCE under a fluorescent lamp (300 lux), in contrast to AM1.5G conditions where the PTB7-based devices performed the best. A PCDTBT-based module with a total active area of 100 cm² delivered, under a 300 lux fluorescent lamp, a PCE of 11.2% corresponding to a maximum power of 9.38 µW·cm⁻². Modules (8 cells) based on a proprietary formulation, with an active area of 3.67 cm² achieved an output power of 43.4 µW·cm⁻² as reported by Aoki et al.[158] OPV modules consisting of 6 cells connected in series with a total active area of 9.5 cm² (1.6 cm² per cell) were prepared by Arai et al.[159] on glass and PET substrates using a PAL of BDT-2T-ID:PNP. Under a white LED

Table 1. Performance of ITO-based large area (≥1.0 cm^2) OPV devices (cells and modules), under indoor light.

Device structure	Photoactive layer (PAL)	PAL deposition technique	PAL solvent	PAL thick [nm]	PAL atmos	Cell (C) or Module (M)	Total Active Area [cm^2]	Light source	Light intensity (lux)	P_{in} [μW·cm^{-2}]	P_{out} [μW·cm^{-2}]	PCE [%]	Year	Ref.
Glass/ITO/ PEDOT:PSS/PAL/ PFN-Br/Al	PBDB-TF:IO-4Cl	Spin-coated	Hal	100	Inert	C	1.0	LED (2700 K)	1000	302.2	78.8	26.1	2019	[85]
		Blade-coated		179			4.0				72.1	23.9		
Glass/ITO/ PEDOT:PSS/PAL/ PFN-Br/Al	PM6:IT-4F	Spin-coated	Hal	100	Inert	C	1.07	LED (2700 K)	1000	302.2	62.8	20.8	2019	[105]
	PM6:ITCC										66.5	22.0		
Glass/ITO/ZnO/ TPD-n:IT-4F/ MoO$_3$/Ag	TPD-3F:IT-4F	Blade-coated	—	—	—	C	20.4	TL84 fluorescent lamp	1000	185	40.2	21.8	2020	[152]
ITO/PEDOT:PSS/ PAL/Al	PCDTBT:PC$_{71}$BM	Spin-coated	Hal	70	Inert	M(8)	100	Fluorescent lamp	300	83.6	9.38	11.2	2016	[157]
Glass/ITO/ETL/ PAL/PEDOT:PSS/Al	Merck formulation	Spin-coated	—	200		M(8)	3.67	Fluorescent lamp	1000	—	43.4	—	2017	[158]
Glass/ITO/ZnO/ PAL/MoO$_3$/Ag	BDT-2T-ID:PNP	Spin-coated	Hal	150-200	—	M(6)	9.6	White LED	200	76.8	11.7	15	2019	[159]
PEN/ITO/ZnO/ PAL/MoO$_3$/Ag											10.6	14		
PET/ITO/AZO/ PAL/MoO$_3$/Ag	1DTP-ID:PNP	Spin-coated	Hal	150-190	—	M(6)	9.6	White LED	200	≈58.5	9.94	≈17	2019	[160]
Glass/ITO/ZnO/ PAL/MoOx/Ag	PBDB-TSCl:IT-4F	Spin-coated	Hal	—	—	M(10)	58.5	Fluorescent lamp	1000	298.5	37.06	12.42	2020	[161]
									3700	1182.1	169.73	14.36		
	PBDB-TF:IT-4F								1000	298.5	19.48	6.53		
									5000	1607.5	172.69	10.74		

illumination at 200 lux, the module (on a glass substrate) achieved an output power of 11.7 μW·cm^{-2}, corresponding to a PCE ≈15%, and the module on PET achieved an output power of 10.6 μW·cm^{-2}. In related work, the same authors[160] studied similar OPV modules based on the PAL system 1DTP-ID:PNP, which could generate a power of 95.4 μW under a lamp producing 200 lux, corresponding to a PCE of ≈17% and a V_{OC} = 4.05 V. More recently, Park et al.[161] tested a novel polymer donor (PBDB-TSCl), blended with the NFA IT-4F in OPV modules with a total active area of 58.5 cm^2 composed of 10-stripe cells connected in series with the complete structure being glass/ITO/ZnO/PBDB-TSCl:IT-4F/MoOx/Ag. These modules demonstrated a PCE of 12.42% under 1000 lux; a value much greater than the PCE of 6.53% produced by reference modules based on PBDB-TF.

2.2.2. Vacuum-Free (Evaporation-Free) Conditions

Some of the earliest (2009 and 2010) reports of OPV modules processed without vacuum deposition steps (except for the sputtered ITO substrate), were made by Krebs and coworkers.[115,162–164] In 2009, these authors introduced one of the first industrial manufacturing processes in an ambient atmosphere (known as ProcessOne) that was used to create flexible ITO-based OPV modules.[163] ProcessOne uses a roll of PET substrate with a sputtered ITO layer and involves several steps, including the deposition by screen printing of a silver back electrode under ambient conditions. ProcesseOne modules with areas up to 360 cm^2 were reported by the DTU group in 2010,[115] but the corresponding PCEs were low (<2%).

After these early vacuum-free studies, several others have addressed the upscaling of OPV modules using vacuum-free processing[103,107,147,165–177] with strategies used to deposit the top electrodes including spray coating,[165,172] screen-printing,[103,147,166,170,176] rotary screen printing,[169,174] inkjet printing,[166,173] blade-coating,[107,167,175,177] and gravure printing.[168] However, despite all these studies, only a few reported modules displayed PCEs close to or higher than 5.0%.[171,175,176]

In 2016, Berny et al.[103] reported modules, produced under ambient conditions, based on a PBTZT-stat-BDTT-8:PC$_{61}$BM PAL blend with screen-printed top Ag-grid electrodes. Modules composed of 9 serially connected cells patterned using a high precision laser, had a total active area of 114.5 cm^2 and a GFF of 95%. These devices displayed an average PCE of 4.3% and were assembled in solar trees at the Milan Expo in 2015, as illustrated in **Figure 9**.

Laser patterning (fs) was used by Lucera et al.[171] to produce, semi-transparent blade-coated modules (on rigid glass/FTO)
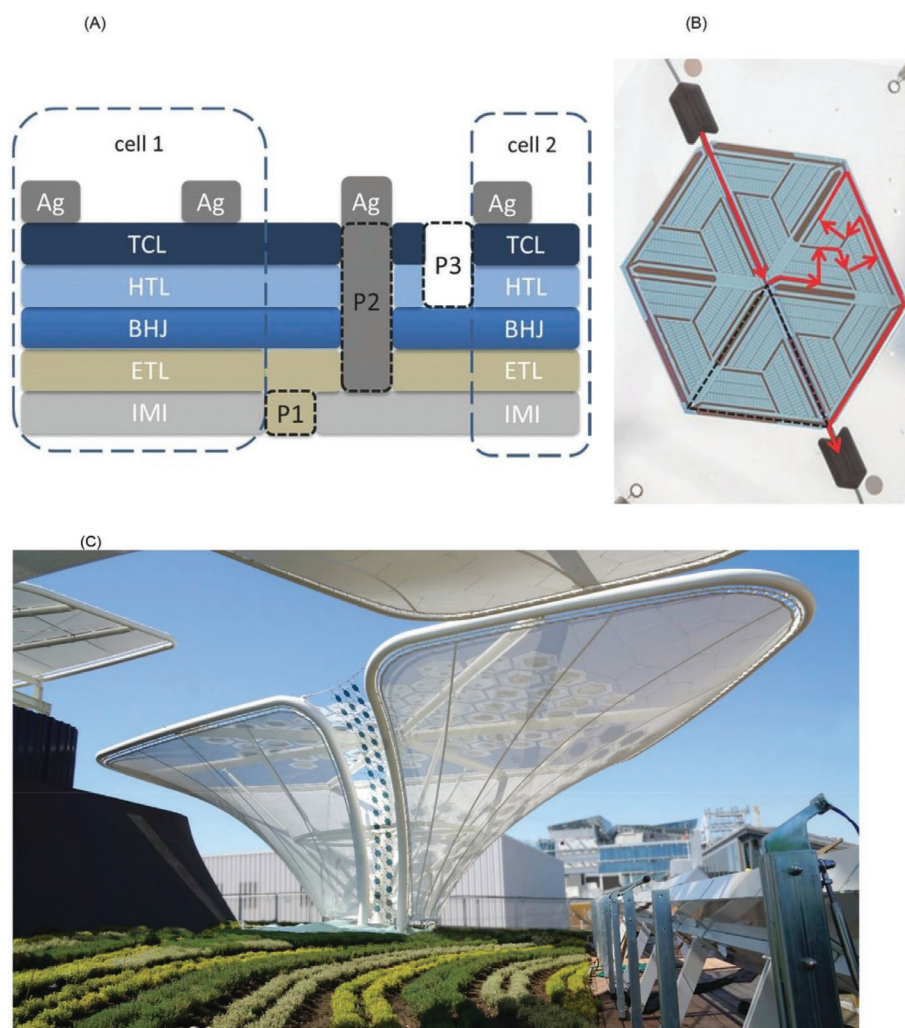
Figure 9. A) Schematic of the module layout. The interconnect P2 is made by laser scribing. The distance between two cells (beginning of P1 to end of P3) is 1 mm. B) Close-up of a small module installed in an EXPO tree. One of the small modules consists of six submodules, each in a triangular shape (dashed line), which are all connected in parallel. One triangular module is made of nine cells, all connected in series. The red arrow symbolizes the current pathway for one distinct triangular submodule from the anode to the cathode. C) large scale deployment of OPV modules in solar trees at the Milan Expo 2015. Reproduced with permission.[103] Copyright 2016, John Wiley & Sons.

and slot-die coated modules (on flexible PET/IMI), based on a PBTZT-stat-BDTT-8:PC$_{61}$BM PAL. The flexible PET/IMI-based modules consisted of 19 individual cells, with a total active area of 68.76 cm^2 (3.61 cm^2 per cell) and achieved a PCE of 4.3%. The rigid glass/FTO-based modules consisted of 30 individual cells, with a total active area of 197.40 cm^2 (6.58 cm^2 per cell) and reached a PCE of 4.8%. Glass-based modules, with GFF > 94% and transparency > 10%, were demonstrated in a BIPV insulating glass window.

Fully blade-coated modules, including AgNW top electrodes and consisting of 12 individual cells monolithically connected in series with a total area of 64.0 cm^2 were developed by Strohm et al.[175] As a PAL, two donor:acceptor combinations were explored (P3HT:PCBM and P3HT:IDTBR) and for modules based on the IDTBR acceptor, both halogenated and non-halogenated solvents were used for the PAL deposition. Laser patterning allowed monolithic interconnection of cells, producing narrow interconnect areas with high precision and good

reproducibility, achieving GFF values of ≈93% for all modules (total active area of 59.52 cm^2). PCBM-based modules delivered a maximum PCE of 2.4% and IDTBR-based modules delivered maximum PCEs of 5.0% and 4.7% when processed from CB and from *o*-methylanisole, respectively.

Han et al.[176] fabricated inverted structure ITO/ZnO/PAL/HTLs/Ag OPV modules by ProcessOne, with devices incorporating screen-printed top Ag electrodes. Modules using bilayer HTLs (WO$_3$/HTL) with 10 cells connected in series and having a total active area of 80 cm^2 achieved an impressive PCE of 5.25%.

3. Upscaling of Indium-Tin-Oxide-Free Cells and Modules

OPVs have evolved around ITO as the front electrode, because of its high transparency, low sheet resistance (8–12 Ω·□$^{-1}$ on

glass substrates) and industry proven reliability. However, ITO presents several problems:

i) ITO is expensive due to the scarcity of indium and due to the vacuum sputtering processing needed in its preparation. Some life cycle analysis studies have concluded that ITO has a substantially negative impact on the EPBT of OPVs;[178–182]
ii) ITO is brittle and not suitable for highly flexible substrates;
iii) ITO processing, especially at higher conductivity, requires high temperature annealing, which is incompatible with plastic-based flexible substrates, such as, polyethylene naphthalate (PEN) and PET.
iv) ITO has a relatively high sheet resistance (typically $> 40\ \Omega \cdot \square^{-1}$ on plastic substrates and $> 8\ \Omega \cdot \square^{-1}$ on glass substrates) which is problematic when fabricating large-area OPVs.

All these shortcomings make the replacement of ITO an important and desirable goal on the pathway to commercially and technically viable OPVs.[183–185] Several strategies have been followed to replace the ITO bottom electrodes either with other transparent conducting electrodes (TCEs) or with opaque electrodes (back illumination). These strategies are summarized in **Figure 10** and include the use of current collecting metal grids, metal nanowires, ultrathin metal films (UTMFs), carbon-based electrodes, and conducting polymer based electrodes as transparent electrodes, as well as, the use of thick metal films as opaque electrodes. Although some recent literature reviews have addressed work to develop ITO-free OPVs,[186–190] their focus was not on large area cells and modules.

The most relevant ITO-free large area OPV cells and modules are described along this section and their performances are indicated in Table S3, Supporting Information, and represented in **Figure 11**.

3.1. Upscaling Using Metal-Based Transparent Conducting Electrodes as Bottom (Front) Electrodes

Metal-based TCEs, have been extensively investigated as potential substitutes for ITO in OPV devices and some reviews on
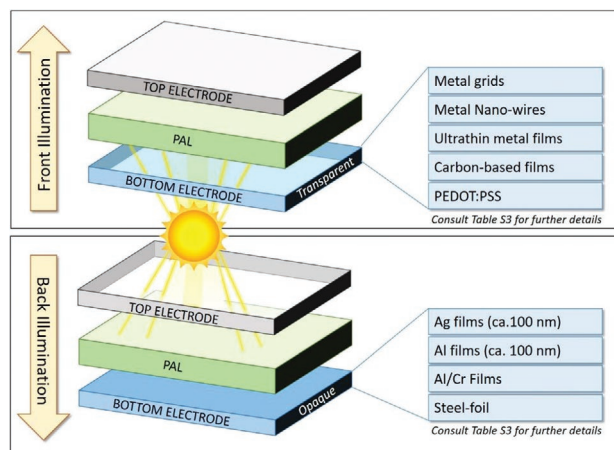

Figure 10. a) Transparent bottom electrodes with front illumination. b) Opaque bottom electrodes with back illumination.
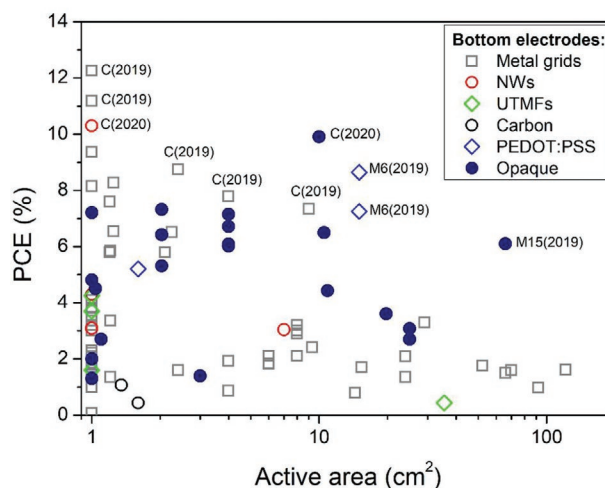

Figure 11. Performance of large area ($\geq 1\ cm^2$) ITO-free devices, cells (C), and modules (Mx, where x is the number of cells), under AM1.5G conditions. The most promising devices have been reported very recently, as indicated inside brackets.

this topic have been published,[191,192] although these were not focused on large area OPVs. Silver (Ag), copper (Cu), and gold (Au) are (in this order), the most highly conductive metals and their use in metal-based TCEs for large area OPV cells and modules has been extensively explored in different forms, including as current collecting metal grids, UTMFs, metal nanowires among others, and is reviewed in this sub-section.

3.1.1. Metal Grids (Meshes) as Transparent Bottom Electrodes

Metal grids can be either positioned above the substrate or embedded into the substrate. A printed grid, with raised topography above the substrate, has the advantage that it only requires one single printing step. As a disadvantage, these electrodes may suffer from high surface roughness, resulting in the possibility of electrical short-circuits between the TCEs and the top electrode. As a way to attenuate this effect, such grids needs to be very thin, however very thin grids needs a certain width to guarantee a good electrical conductivity which leads to a loss in transparency.

An embedded grid has the advantages of creating both a smooth substrate topography and allowing the use of thicker metal grids with a very high aspect ratio (height/width). This results in grids that both have very high conductivity and optical transparency. The disadvantages of this approach are that grid fabrication requires at least two distinct processing steps (thermal imprinting and filling with metal) and an associated lower production speed.

Metal grids can have different geometries, including circular, linear, and hexagonal (honeycomb). The ideal geometry of a current-collecting grid should provide an optimal balance between transparency and conductivity. A higher transparency can be obtained by using thinner lines and a larger pitch size (distance between lines). By contrast, a higher conductivity can be achieved using thicker lines and a smaller pitch size.
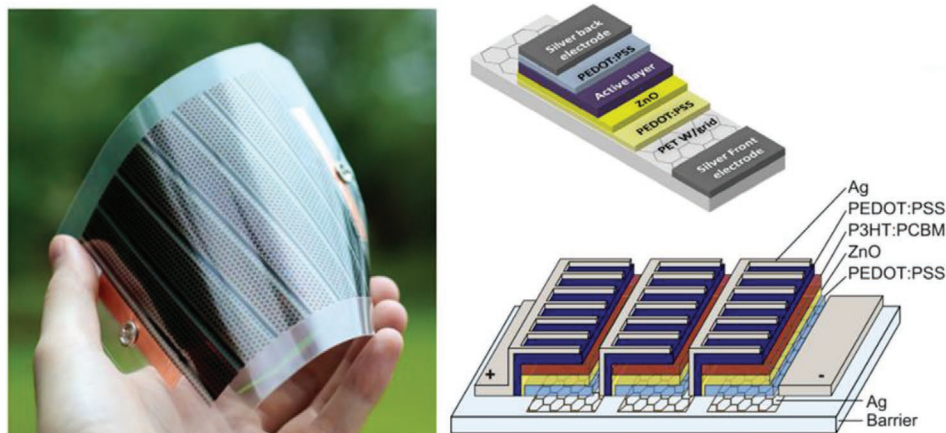
**ADVANCED
SCIENCE NEWS**

www.advancedsciencenews.com

**ADVANCED
ENERGY
MATERIALS**

www.advenergymat.de

Figure 12. Examples of Flextrode-based OPV devices. Reproduced with permission.[201,207] Copyright 2013, Elsevier.

In 2005 Cheknane et al.[193] determined the best theoretical compromise between shadowing effects and series resistance effects, caused by using a metallic grid having a circular geometry. Later, the same author[194] compared circular and linear geometries and concluded that devices with a circular grid should achieve a higher FF and PCE. Similar studies on the best compromise between transparency and conductivity were performed for linear grids by Tvingstedt et al.[195] and later by Galagan et al.[196] In practice, linear and honeycomb grids have been far more popular than the circular grids. A honeycomb pattern has an important advantage over a linear pattern, as line breaks have less impact in overall current collection, since charges can be redirected through alternative paths along the grid.

In one of the first reports on the use of metal grids in OPVs, Kang et al.[197] demonstrated the fabrication via a R2R compatible nano-imprint lithography technique of nano-patterned metal-grid TCEs composed of Ag, Au, and Cu having a thickness of 40 nm. Small cells fabricated using these grids as bottom electrodes achieved a PCE similar to reference ITO-based cells.

Silver, being the most highly conductive metal, has been by far the most studied metal for TCE applications. In 2007, Tvingstedt et al.[195] demonstrated a soft lithographic method for depositing linear grid Ag electrodes. The best theoretical compromise between transparency and conductivity was determined as a function of pitch size. Silver grid-covered substrates were coated with the highly conductive polymer DEG-PEDOT:PSS to reduce surface roughness and associated risk of short circuits. The small cells fabricated achieved a PCE comparable to ITO-based devices.

Frederik Krebs at DTU and his coworkers have been a leading group in the development of high throughput R2R mass-production methods for large area OPV cells and modules. These authors have developed an extensive and important body of work on the R2R upscaling of OPVs based on Ag-grid TCEs. Part of this work focused on the standard P3HT:PCBM PAL system[198–209] and addressed issues such as: i) Printing/deposition of the silver grid bottom (front) electrodes using techniques, such as, thermal imprinting, inkjet printing, flexographic printing, and photonic sintering;[198–200]

ii) the printing of the top (back) electrodes using techniques such as flatbed screen printing, rotary screen printing, inkjet printing, and flexographic printing;[201–203] iii) the fabrication of tandem devices where the entire layer stack was prepared by printing or coating, that is, without vacuum;[204] iv) the optimization of the slot-die coated PAL morphology with additives;[205] and v) round-robin inter-laboratory device reproducibility.[206]

In 2013, Krebs et al.[208] introduced a new candidate for the replacement of ITO-based substrates; the flextrode. Flextrode substrates, or flextrodes, are made of a highly conducting Ag grid flexographically printed on a PET substrate and have the structure PET/Ag-grid/PEDOT:PSS/ZnO (see **Figure 12**). Flextrodes exhibit a sheet resistance of $\approx$10 $\Omega \cdot \square^{-1}$ and an optical transmittance over the visible region of $\approx$60%, with their electrical and optical properties being studied in detail.[210] Since their introduction, flextrodes have been used by Krebs and coworkers in a large number of upscaling studies and currently, flextrodes are commercialized by the company InfinityPV, a spin-off from DTU.[211]

Using flextrode bottom electrodes and screen printed top Ag-grid electrodes, Krebs et al.[207] described the all-solution processing of ITO-free OPV modules, and named this process as IOne, as opposed to the ITO-based ProcessOne as described in Section 2.

Krebs and coworkers have also applied high throughput R2R mass-production methods to fabricate OPV devices based on PAL systems other than the classical P3HT:PCBM[209,212–221] and addressed issues such as: i) Use of new polymer donors[209,212–216] and new small molecule donors[217] with PCBM; ii) testing of fullerene-free systems;[218,219] iii) PAL morphology optimization with additives;[220] and iv) tandem devices.[214,221]

Upscaling work on ITO-free OPV devices based on Ag-grid bottom electrodes has also been explored by other groups,[78,92,101,222–231] either using a P3HT:PCBM PAL[78,222–225] or other PALs.[78,92,101,225–231] Most of this work focused on the optimization of the Ag-grid electrodes including grid geometry (honeycomb, linear),[222] the height and width of grid lines and busbars,[223] grid pitch,[228] and the properties of PEDOT.[224,229] Other work was more focused on the use of new PALs in Ag-grid based OPVs,[92,230,231] including fullerene-free systems.[231]

ADVANCED
SCIENCE NEWS
www.advancedsciencenews.com

ADVANCED
ENERGY
MATERIALS
www.advenergymat.de

Jin et al.[228] prepared fully printed Ag-grid/PEDOT:PSS TCEs with different grid pitches (GP = 1, 2, and 4 mm). All these TCEs exhibited a high optical transmittance ($T_{550nm} \approx 90\%$), low surface roughness (rmsr ≈ 1 nm), high flexibility (bending radius of ≈1 mm) with R_{sheet} varying between ≈4 $\Omega \cdot \square^{-1}$ (GP = 1 mm) and ≈20 $\Omega \cdot \square^{-1}$ (GP = 4 mm). Flexible OPVs based on TCE-GP of 1 mm with an active area of 2.10 cm^2 and based on a PTB7:PC$_{71}$BM PAL, exhibited a relatively high PCE of 5.79%; a value higher than reference devices with same size based on ITO (3.85%).[228] Lu et al. used the additives 5% DMSO and 0.1% fluoro-surfactant Capstone FS-31, v/v[229] to improve the conductivity and the wettability of PEDOT:PSS on a PET substrate. Devices based on a PTB7-Th:PC$_{71}$BM PAL with active area of 2.25 cm^2 and with different Ag patterns exhibited very similar PCEs (max of 6.51%) suggesting that it is the cover ratio rather than the shape of the patterns that has stronger influence on device performance. Zhang et al.[92] reported cells with Ag-grid bottom electrodes and a ternary PAL blend of PTB7-Th:p-DTS(FBTTH$_2$)$_2$):PC$_{71}$BM, with active area of 1.25 cm^2 and achieved an impressive PCE of 8.28%. This is one of the highest efficiencies reported so far for OPV devices based on Ag-grid bottom electrodes with an active area ≥1 cm^2. OPV cells based on the ternary PAL blend PAL PffBT4T-2OD:PC$_{61}$BM:PC$_{71}$BM, with active area ≈1.2 cm^2 and the structure PET/Ag-mesh/PEDOT:PSS/ZnO/PAL/top-electrode were reported by Czolk et al.[101] Here, a mixture of AgNWs:PEDOT:PSS and evaporated MoOx/Ag were tested as top electrodes with corresponding average PCEs reported of 5.8% and 7.6%, respectively. Helgesen et al.[230] upscaled the synthesis of the polymer PBDTTTz-4 from milligram to gram scale by applying continuous flow synthesis. This was then blended with PCBM and used in roll coated cells and modules with Ag-grid/PEDOT:PSS bottom electrodes. Modules, consisting of 16 cells connected in series with a total active area of 29 cm^2 exhibited an average PCE of 3.3%.[230] Fan et al.[231] reported fullerene-free cells based on a PAL of PM6:IDIC and with Ag-grid bottom electrodes. Devices with an active area of 1.25 cm^2 exhibited a PCE of 6.54%.

OPV studies based on TCEs with other metal grids, such as, Cu grids or multi-metal grids are much rarer. However, TCEs based on Cu meshes have been studied due to their very low cost. For instance, copper nanoparticle inks have been reported as being six times cheaper than Ag nanoparticle inks, and this could further reduce the fabrication cost of OPV devices. Cu is well suited for OPV applications due to its much lower cost and similar work function to ITO (≈4.7 eV). Although Cu grids have been tested in small area (<1 cm^2) OPVs,[232–234] no reports are known of its application in larger areas (>1 cm^2).

Multi-metal grids have been also explored.[235–238] Choi et al.[235] developed embedded Cu/Au metal grids consisting of an Au grid-layer on top of an electroplated copper grid-layer on a flexible SU8 polymer substrate. Using this, OPVs cells based on a P3HT:ICBA PAL with an active area of 9.3 cm^2 exhibited a PCE of ≈2.4%.

Sputtered tri-layer Mo/Al/Mo (MAM) grids have been explored as bottom TCEs in large area OPV devices.[236,237] Galagan et al.[236] studied the relationship between the resistance of MAM grids, the size of the OPV cells (active areas from 2.4 to 14.4 cm^2) and their PCE using P3HT:PCBM based devices. Here, an observed PCE drop (1.6% to 0.8%) was observed when scaling up devices from 2.4 to 14.4 cm^2 and was found to depend both on the metal-grid sheet resistance (R_S) and on the light intensity. Interestingly, for a R_S of 9.64 $\Omega \cdot \square^{-1}$, a PCE drop of 75% was found at 1 Sun illumination, with this reducing to only 25% at 0.13 Sun, indicating that for indoor applications, scaling up the OPV cell dimensions has a much less effect on PCE. Mo/Al/Mo metal grids have also been used by Eggenhuisen et al.[237] to produce modules with a total active area of 92 cm^2. However, these modules achieved a very low PCE of 0.98%.

More recently, Han et al.[238] reported Ag/Cu grid TCEs having a honeycomb structure and very low sheet resistance <1 $\Omega \cdot \square^{-1}$ with high average transparency (84%). The grids developed were 3 µm in width and 3 µm in depth and were almost completely embedded in the PET substrate and only covered ≈3% of the substrate (see **Figure 13**). Such grids were surface planarized using highly conductive PEDOT:PSS (E100) and then tested in large area OPV cells. The highest efficiency cells, (having an active area of 1.0 cm^2) utilized a PAL of NF3000-P:NF3000-N and a CIL of ZnO/zirconium-acetylacetonate (ZrAcac) and achieved a very impressive PCE of 12.26% (certificated PCE of 11.45%). This is currently a performance record for large area ITO-free devices. Such TCEs were also tested in larger area devices with an impressive PCE of 8.75, 7.79, and 7.35% attained for active areas of 2.4, 4, and 9 cm^2, respectively.
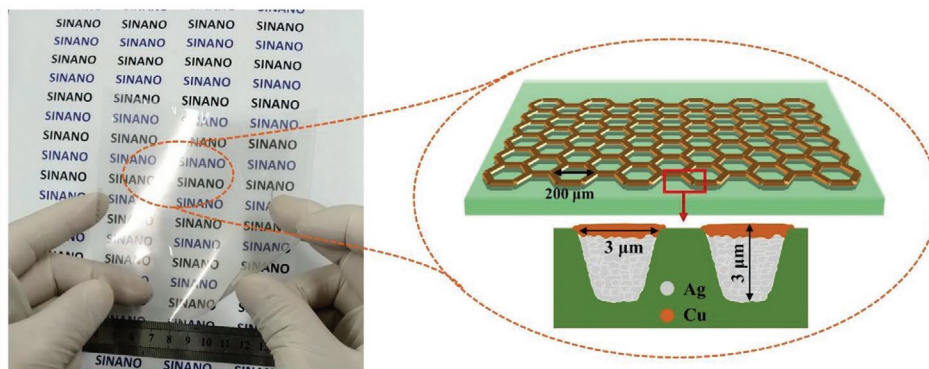

Figure 13. Photograph and the schematic diagram of the large-area PET/Ag/Cu electrode. Reproduced with permission.[238] Copyright 2019, John Wiley & Sons.

3.1.2. Metal Nanowires as Transparent Bottom Electrodes

Metal nanowires (NWs), and particularly silver and copper nanowires (AgNWs and CuNWs), have been investigated as promising alternatives for ITO-based electrodes. TCEs based on AgNWs that were around 8.7 μm long and 100 nm diameter, were first demonstrated in 2008, in a seminal work by Peumans and coworkers,[239] and their scalability has been demonstrated by the same authors in 2010.[240] Since then, a significant number of studies have addressed the use of transparent AgNWs-based bottom electrodes in OPVs, although the majority of these studies were limited to small area devices (<1 cm^2)[241–246] and are the subject of previous reviews.[191,247,248] The reports of large area OPVs based on AgNWs bottom electrodes are still very scarce in literature.[102,249–252]

The DTU group[249] rotary screen printed AgNW-based TCEs covered with ZnO, displaying a transmittance ≈84% over the spectral range 550–800 nm and had a R_S of 10–20 Ω·□$^{-1}$. OPV cells based on these bottom TCEs with active area of 1.0 cm^2 and structure PET/AgNW/ZnO/PAL/PEDOT:PSS/Ag-grid were fabricated using different polymer:PCBM PALs. The highest efficiency devices were based on a PAL blend of PBDTTTz-4:PCBM and achieved a PCE of 3.30%.[249] Fully inkjet printed OPV cells, with AgNW bottom and top electrodes and with active area of 1.0 cm^2 were demonstrated by Maisch et al.[250] who achieved a PCE of 4.3% based on a PV2000:PC$_{71}$BM PAL. Zhao et al.[102] used AgNW-based TCEs, deposited on PET substrates using slot-die printing to produce OPV cells having the structure PET/AgNWs/ZnO/PAL/MoOx/Ag with an active area of 7 cm^2 where the PAL was a PPDT2FBT:PC$_{71}$BM blend. These cells achieved a PCE of 3.04% when the PAL was coated on substrate at 40 °C. Very recently, Sun et al.[252] reported all-solution processed OPV cells with the structure AgNWs@PI/ZnO/PBDB-T-2F:IDIC:Y6/HXMoO3/PEDOT:PSS/AgNWs having an active area of 1.0 cm^2 which reached a PCE of 10.3%. This represents one of the highest efficiencies ever reported for OPV devices based on AgNWs bottom electrodes.

Although AgNW-based bottom electrodes exhibit a good balance between conductivity and transmittance and are amenable to R2R processing, some stability issues have been reported. The electrical conductivity of AgNWs degrades under simultaneous presence of high humidity and high temperature,[253] under electrical stress[253,254] and under UV-light exposure.[255] Another disadvantage of AgNWs lies in the occurrence of short circuits (shunting) due to inter-electrode penetration.[241]

Despite several reports on the application of copper nanowires (CuNWs) in TCEs,[256,257] the few literature studies that report their use as bottom electrodes in OPVs are limited to small area devices.[258,259] No literature studies are known on large area (≥1 cm^2) OPV devices with CuNW-based electrodes.

3.1.3. Ultrathin Metal Films as Transparent Bottom Electrodes

UTMFs are continuous metallic films, typically with thickness <10 nm, that have a high transmittance and exhibit a low sheet resistance. UTMFs possess high compatibility with organic semiconductor materials and are very flexible due to their low thickness and high mechanical ductility. UTMFs are scalable to large areas and, compared to metallic grids, have the advantage that they do not require any patterning processes. However, the growth of UTMFs follows the Volmer–Weber mechanism, resulting in a rough and discontinuous morphology with poor optoelectronic properties due to poor adhesion to substrates. Different strategies have been developed for preparing ultrasmooth UTMFs with superior transmittance and conductivity by successfully suppressing the Volmer–Weber mechanism. Addressing these strategies is outside the scope of this review and interested readers are referred to a recent comprehensive review on this topic.[260]

In 2012, the DTU group[261] demonstrated fully solution processed semi-transparent Ag-based UTMF electrodes (thickness < 20 nm) spin-coated on flexible PET substrates from diluted Ag-inks. These electrodes had a sheet resistance as low as 5 Ω·□$^{-1}$ and transmittance of ≈30% at 550 nm and were tested in OPVs devices based on a P3HT:PCBM PAL. Devices with an active area of 1 cm^2 and R2R processed modules with an active area of 35.5 cm^2 exhibited PCEs of ≈1.6% and ≈0.44%, respectively.[261] Stec et al.[262] produced 8 nm thick Cu, Ag, Au, and Cu/Ag UTMF bilayer electrodes on flexible chemically surface modified PET and PEN substrates. OPV devices employing 8 nm Ag and Au electrodes, based on the PAL PCDTBT:PC$_{71}$BM and with an active area of 1 cm^2, achieved PCEs of 3.7% (Ag) and 4.25% (Au) comparable to the PCE of 4.10% for ITO-based reference devices. The UTMFs however were more resistant to repeated bending.

3.2. Upscaling Using Carbon-Based Transparent Conducting Electrodes as Bottom Electrodes

Studies on the application of carbon-based TCEs in large area OPV cells and modules have focused on the use of carbon nanotube (CNT)-based and graphene-based electrodes, and these are briefly reviewed in this sub-section.

3.2.1. Carbon Nanotubes-Based Transparent Conducting Electrodes

CNTs have some outstanding properties such as high electrical conductivity and excellent mechanical and thermal properties that make them attractive for electrode applications in OPV devices. However, most of these properties are along their axial direction, that is, highly anisotropic, which makes their industrial application very challenging.

The first application of CNT-based bottom TCE as a replacement of the ITO electrode in OPVs, was reported in 2005 by Du Pasquier et al.[263] in a small area device that achieved a PCE of ≈1%. Since then, a considerable number of studies have tested the use of CNTs as bottom TCE in OPVs and these studies have been discussed in a large number of reviews broadly related with the use of CNTs in thin film TCEs and the application of these TCEs in OPV devices.[264–272]

While some progress has been made regarding the application of CNT-based TCEs in OPVs,[273] this research topic is still on its infancy, due to the complexities involved, and no literature studies are known on large area (>1 cm^2) OPVs using CNT-based TCEs.

3.2.2. Graphene-Based Transparent Conducting Electrodes

Graphene combines a good optical transmittance, electrical conductivity, chemical stability, and flexibility making it a very attractive material for electrode applications.[274,275] The first example application of graphene-based bottom TCE in small area OPVs was reported by Peumans and coworkers in 2008.[276] Since then, the application of graphene in TCEs and of these TCEs as bottom electrode in OPV devices has been extensively investigated as described in several literature reviews.[270,271,277–286] However, despite all the progress achieved, the majority of the most important studies focus on small area OPV devices.[287–290] Reports of OPV devices based on graphene bottom electrodes and with large active area (≥ 1 cm^2) are still very scarce in the literature[291,292] and these are briefly described below.

Konios et al.[291] developed a laser-based patterning technique, compatible with plastic substrates, for the production of reduced graphene oxide micromesh (rGOMM) electrodes over large areas. This technique was used to increase the transparency of reduced graphene oxide films from ≈20% to up to ≈85%, with only a minor increase in the respective sheet resistance value. These rGOMM electrodes were tested in OPV cells with area of 1.35 cm^2, based on PCDTBT:PC$_{71}$BM active layers, and exhibited an average PCE of 1.07% compared with 1.38% for a similar ITO-based reference device.

More recently, La Notte et al.[292] prepared a 4-layer (4L) graphene electrode doped with SOCl$_2$ by chemical vapor deposition and transferred it to glass. This was then used as cathode in OPV devices having an inverted structure. The 4L-graphene electrode had a transmittance value of 88.1% at 550 nm and a sheet resistance R_s of 30 $\Omega \cdot \square^{-1}$. Devices were prepared with the structure: Glass/graphene/PEDOT:PSS/ZnO/PEIE/PffBT4T-2OD:PC$_{71}$BM/V$_2$O$_5$/Ag. A mini-module composed of 3 cells, based on the 4L-graphene electrode, and with total active area of 1.6 cm^2 exhibited a PCE of 0.44% (**Figure 14**).

3.3. Upscaling Using Conducting Polymer Transparent Conducting Electrodes as Bottom Electrodes

PEDOT:PSS is an electrically conductive complex of poly(3,4-ethylenedioxythiophene) (PEDOT) and poly(4-styrenesulfonate) (PSS) where the PSS works as a dispersion agent in aqueous medium.[293] PEDOT:PSS electrodes have been tested as potential substitute for the ITO electrode in OPVs.[294]

In 2004, Aernouts et al.[295] made the first reports of the use of a highly conductive PEDOT:PSS anode as a potential substitute for ITO in OPV devices. Other studies have then followed using small area devices.[296–300] Due to the relatively large optical absorption coefficient of PEDOT:PSS, PEDOT:PSS films need to have a thickness below 100 nm to maintain a high transmittance. This significantly raises the sheet resistance of the electrodes limiting the application potential of pure PEDOT:PSS-based devices.

In a 2019 study, Wang et al.[301] prepared TCEs based on high conductivity PEDOT:PSS PH 1000 on ultrathin (100 µm-thick) flexible glass substrates, with optimized TCEs exhibiting a R_S of ≈30 $\Omega \cdot \square^{-1}$ and a transmittance of ≈77% at 550 nm, with a broad transparency window observed between 300 and 800 nm. OPV cells with active area 1.6 cm^2 and with the structure glass/PEDOT:PSS PH1000/MoOx/BQR:PC$_{71}$BM/Ca/Al achieved a PCE of 5.2% (compared to 8.0% for devices with small area of 0.2 cm^2). Also in 2019, Meng et al.[68] produced flexible modules composed of 6 cells with a total active area of 15 cm^2 having the structure PET/hc-PEDOT:PSS/ZnO/PAL/MoO$_3$/Ag, where the high conductivity (hc-) PEDOT:PSS, the ZnO, and the PAL were slot-die-coated. Modules prepared with the PAL blends PTB7-Th:PC$_{71}$BM and PBDB-T:ITIC achieved average/maximum PCEs of 7.25/7.58% and 8.64/8.90%, respectively. These represent the highest efficiency values reported so far for large area OPVs based on PEDOT:PSS bottom electrodes.

3.4. Upscaling Using Opaque Bottom Electrodes with Top (backside) Illumination

A different strategy for the replacement of ITO as the bottom electrode consists in using opaque bottom electrodes and illuminating the devices from the top (backside).

In 2009 Frederik Krebs[302] reported on the use of opaque bottom electrodes made of Cu(50 µm)/Ti (100 nm) in large area modules illuminated from top. This strategy has since been followed by others[36,100,303–316] and the list of opaque electrodes tested includes mostly thick (typically ≈100 nm) silver[36,100,303–310] and aluminum films[311–313] among others.[314–316]

In 2015, Huang et al.[100] reported top-illuminated single cells with an active area of 1 cm^2 and with a thick (100 nm) opaque Ag bottom electrode exhibiting a PCE of 7.21%, based on a
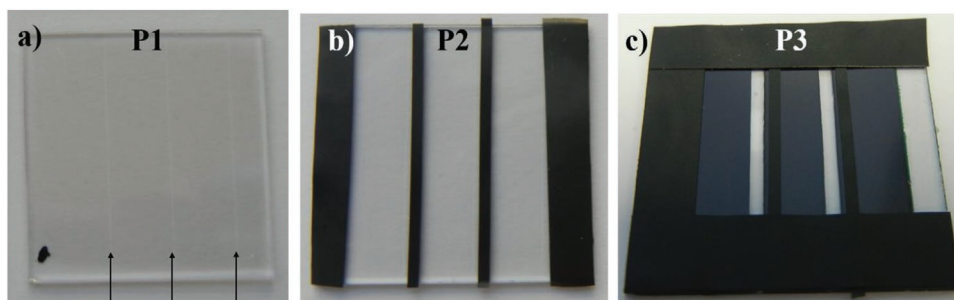

Figure 14. Photo of the graphene sample at each patterning step: a) P1 by laser scribing, b) P2 by shadow mask, and c) P3 by shadow mask. Reproduced with permission.[292] Copyright 2018, Elsevier.

ADVANCED
SCIENCE NEWS
www.advancedsciencenews.com

ADVANCED
ENERGY
MATERIALS
www.advenergymat.de

PBDTT-F-TT:PC$_{71}$BM PAL. The cells had the inverted architecture glass/thick-Ag/FPI-PEIE/PAL/MoO$_3$/UTMF-Ag/TeO$_2$, where "MoO$_3$/UTMF-Ag/TeO$_2$" is a UTMF-based microcavity semi-transparent top-electrode that allows for efficient light in-coupling. This PCE was considerably higher than the PCE of reference ITO-based inverted cells (5.70%). In the same year, Zuo et al.[304] reported OPV cells with an active area of 4 cm^2 using an opaque 100 nm thick Ag film (on glass or PET) as bottom electrode, and ultrathin thickness-gradient Ag TCE as top electrode. Devices based on a PTB7-Th:PC$_{71}$BM PAL achieved PCEs of 7.15% and 7.09% on glass and PET substrates respectively. Later, the same authors[305] produced similar cells with opaque Ag bottom electrodes which were also based on a PTB7-Th:PC$_{71}$BM PAL, but where the ultrathin thickness-gradient Ag top electrode was replaced by a triangular shaped Ag-grid. The 4 cm^2 cells on glass substrates achieved a PCE of 6.93%. Mao et al.[36] reported 10.5 cm^2 active area flexible tandem cells using an opaque Ag film (80 nm) as bottom electrode. Cells using two different PALs, namely PAL1 = P3HT:ICBA and PAL2 = PTB7-Th:PC$_{61}$BM, yielded maximum PCE values of 6.50%. Compared to single junction cells, tandem cells are less susceptible to parasitic area upscaling effects and exhibit a superior tolerance to defects. Producing tandem cells, the authors demonstrated that a toy electric car could be powered to run under sunlight[317] (**Figure 15**). Opaque Ag films covered with TiOx were used by Lin et al.[307,308] to produce OPV cells with an active area of 2.03 cm^2. Cells based on a blade-coated PTB7-Th:ITIC PAL achieved a PCE of 7.60%[307] and cells based on a blade-coated all-polymer PAL (PTB7-Th:PNDI-T10) achieved a maximum PCE of 6.65%.[308] Very recently, Jiang et al.[310] demonstrated the growth of a very smooth Ag layer (rms = 1.06 nm) with a thickness of 70 nm (opaque) on top of a chemically reactive hydrogen molybdenum bronze (HxMoO$_3$) surface. Top-illuminated 10 cm^2 NFA-based OPV cells with structure glass/HxMoO$_3$/opaque Ag (70 nm)/PAL/HxMoO$_3$/ultrathin Ag (8 nm)/MoO$_3$, where the PAL consisted of PM6:IT-4F, achieved an impressive PCE of 10.24%.[310]

Using an opaque Al film (100 nm thick) as bottom electrode, Ibraikulov et al.[313] produced modules of 15 monolithic cells connected in series, based on a blade-coated PAL of PF2:PC$_{71}$BM, with an impressive total active area of 66 cm^2 (GFF = 69%) that achieved a PCE of 6.1%.
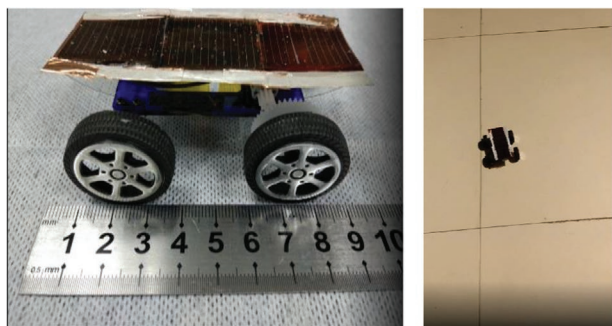

Figure 15. Frames from a movie showing a toy electric car being powered to run under sunlight. It uses a flexible tandem OPV with structure PES/Ag/PEI/PAL1/m-PEDOT:PSS/PEI/PAL2/ hc-PEDOT:PSS/Ag-grid. The movie, from the work of Mao et al.,[36] can be found in the URL at ref. [317]. Reproduced with permission.[36] Copyright 2017, Royal Society of Chemistry.

4. Encapsulation and Stability Testing of Large Area Devices

OPV devices will only become a commercial success if they can have both a high PCE and exhibit long-term stability at a reasonable price. After rapid recent improvements observed in PCE, increasing the operational lifetime of OPV devices has become particularly important for practical applications.

Important advances in the stability of OPV devices have been made recently. Du et al.[318] reported small area OPV cells exhibiting a PCE of ≈8% along with an extrapolated operational lifetime approaching 10 years. Xu et al.[319] demonstrated small area OPV cells with a PCE of 10% combined with an extrapolated potential lifetime of 22 years, based on an estimated absorbed optical energy dose. Despite these significant improvements on the lifetime of small area OPVs, the lifetime of large area OPVs, which indirectly determine the EPBT is still poor compared to the 25 years that inorganic silicon-based solar cells can last. Therefore, significant improvements still need to be made in terms of stability to make OPV technology attractive for mass production and commercialization.

The factors that contribute to the reduction in operational efficiency of OPV cells and modules over time are several and have been clearly identified.[320–329] Degradation factors that are common to all OPV devices include: photochemical and photophysical degradation of the active layer materials and interfaces;[330–332] morphological degradation[333,334] due to high thermal stress under operation; as well as, a series of degradation events that can be initiated by the ingress of H$_2$O and O$_2$ in poorly sealed devices.[335–337] Additionally, there are some degradation factors specific to OPV modules, including electrical stress[338] and degradation at the cell interconnections. A detailed description of all these degradation factors and corresponding mechanisms is beyond the scope of this review, and the interested readers are directed to some existing reviews on this topic.[320–329]

Some strategies to improve the stability of OPV cells and modules have focused on improving the intrinsic stability of the materials and interfaces. For example, chemical modification of polymer donors, either modification of backbone or side chains, has proved effective to improve the stability of OPV devices.[212,339,340] An increase in the polymer molecular weight[341–343] and in polymer regioregularity[333] have also been shown to produce more stable devices. NFA-based OPVs, have been demonstrated to exhibit, in general, considerably higher thermal and photochemical stability than the corresponding fullerene based OPVs.[82,218,344–347] Also, among NFAs, end-group and side-chain modifications have shown to strongly influence both device photo-stability and morphological stability.[318] Therefore, in outdoor conditions and especially in tropical regions where high stability at elevated temperature is crucially important, replacing fullerene by NFAs is a promising strategy to extend the device lifetime up to the commercial requirements. Ternary blending of the PAL through the addition of compatibilizers with light harvesting properties[94,348–351] has proved to be a powerful strategy to improve the morphological stability of the PAL with an associated increase in the lifetime of OPVs which is often also with associated enhancements in PCE. Replacement of the PEDOT:PSS HTL

either by thin films of solution-processed molybdenum oxide (MoOx)[352] or by a thin V_2O_5 layer;[353] the plasma treatment of interfacial layers;[354] the replacement of the front and back electrodes;[251,355] as well as, the choice of more favorable device architectures[355–358] has also been used successfully to improve the OPVs lifetime. UV-blocking filters that can attenuate most UV photons below 400 nm have also proved successful in extending lifetime.[359] Other strategies have focused on preventing the ingress of H_2O and O_2 through encapsulation of the devices (extrinsic stability).[339,358,360–367] However, most of these strategies have either been applied only to small area devices (<1 cm^2) or, when applied to larger areas, have resulted in devices with relatively modest lifetimes (<<1 year).

In this section we present and discuss the most relevant stability studies performed on large area (≥1 cm^2) OPV cells and modules. It should be noted that the vast majority of these studies focus on devices based on P3HT:PC$_{61}$BM blends, chosen primarily because of the commercial availability of P3HT and PC$_{61}$BM in the quantities required for large scale production and at a reasonable price. Also, for these reasons, the majority of such studies focus on mitigating extrinsic degradation factors (H_2O and O_2) through the development of different encapsulation strategies, rather than on improving the intrinsic stability of the devices. Although the P3HT:PC$_{61}$BM system has promising stability, the corresponding devices exhibit a PCE well below the commercial requirements (maximum small area PCE ≈5%) and therefore, the interest in this system is currently purely academic.

4.1. Stability Testing and Encapsulation

OPV devices typically suffer an initial period of faster reduction in their PCE, known as the "burn-in" period, after which a much slower and typically linear reduction of PCE occurs with time (**Figure 16**a). Two different lifetime parameters, namely T_{80} and T_{s80}, are typically used to quantify the operational lifetime of OPV devices.[358,368,369] The T_{80} lifetime is the time it takes for the PCE of the cell or module to decrease to 80% of its very initial value. The T_{s80} lifetime is defined as the time needed for the PCE of the device to decrease to 80% of its value at the end of the burn-in period. Interestingly, recent studies have shown that NFA-based OPVs may not have a burn-in period.[347]

Until 2010 there were no specific standards for OPV lifetime testing and the standard IEC61646, originally created for amorphous silicon thin film solar cells was often used. However, as the degradation mechanisms of silicon based PVs and OPVs are different, an International Summit on Organic solar cell Stability (ISOS) in 2011 established a set of guidelines to allow ready comparison of data obtained by different laboratories.[370] Five main testing protocols were created with each protocol containing three levels of complexity, named levels 1, 2, and 3, corresponding respectively to "Basic," "Intermediate," and "Advanced." The five protocols created were: i) Dark tests (ISOS-D-1; ISOS-D-2; and ISOS-D-3); ii) Outdoor tests (ISOS-O-1; ISOS-O-2; and ISOS-O-3); iii) Laboratory weathering tests (ISOS-L-1; ISOS-L-2; and ISOS-L-3); iv) Thermal cycling tests (ISOS-T-1; ISOS-T-2; and ISOS-T-3) and v) Solar-thermal-humidity cycling tests (ISOS-LT-1; ISOS-LT-2; and ISOS-LT-3). More details about these

testing protocols can be found in the literature.[370] ISOS-T and ISOS-LT tests are rarely used due to their complexity and low stability of most OPVs under such harsh conditions. In the following discussion, particular emphasis is placed on the results from outdoor stability tests (ISOS-O) as these most closely represent operation under real conditions.

A novel OPV lifetime diagram (entitled o-diagram), see Figure 16b, was proposed by Krebs and coworkers for comparing lifetimes of different OPV technologies and/or different test conditions.[371] O-diagrams plot the initial device performance versus the T_{80} values in a Log4 scale (units of days); base 4 is used since it allows the scale to be associated with common time units (hours, days, months, seasons, years).

OPVs degrade in ambient air mostly because of moisture and oxygen, and therefore OPV cells are usually fabricated inside a glove box and are encapsulated before exposure to ambient air. The most common encapsulation method sandwiches the OPV device between two or more barrier films whose edges are glued together with a sealant. In the encapsulation of OPVs, barrier films and sealants with low water vapor transmission rate (WVTR ≈ 10^{-6} gm^{-2}day^{-1}) and low oxygen transmission rate (≈10^{-3} cm^{3}m^{-2}day^{-1}) need to be used to improve lifetime[364] and a certain edge sealing distance between the barrier film edge and the OPV edge should be left to avoid O_2 and H_2O edge ingress. Although sealants can be pressure sensitive, hot-melt, or UV curable epoxy-based adhesives, a study suggests that UV curable epoxy-based adhesives are the most effective.[373]

Rigid glass panels are the most hermetic barriers films known for OPVs, where OPV cells and modules can be sandwiched in between two panels.[374] Large area rigid glass-glass encapsulation can be used for example in building integrated OPV products, such as, glass facades.[375] In the most common encapsulation method, large area devices are laminated between films of cross-linkable ethylene vinyl acetate in vacuum, under compression and up to 150 °C, which requires the PAL to be stable for ≈2 h at 150 °C to ensure glass sealing.[103,376] However, recent progress in laser assisted glass sealing will likely soon make this compression method obsolete, as it can guarantee the hermetic glass sealing at a process temperature <80 °C. Although glass encapsulation using laser-assisted glass-frit sealing has been much studied to seal other related photovoltaic technologies, such as large area dye sensitized solar cells (DSSC)[377] and perovskite[378] solar cells, no studies are currently known in literature on the use of this technology to glass seal large area OPVs. Furthermore, the use of ultrathin flexible glass substrates on OPVs, compatible with R2R processing, is still very limited.[379,380] Despite encapsulation being known to play a decisive role in increasing the stability of OPV devices,[381] limited information is usually provided about the encapsulation procedures. An analysis of literature data on rigid (front and back glass) and flexible (mostly PET foils) encapsulated devices have shown that device lifetime is mostly limited by the quality of the edge sealing and not by the water vapor or oxygen permeability of the barrier films (glass and PET).[382] Solving the problem of efficient edge sealing has been highlighted as a crucial step toward improving the lifetime of devices.[374,382,383]

Several other materials have been tested as effective encapsulation barrier layers to inhibit atmosphere-induced degradation. These include graphene oxide based barrier films,[384] ultra-thin
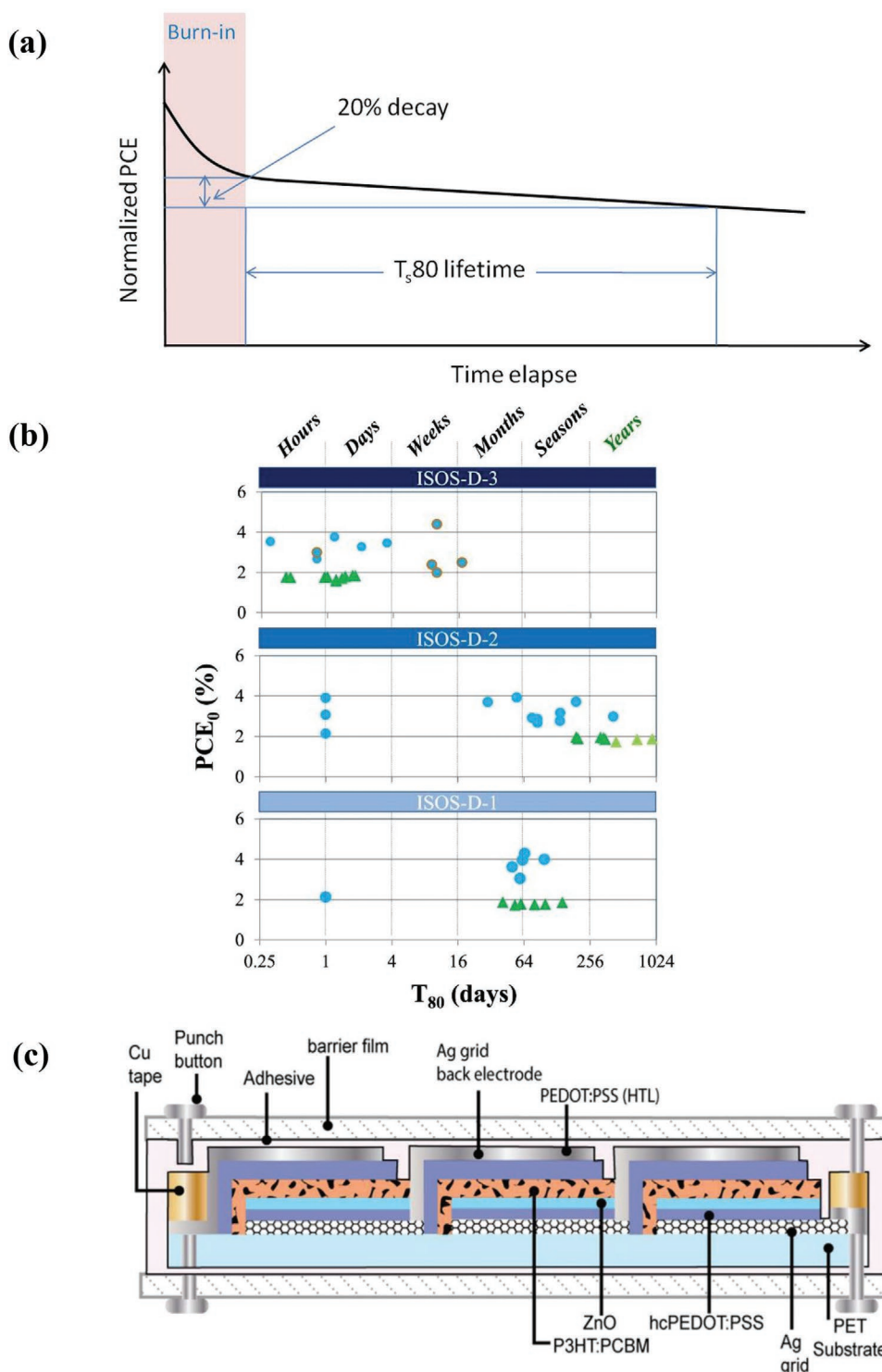
Figure 16. a) Typical degradation behavior of an OPV device. Reproduced with permission.[368] Copyright 2018, John Wiley & Sons. b) Lifetime diagram for intercomparison of lifetime of different OPV devices. X axes present logarithmic function with base 4, which is associated with the time unites shown above the plot. Y axes represent the PCE of the device at the T_0 point, from where T_{80} was calculated. Reproduced with permission.[371] Copyright 2015, John Wiley & Sons; c) Encapsulation scheme of the ITO-free IOne modules. Reproduced with permission.[372] Copyright 2011, Elsevier.

AlOx layers deposited by ALD,[385] multilayer stacks of MgF_2/MoO_3,[386] ZnO/UV-resin,[387] among others. However, all of these strategies[384–387] have been so far limited to small area devices (<1 cm²).

**ADVANCED
SCIENCE NEWS**

www.advancedsciencenews.com

**ADVANCED
ENERGY
MATERIALS**

www.advenergymat.de

4.2. Stability of Large Area Cells and Modules

This sub-section reviews the most relevant studies on the stability performed of large area OPV devices, giving emphasis to outdoor stability studies (ISOS-O) and laboratory weathering tests (ISOS-L). As mentioned above, these studies mostly focus on P3HT:PC$_{61}$BM PAL system and on different encapsulation strategies to mitigate the deleterious action of extrinsic degradation factors (H$_2$O and O$_2$). Table S4, Supporting Information, summarizes the most important results obtained applying ISOS-O and ISOS-L protocols where, as a benchmark for stability, only tests and lifetimes with duration > 1 year are indicated.

One of the earliest demonstrations of the encapsulation of large area OPV devices was made by Krebs et al.[388] in 2004. Devices based on MEH-PPV with an area of 100 cm^2 were laminated using PET, however the lamination had a negative effect on the lifetime. In 2006, Krebs[389] encapsulated a cell based on P3HT:PCBM with active area of 10 cm^2 using a thick glass substrate and an aluminum backplate that were sealed using a glass fibre reinforced thermosetting epoxy (prepreg), requiring a thermosetting time of 12 h. Typical devices achieved a PCE of 0.48% immediately after encapsulation, which dropped to 0.31% after ≈1 year under ambient conditions.

In 2008, flexible P3HT:PCBM based modules with an initial PCE > 1% and packaged with transparent barrier films were tested at the Konarka rooftop testing setup in Lowell (USA)[390] and exhibited no performance losses after a 14 month testing period.

Gevorgyan et al.[391] used ProcessOne to produce modules with 16 serially connected cells employing an inverted structure ITO/ZnOx/P3HT:PCBM/PEDOT:PSS/Ag-paste and with a total active area of ≈35.5 cm^2. The modules were encapsulated using a UV filter/barrier (Amcor) with a pressure sensitive adhesive (467 MPF, 3M) and demonstrated initial PCE values between 0.7% and 1.4%. Their outdoor stability was then tested in 6 laboratories in 4 countries (Germany, Israel, Australia, and Denmark). In addition to the encapsulation, the device terminals were protected against H$_2$O and O$_2$ diffusion which proved to be crucially important. The most stable modules had well sealed terminals and demonstrated a T_{80} > 416 days contrary to modules with unprotected device terminals which exhibited T_{80} < 21 days.

Sapkota et al.[316] used UV curing epoxy glue together with glass plates or flexible barrier films to encapsulate backside illuminated OPV cells having an active area of 1.1 cm^2 and with the inverted geometry Cr/Al/Cr/P3HT:PCBM/PEDOT:PSS/metal-grid. Devices encapsulated between two glass plates were able to maintain 90% of their initial PCE (2.7%) after >12 000 h following continuous illumination at 1000 W m^{-2} (similar to AM1.5G but with low UV content) and at an ambient temperature of ≈50 °C and ≈6% RH.

Fully printed *IOne* modules with active areas of 70–100 cm^2 and PET/Ag-grid/PEDOT:PSS/ZnO/P3HT:PCBM/ PEDOT:PSS/Ag-grid structure were tested by Krebs and coworkers[392] for outdoor stability assessment over 1 year, with devices located in Denmark (ISOS-O-3) and the Netherlands (ISOS-O-1). Modules with different PET substrate thickness (45 μm; 125 μm) were laminated between two sheets of food packaging barrier using a UV curable adhesive and with different edge sealing margins (<<1 cm and >1 cm). The best modules, in both countries, had a PET substrate thickness of 125 μm and an edge sealing margin >1 cm, and exhibited T_{80} > 1 year. Large area (100 cm^2), R2R processed P3HT:PCBM based OPV modules that were manually laminated between barrier foils using a UV-curable adhesive were tested by Angmo et al.[372] for their stability. The encapsulation was performed feeding the "barrier/adhesive/module/adhesive/barrier" through the nip pressure of a R2R coater to achieve homogenous distribution of the adhesive and thereafter curing the adhesive under UV light. Before encapsulation, the module terminal contacts/busbars were covered with a copper tape and metal snap fasteners were punched through over them after encapsulation (Figure 16c). Impressive values of T_{80} > 2 years were obtained, under protocols ISOS-O-3 and ISOS-D-2. The results suggested that O$_2$ permeation may be responsible for degradation mainly under outdoor conditions, whereas WVTR has a larger impact under dark conditions.

Weerasinghe et al.,[393] tested the outdoor stability (ISOS-O-2) of fully-printed OPV modules (having an active area ≈50 cm^2), comprising of 5 individual cells connected in series and with a PET/ITO/ZnO/P3HT:PCBM/PEDOT:PSS/Ag configuration. Various encapsulation architectures (partial, perforated, and complete) were tested using commercially available flexible barrier films and adhesives. Completely encapsulated modules showed no evidence of PCE loss after 13 months of outdoor exposure and a T_{80} of at least 3 years was anticipated. No absolute values of PCE were reported.

Other stability studies of large area OPV cells and modules have been performed testing different experimental variables such as: i) Single-junction versus tandem devices;[394] ii) different encapsulation protocols (complete; partial);[170] iii) different encapsulation barrier foils;[209] iv) different adhesives (UV-curable; pressure-sensitive);[207] v) the effect of edge sealing;[374,383] vi) the lifetime reproducibility among different laboratories;[371] and vii) combined application of different stress factors on the adhesion of OPV interfaces in large area R2R devices.[395] However, in all of these studies the reported values of T_{80} were <<1 year.

The vast majority of the stability tests reviewed above for large area devices were based on a P3HT:PCBM PAL and therefore, despite some encouraging stability results obtained (T_{80} > 1 year), their initial PCE values were rather low (typically < 3%). Therefore, demonstrating OPV devices with simultaneously high PCE (>10%), large area (>>100 cm^2) and high stability (T_{80} > 10 years)—the ultimate goal of the OPV field—has still not been reached. However, some recent studies suggest that real progress is being made in this regard. For example a recent study by Chang et al.[145] explored carefully encapsulated modules based on a PV2000:PCBM PAL having a total active area of 23.7 cm^2 and an initial PCE of 7.56%; here it was shown that modules were able to maintain 91.7% of their initial PCE value after 1000h under AM1.5G light-soaking. Furthermore, Distler et al.[125] fabricated PM6:Y6-based modules with areas of 26 and 204 cm^2 having PCEs of 12.6% and 11.7%, respectively; again no significant degradation was observed during the in-house characterization measurements and certification process, which lasted several days and included extended AM1.5G irradiation at 1000 W m^{-2}.

5. Conclusions and Future Directions

The field of OPVs has witnessed a rapid development in very recent years, mainly due to the development of new polymer donors and NFAs. To date, the PCE of ITO-based single cells with active area ≥ 1.0 cm^2 has reached over 15%, and the PCE of ITO-based modules having active areas ≥ 10 cm^2 and ≥ 100 cm^2 has reached over 14% and 12% respectively. These are very encouraging results with this progress all being made in the last year. These devices were prepared using vacuum processing steps, however the PCE of devices prepared using vacuum-free techniques still lags far behind. Although vacuum processing increases the complexity and cost of device fabrication, it is not incompatible with upscaling. Therefore, unless the efficiency gap between vacuum and vacuum-free processed devices can be reduced considerably in the future, it is likely that vacuum-processing will form an integral part of any future OPV device manufacture process.

The most successful ITO-free strategy, particularly for larger area devices ≥ 10 cm^2, has consisted in the use of highly conductive thick metal films (≈ 100 nm) as opaque bottom electrodes in back illuminated devices; here PCEs of 10.24% and 6.1% in devices with active areas of 10 and 66 cm^2, respectively, are among the most impressive efficiencies reported so far. To create ITO-free devices with a bottom TCE, most research has been concentrated on the development of silver grids. Here metal grids suffer from the inherent limitation that high conductivity and high transparency are difficult to combine in a single material and a trade-off has to be met between these two properties. However, recent studies using hexagonal Ag/Cu grids reported PCEs >12% in 1.0 cm^2 cells; a value that currently represents a record PCE for large area ITO-free devices. Although the use of high conductivity PEDOT:PSS as bottom electrode has received far less attention, some recent reports suggest this to be a promising strategy; here a PCE of 8.90% was reported in devices having an active area of 15 cm^2.

Despite these impressive very recent developments, the large majority of upscaling studies performed so far (particularly to very large areas of >100 cm^2) have been performed using the standard P3HT:PCBM blend system due to the higher availability and lower price of these materials compared to other donor:acceptor pairs. However, the P3HT:PCBM system typically exhibits low PCE ($\leq 4\%$) even in small area (a few mm^2) devices. It is therefore difficult to judge the real effect of upscaling on PCE using a system that intrinsically exhibits low performance. More systematic upscaling studies are needed using donor:acceptor pairs that demonstrate high performances (>10%) in small area devices, with special focus on systems containing NFAs.

Long-term device stability is also needed for commercial applications and requires improvements in both intrinsic and extrinsic stability. Here, the replacement of fullerenes by NFAs seems a promising strategy as these materials appear to have higher intrinsic stability and should result in an increase in device lifetime. In parallel, more effort should be placed in developing new encapsulation strategies to enhance the extrinsic stability of devices. Encapsulation studies have so far been relatively scarce and mostly rely on the use of epoxy-based adhesives as sealants. Surprisingly, glass frit sealing technology which has been intensively studied for encapsulating large area DSSCs and perovskite solar cells, has still not been tested in large area OPVs. Notably for BIPV applications in which OPV devices are embedded in glass requires devices to be stable for at least 2 h at 120 °C during the lamination process. However, this demanding requirement is partially lifted due to recent advances in laser assisted glass frit sealing, as encapsulation can now be performed in a few minutes at temperatures as low as 80 °C. As far as we are aware, these new advances in laser assisted glass frit sealing have not been tested in large area OPVs.

The development of flexible OPV technologies remains a highly attractive goal. Previously this mainly meant depositing devices on PET or PEN substrates. However, ultra-thin flexible glass is becoming increasingly popular amongst a range of related technologies, and its implementation in OPVs devices also looks to be a very attractive prospect.

The ultimate objective of these developments is to combine high efficiency performance and high stability in large area modules, with the 10-10 target, that is, 10% efficiency and 10 years stability being a key goal. Outdoor operational lifetime studies of OPV modules now report lifetimes of several years. Despite the fact that there is still a way to go to reach the 10-10 target, this represents an encouraging result considering that 10 years ago, typical device lifetimes were in the range of a few days to weeks.

Conflict of Interest

D.G.L is co-founder and Chairman of the materials science company Ossila Ltd, who retail materials and equipment used in the research and development of organic photovoltaic devices.

[1] C. W. Tang, *Appl. Phys. Lett.* **1986**, *48*, 183.

[2] N. S. Sariciftci, L. Smilowitz, A. J. Heeger, F. Wudl, *Science* **1992**, *258*, 1474.

[3] G. Yu, J. Gao, J. C. Hummelen, F. Wudl, A. J. Heeger, *Science* **1995**, *270*, 1789.

[4] H. Gaspar, F. Figueira, L. Pereira, A. Mendes, J. C. Viana, G. Bernardo, *Materials* **2018**, *11*, 2560.

[5] R. Ganesamoorthy, G. Sathiyan, P. Sakthivel, *Sol. Energy Mater. Sol. Cells* **2017**, *161*, 102.

[6] P. Cheng, G. Li, X. W. Zhan, Y. Yang, *Nat. Photonics* **2018**, *12*, 131.

[7] J. Q. Zhang, H. S. Tan, X. G. Guo, A. Facchetti, H. Yan, *Nat. Energy* **2018**, *3*, 720.

[8] C. Q. Yan, S. Barlow, Z. H. Wang, H. Yan, A. K. Y. Jen, S. R. Marder, X. W. Zhan, *Nat. Rev. Mater.* **2018**, *3*, 18003.

[9] J. H. Hou, O. Inganas, R. H. Friend, F. Gao, *Nat. Mater.* **2018**, *17*, 119.

[10] A. Wadsworth, M. Moser, A. Marks, M. S. Little, N. Gasparini, C. J. Brabec, D. Baran, I. McCulloch, *Chem. Soc. Rev.* **2019**, *48*, 1596.

[11] R. S. Gurney, D. G. Lidzey, T. Wang, *Rep. Prog. Phys.* **2019**, *82*, 036601.

[12] L. J. Ma, S. Q. Zhang, J. W. Wang, Y. Xu, J. H. Hou, *Chem. Commun.* **2020**, *56*, 14337.

[13] Best Research-Cell Efficiency Chart—NREL, https://www.nrel.gov/pv/cell-efficiency.html (accessed: March 2021).

[14] Z. Zheng, H. Yao, L. Ye, Y. Xu, S. Zhang, J. Hou, *Mater. Today* **2020**, *35*, 115.

[15] C. An, Z. Zheng, J. Hou, *Chem. Commun.* **2020**, *56*, 4750.

[16] D. Gedefaw, X. Pan, M. R. Andersson, *Front. Mater.* **2020**, *7*, 280.

[17] B. Zheng, L. J. Huo, Y. F. Li, *NPG Asia Mater.* **2020**, *12*, 3.

[18] C. H. Duan, L. M. Ding, *Sci. Bull.* **2020**, *65*, 1422.

[19] G. P. Kini, S. J. Jeon, D. K. Moon, *Adv. Mater.* **2020**, *32*, 1906175.

[20] H. F. Yao, J. W. Wang, Y. Xu, S. Q. Zhang, J. H. Hou, *Acc. Chem. Res.* **2020**, *53*, 822.

[21] Q. Q. Zhao, J. F. Qu, F. He, *Adv. Sci.* **2020**, *7*, 2000509.

[22] Y. Z. Lin, J. Y. Wang, Z. G. Zhang, H. T. Bai, Y. F. Li, D. B. Zhu, X. W. Zhan, *Adv. Mater.* **2015**, *27*, 1170.

[23] J. Yuan, Y. Zhang, L. Zhou, G. Zhang, H.-L. Yip, T.-K. Lau, X. Lu, C. Zhu, H. Peng, P. A. Johnson, M. Leclerc, Y. Cao, J. Ulanski, Y. Li, Y. Zou, *Joule* **2019**, *3*, 1140.

[24] H. S. Ryu, S. Y. Park, T. H. Lee, J. Y. Kim, H. Y. Woo, *Nanoscale* **2020**, *12*, 5792.

[25] M. Mainville, M. Leclerc, *ACS Energy Lett.* **2020**, *5*, 1186.

[26] I. Mathews, S. N. Kantareddy, T. Buonassisi, I. M. Peters, *Joule* **2019**, *3*, 1415.

[27] F. C. Chen, *Adv. Opt. Mater.* **2019**, *7*, 1800662.

[28] S. Biswas, H. Kim, *Polymers* **2020**, *12*, 1338.

[29] Y. Zhang, C. Duan, L. Ding, *Sci. Bull.* **2020**, *65*, 2040.

[30] Y. Cui, L. Hong, J. H. Hou, *ACS Appl. Mater. Interfaces* **2020**, *12*, 38815.

[31] X. Y. Hou, Y. W. Wang, H. K. H. Lee, R. Datt, N. U. Miano, D. Yan, M. Li, F. R. Zhu, B. Hou, W. C. Tsoi, Z. Li, *J. Mater. Chem. A* **2020**, *8*, 21503.

[32] H. K. H. Lee, J. Y. Wu, J. Barbe, S. M. Jain, S. Wood, E. M. Speller, Z. Li, F. A. Castro, J. R. Durrant, W. C. Tsoi, *J. Mater. Chem. A* **2018**, *6*, 5618.

[33] L. K. Ma, Y. Z. Chen, P. C. Y. Chow, G. Y. Zhang, J. C. Huang, C. Ma, J. Q. Zhang, H. Yin, A. M. H. Cheung, K. S. Wong, S. K. So, H. Yan, *Joule* **2020**, *4*, 1486.

[34] Champion Photovoltaic Module Efficiency Chart—NREL, https://www.nrel.gov/pv/module-efficiency.html (accessed: March 2021).

[35] J. E. Carle, M. Helgesen, O. Hagemann, M. Hosel, I. M. Heckler, E. Bundgaard, S. A. Gevorgyan, R. R. Sondergaard, M. Jorgensen, R. Garcia-Valverde, S. Chaouki-Almagro, J. A. Villarejo, F. C. Krebs, *Joule* **2017**, *1*, 274.

[36] L. Mao, J. Tong, S. Xiong, F. Jiang, F. Qin, W. Meng, B. Luo, Y. Liu, Z. Li, Y. Jiang, C. Fuentes-Hernandez, B. Kippelen, Y. Zhou, *J. Mater. Chem. A* **2017**, *5*, 3186.

[37] L. Mao, L. L. Sun, B. W. Luo, Y. Y. Jiang, Y. H. Zhou, *J. Mater. Chem. A* **2018**, *6*, 5817.

[38] Z. Zhan, J. An, Y. Wei, V. T. Tran, H. Du, *Nanoscale* **2017**, *9*, 965.

[39] X. J. Peng, J. Yuan, S. Shen, M. Gao, A. S. R. Chesman, H. Yin, J. S. Cheng, Q. Zhang, D. Angmo, *Adv. Funct. Mater.* **2017**, *27*, 1703704.

[40] A. Reale, L. La Notte, L. Salamandra, G. Polino, G. Susanna, T. M. Brown, F. Brunetti, A. Di Carlo, *Energy Technol.* **2015**, *3*, 385.

[41] F. Aziz, A. F. Ismail, *Mater. Sci. Semicond. Process.* **2015**, *39*, 416.

[42] G. Wang, M. A. Adil, J. Zhang, Z. Wei, *Adv. Mater.* **2019**, *31*, 1805089.

[43] A. S. Gertsen, M. F. Castro, R. R. Søndergaard, J. W. Andreasen, *Flexible and Printed Electron.* **2020**, *5*, 014004.

[44] R. R. Søndergaard, M. Hösel, F. C. Krebs, *J. Polym. Sci., Part B: Polym. Phys.* **2013**, *51*, 16.

[45] R. Sondergaard, M. Hosel, D. Angmo, T. T. Larsen-Olsen, F. C. Krebs, *Mater. Today* **2012**, *15*, 36.

[46] F. C. Krebs, *Sol. Energy Mater. Sol. Cells* **2009**, *93*, 394.

[47] H. Youn, H. J. Park, L. J. Guo, *Small* **2015**, *11*, 2228.

[48] M. Hösel, H. F. Dam, F. C. Krebs, *Energy Technol.* **2015**, *3*, 293.

[49] I. Burgués-Ceballos, M. Stella, P. Lacharmoise, E. Martínez-Ferrero, *J. Mater. Chem. A* **2014**, *2*, 17711.

[50] J. Lee, S. A. Park, S. U. Ryu, D. Chung, T. Park, S. Y. Son, *J. Mater. Chem. A* **2020**, *8*, 21455.

[51] S. Zhang, L. Ye, H. Zhang, J. Hou, *Mater. Today* **2016**, *19*, 533.

[52] Z. W. Ma, B. Zhao, Y. S. Gong, J. P. Deng, Z. A. Tan, *J. Mater. Chem. A* **2019**, *7*, 22826.

[53] X. P. Xu, L. Y. Yu, H. Yan, R. P. Li, Q. Peng, *Energy Environ. Sci.* **2020**, *13*, 4381.

[54] C. J. Brabec, A. Distler, X. Y. Du, H. J. Egelhaaf, J. Hauch, T. Heumueller, N. Li, *Adv. Energy Mater.* **2020**, *10*, 2001864.

[55] S. Park, T. Kim, S. Yoon, C. W. Koh, H. Y. Woo, H. J. Son, *Adv. Mater.* **2020**, *32*, 2002217.

[56] H. Kang, G. Kim, J. Kim, S. Kwon, H. Kim, K. Lee, *Adv. Mater.* **2016**, *28*, 7821.

[57] M. Jorgensen, J. E. Carle, R. R. Sondergaard, M. Lauritzen, N. A. Dagnaes-Hansen, S. L. Byskov, T. R. Andersen, T. T. Larsen-Olsen, A. P. L. Bottiger, B. Andreasen, L. Fu, L. J. Zuo, Y. Liu, E. Bundgaard, X. W. Zhan, H. Z. Chen, F. C. Krebs, *Sol. Energy Mater. Sol. Cells* **2013**, *119*, 84.

[58] R. Po, A. Bernardi, A. Calabrese, C. Carbonera, G. Corso, A. Pellegrino, *Energy Environ. Sci.* **2014**, *7*, 925.

[59] P. Doggart, N. Bristow, J. Kettle, *J. Appl. Phys.* **2014**, *116*, 103103.

[60] W. C. Zhao, S. Q. Zhang, Y. Zhang, S. S. Li, X. Y. Liu, C. He, Z. Zheng, J. H. Hou, *Adv. Mater.* **2018**, *30*, 1704837.

[61] S. Dong, K. Zhang, B. Xie, J. Xiao, H.-L. Yip, H. Yan, F. Huang, Y. Cao, *Adv. Energy Mater.* **2019**, *9*, 1802832.

[62] R. Sun, J. Guo, C. Sun, T. Wang, Z. Luo, Z. Zhang, X. Jiao, W. Tang, C. Yang, Y. Li, J. Min, *Energy Environ. Sci.* **2019**, *12*, 384.

[63] R. Sun, Q. Wu, J. Guo, T. Wang, Y. Wu, B. B. Qiu, Z. H. Luo, W. Y. Yang, Z. C. Hu, J. Guo, M. M. Shi, C. L. Yang, F. Huang, Y. F. Li, J. Min, *Joule* **2020**, *4*, 407.

[64] S. Kim, H. Kang, S. Hong, J. Lee, S. Lee, B. Park, J. Kim, K. Lee, *Adv. Funct. Mater.* **2016**, *26*, 3563.

[65] S. Hong, M. Yi, H. Kang, J. Kong, W. Lee, J.-R. Kim, K. Lee, *Sol. Energy Mater. Sol. Cells* **2014**, *126*, 107.

[66] Y.-C. Huang, H.-C. Cha, C.-Y. Chen, C.-S. Tsao, *Prog. Photovoltaics* **2017**, *25*, 928.

[67] Y. Zhao, G. Wang, Y. Wang, T. Xiao, M. A. Adil, G. Lu, J. Zhang, Z. Wei, *Sol. RRL* **2019**, *3*, 1800333.

[68] X. C. Meng, L. Zhang, Y. P. Xie, X. T. Hu, Z. Xing, Z. Q. Huang, C. Liu, L. C. Tan, W. H. Zhou, Y. M. Sun, W. Ma, Y. W. Chen, *Adv. Mater.* **2019**, *31*, 1903649.

[69] Q. Wu, J. Guo, R. Sun, J. Guo, S. F. Jia, Y. W. Li, J. B. Wang, J. Min, *Nano Energy* **2019**, *61*, 559.

**ADVANCED
SCIENCE NEWS**
www.advancedsciencenews.com

**ADVANCED
ENERGY
MATERIALS**
www.advenergymat.de

[70] S.-Y. Park, Y.-J. Kang, S. Lee, D.-G. Kim, J.-K. Kim, J. H. Kim, J.-W. Kang, *Sol. Energy Mater. Sol. Cells* **2011**, *95*, 852.

[71] J.-W. Kang, Y.-J. Kang, S. Jung, M. Song, D.-G. Kim, C. Su Kim, S. H. Kim, *Sol. Energy Mater. Sol. Cells* **2012**, *103*, 76.

[72] F. Wu, F. Ye, Z. Chen, Y. Cui, D. Yang, Z. Li, X. Zhao, X. Yang, *Org. Electron.* **2015**, *26*, 48.

[73] N. W. Scarratt, J. Griffin, T. Wang, Y. Zhang, H. Yi, A. Iraqi, D. G. Lidzey, *APL Mater.* **2015**, *3*, 126108.

[74] Y.-C. Huang, C.-S. Tsao, H.-C. Cha, C.-M. Chuang, C.-J. Su, U. S. Jeng, C.-Y. Chen, *Sci. Rep.* **2016**, *6*, 20062.

[75] T. Zhang, Z. Chen, D. Yang, F. Wu, X. Zhao, X. Yang, *Org. Electron.* **2016**, *32*, 126.

[76] C. Cai, Y. Zhang, R. Song, Z. Peng, L. Xia, M. Wu, K. Xiong, B. Wang, Y. Lin, X. Xu, Q. Liang, H. Wu, E. Wang, L. Hou, *Sol. Energy Mater. Sol. Cells* **2017**, *161*, 52.

[77] T. M. Eggenhuisen, Y. Galagan, A. Biezemans, M. Coenen, J. Gilot, P. Groen, R. Andriessen, 2014 IEEE 40th Photovoltaic Specialist Conference (PVSC), Denver, CO, June **2014**.

[78] T. M. Eggenhuisen, Y. Galagan, A. Biezemans, T. Slaats, W. P. Voorthuijzen, S. Kommeren, S. Shanmugam, J. P. Teunissen, A. Hadipour, W. J. H. Verhees, S. C. Veenstra, M. J. J. Coenen, J. Gilot, R. Andriessen, W. A. Groen, *J. Mater. Chem. A* **2015**, *3*, 7255.

[79] D. Corzo, K. Almasabi, E. Bihar, S. Macphee, D. Rosas-Villalva, N. Gasparini, S. Inal, D. Baran, *Adv. Mater. Technol.* **2019**, *4*, 1900040.

[80] Q. Kang, B. Yang, Y. Xu, B. Xu, J. Hou, *Adv. Mater.* **2018**, *30*, 1801718.

[81] S. B. Dkhil, M. Pfannmoller, S. Bals, T. Koganezawa, N. Yoshimoto, D. Hannani, M. Gaceur, C. Videlot-Ackermann, O. Margeat, J. Ackermann, *Adv. Energy Mater.* **2016**, *6*, 1600290.

[82] W. C. Zhao, D. P. Qian, S. Q. Zhang, S. S. Li, O. Inganas, F. Gao, J. H. Hou, *Adv. Mater.* **2016**, *28*, 4734.

[83] Y. Cui, H. F. Yao, J. Q. Zhang, T. Zhang, Y. M. Wang, L. Hong, K. H. Xian, B. W. Xu, S. Q. Zhang, J. Peng, Z. X. Wei, F. Gao, J. H. Hou, *Nat. Commun.* **2019**, *10*, 2515.

[84] Y. Cui, H. Yao, J. Zhang, K. Xian, T. Zhang, L. Hong, Y. Wang, Y. Xu, K. Ma, C. An, C. He, Z. Wei, F. Gao, J. Hou, *Adv. Mater.* **2020**, *32*, 1908205.

[85] Y. Cui, Y. M. Wang, J. Bergqvist, H. F. Yao, Y. Xu, B. W. Gao, C. Y. Yang, S. Q. Zhang, O. Inganas, F. Gao, J. H. Hou, *Nat. Energy* **2019**, *4*, 768.

[86] J. H. Yun, H. Ahn, P. Lee, M. J. Ko, H. J. Son, *Macromolecules* **2017**, *50*, 7567.

[87] I. Shin, H. j. Ahn, J. H. Yun, J. W. Jo, S. Park, S.-y. Joe, J. Bang, H. J. Son, *Adv. Energy Mater.* **2018**, *8*, 1701405.

[88] S. Zhang, Y. Qin, J. Zhu, J. Hou, *Adv. Mater.* **2018**, *30*, 1800868.

[89] B. Fan, X. Du, F. Liu, W. Zhong, L. Ying, R. Xie, X. Tang, K. An, J. Xin, N. Li, W. Ma, C. J. Brabec, F. Huang, Y. Cao, *Nat. Energy* **2018**, *3*, 1051.

[90] Y. Cui, H. Yao, L. Hong, T. Zhang, Y. Xu, K. Xian, B. Gao, J. Qin, J. Zhang, Z. Wei, J. Hou, *Adv. Mater.* **2019**, *31*, 1808356.

[91] C. Cui, X. Guo, J. Min, B. Guo, X. Cheng, M. Zhang, C. J. Brabec, Y. Li, *Adv. Mater.* **2015**, *27*, 7469.

[92] J. Zhang, Y. Zhao, J. Fang, L. Yuan, B. Xia, G. Wang, Z. Wang, Y. Zhang, W. Ma, W. Yan, W. Su, Z. Wei, *Small* **2017**, *13*, 1700388.

[93] S. Q. Liu, D. Chen, X. T. Hu, Z. Xing, J. Wan, L. Zhang, L. C. Tan, W. H. Zhou, Y. W. Chen, *Adv. Funct. Mater.* **2020**, *30*, 2003223.

[94] D. Baran, R. S. Ashraf, D. A. Hanifi, M. Abdelsamie, N. Gasparini, J. A. Rohr, S. Holliday, A. Wadsworth, S. Lockett, M. Neophytou, C. J. M. Emmott, J. Nelson, C. J. Brabec, A. Amassian, A. Salleo, T. Kirchartz, J. R. Durrant, I. McCulloch, *Nat. Mater.* **2017**, *16*, 363.

[95] B. Fan, W. Zhong, L. Ying, D. Zhang, M. Li, Y. Lin, R. Xia, F. Liu, H.-L. Yip, N. Li, Y. Ma, C. J. Brabec, F. Huang, Y. Cao, *Nat. Commun.* **2019**, *10*, 4100.

[96] X. Xiao, K. Lee, S. R. Forrest, *Appl. Phys. Lett.* **2015**, *106*, 213301.

[97] Q. Kang, L. Ye, B. W. Xu, C. B. An, S. J. Stuard, S. Q. Zhang, H. F. Yao, H. Ade, J. H. Hou, *Joule* **2019**, *3*, 227.

[98] G. Ji, W. Zhao, J. Wei, L. Yan, Y. Han, Q. Luo, S. Yang, J. Hou, C.-Q. Ma, *J. Mater. Chem. A* **2019**, *7*, 212.

[99] Y. M. Bai, C. Y. Zhao, R. K. Shi, J. Wang, F. Z. Wang, T. Hayat, A. Alsaedi, Z. A. Tan, *Mater. Chem. Front.* **2020**, *4*, 2072.

[100] J. Huang, C. Z. Li, C. C. Chueh, S. Q. Liu, J. S. Yu, A. K. Y. Jen, *Adv. Energy Mater.* **2015**, *5*, 1500406.

[101] J. Czolk, D. Landerer, M. Koppitz, D. Nass, A. Colsmann, *Adv. Mater. Technol.* **2016**, *1*, 1600184.

[102] Y. F. Zhao, W. J. Zou, H. Li, K. Lu, W. Yan, Z. X. Wei, *Chin. J. Polym. Sci.* **2017**, *35*, 261.

[103] S. Berny, N. Blouin, A. Distler, H. J. Egelhaaf, M. Krompiec, A. Lohr, O. R. Lozman, G. E. Morse, L. Nanson, A. Pron, T. Sauermann, N. Seidler, S. Tierney, P. Tiwana, M. Wagner, H. Wilson, *Adv. Sci.* **2016**, *3*, 1500342.

[104] R. Steim, T. Ameri, P. Schilinsky, C. Waldauf, G. Dennler, M. Scharber, C. J. Brabec, *Sol. Energy Mater. Sol. Cells* **2011**, *95*, 3256.

[105] Y. Cui, H. F. Yao, T. Zhang, L. Hong, B. W. Gao, K. H. Xian, J. Z. Qin, J. H. Hou, *Adv. Mater.* **2019**, *31*, 1904512.

[106] J.-F. Salinas, J.-L. Maldonado, G. Ramos-Ortíz, M. Rodríguez, M.-A. Meneses-Nava, O. Barbosa-García, R. Santillan, N. Farfán, *Sol. Energy Mater. Sol. Cells* **2011**, *95*, 595.

[107] E. Pérez-Gutiérrez, J. Lozano, J. Gaspar-Tánori, J.-L. Maldonado, B. Gómez, L. López, L.-F. Amores-Tapia, O. Barbosa-García, M.-J. Percino, *Sol. Energy* **2017**, *146*, 79.

[108] D. Barreiro-Argüelles, G. Ramos-Ortiz, J.-L. Maldonado, E. Pérez-Gutiérrez, D. Romero-Borja, M.-A. Meneses-Nava, J. C. Nolasco, *Sol. Energy* **2018**, *163*, 510.

[109] Y. Liu, T. T. Larsen-Olsen, X. Zhao, B. Andreasen, R. R. Søndergaard, M. Helgesen, K. Norrman, M. Jørgensen, F. C. Krebs, X. Zhan, *Sol. Energy Mater. Sol. Cells* **2013**, *112*, 157.

[110] D. Angmo, J. Sweelssen, R. Andriessen, Y. Galagan, F. C. Krebs, *Adv. Energy Mater.* **2013**, *3*, 1230.

[111] H. Booth, *J. Laser Micro/Nanoeng.* **2010**, *5*, 183.

[112] K. Sugioka, Y. Cheng, *Light: Sci. Appl.* **2014**, *3*, e149.

[113] K. Sugioka, *Nanophotonics* **2017**, *6*, 393.

[114] K. C. Phillips, H. H. Gandhi, E. Mazur, S. K. Sundaram, *Adv. Opt. Photonics* **2015**, *7*, 684.

[115] F. C. Krebs, T. Tromholt, M. Jørgensen, *Nanoscale* **2010**, *2*, 873.

[116] L. Lucera, P. Kubis, F. W. Fecher, C. Bronnbauer, M. Turbiez, K. Forberich, T. Ameri, H.-J. Egelhaaf, C. J. Brabec, *Energy Technol.* **2015**, *3*, 373.

[117] F. C. Krebs, H. Spanggard, T. Kjær, M. Biancardo, J. Alstrup, *Mater. Sci. Eng., B* **2007**, *138*, 106.

[118] R. Tipnis, J. Bernkopf, S. Jia, J. Krieg, S. Li, M. Storch, D. Laird, *Sol. Energy Mater. Sol. Cells* **2009**, *93*, 442.

[119] P. Kubis, N. Li, T. Stubhan, F. Machui, G. J. Matt, M. M. Voigt, C. J. Brabec, *Prog. Photovoltaics* **2015**, *23*, 238.

[120] N. Li, P. Kubis, K. Forberich, T. Ameri, F. C. Krebs, C. J. Brabec, *Sol. Energy Mater. Sol. Cells* **2014**, *120*, 701.

[121] P. Kubis, L. Lucera, F. Machui, G. Spyropoulos, J. Cordero, A. Frey, J. Kaschta, M. M. Voigt, G. J. Matt, E. Zeira, C. J. Brabec, *Org. Electron.* **2014**, *15*, 2256.

[122] L. Lucera, F. Machui, P. Kubis, H. D. Schmidt, J. Adams, S. Strohm, T. Ahmad, K. Forberich, H. J. Egelhaaf, C. J. Brabec, *Energy Environ. Sci.* **2016**, *9*, 89.

[123] C. Moorhouse, D. Karnakis, C. Kapnopoulos, A. Laskarakis, E. Mekeridis, S. Logothetidis, *J. Laser Micro/Nanoeng.* **2015**, *10*, 195.

[124] S. Röttinger, B. Schwarz, S. Schäfer, R. Gauch, B. Zimmermann, U. Würfel, *Sol. Energy Mater. Sol. Cells* **2016**, *154*, 35.

[125] A. Distler, C. J. Brabec, H.-J. Egelhaaf, *Prog. Photovoltaics* **2021**, *29*, 24.

[126] I. Etxebarria, J. G. Tait, R. Gehlhaar, R. Pacios, D. Cheyns, *Org. Electron.* **2013**, *14*, 430.

[127] J. G. Tait, L. L. Notte, D. Melkonyan, R. Gehlhaar, D. Cheyns, A. Reale, P. Heremans, *Sol. Energy Mater. Sol. Cells* **2016**, *144*, 493.

[128] N. Agrawal, M. Z. Ansari, A. Majumdar, R. Gahlot, N. Khare, *Sol. Energy Mater. Sol. Cells* **2016**, *157*, 960.

[129] J. Lee, H. Back, J. Kong, H. Kang, S. Song, H. Suh, S.-O. Kang, K. Lee, *Energy Environ. Sci.* **2013**, *6*, 1152.

[130] S. Hong, H. Kang, G. Kim, S. Lee, S. Kim, J.-H. Lee, J. Lee, M. Yi, J. Kim, H. Back, J.-R. Kim, K. Lee, *Nat. Commun.* **2016**, *7*, 10279.

[131] S. Dong, K. Zhang, X. Liu, Q. Yin, H. L. Yip, F. Huang, Y. Cao, *Sci. China: Chem.* **2019**, *62*, 67.

[132] P.-T. Tsai, K.-C. Yu, C.-J. Chang, S.-F. Horng, H.-F. Meng, *Org. Electron.* **2015**, *22*, 166.

[133] P. T. Tsai, K. C. Lin, C. Y. Wu, C. H. Liao, M. C. Lin, Y. Q. Wong, H. F. Meng, C. Y. Chang, C. L. Wang, Y. F. Huang, S. F. Horng, H. W. Zan, Y. C. Chao, *ChemSusChem* **2017**, *10*, 2778.

[134] Y. Q. Wong, H.-F. Meng, H. Y. Wong, C. S. Tan, C.-Y. Wu, P.-T. Tsai, C.-Y. Chang, S.-F. Horng, H.-W. Zan, *Org. Electron.* **2017**, *43*, 196.

[135] K.-M. Huang, Y. Q. Wong, M.-C. Lin, C.-H. Chen, C.-H. Liao, J.-Y. Chen, Y.-H. Huang, Y.-F. Chang, P.-T. Tsai, S.-H. Chen, C.-T. Liao, Y.-C. Lee, L. Hong, C.-Y. Chang, H.-F. Meng, Z. Ge, H.-W. Zan, S.-F. Horng, Y.-C. Chao, H. Y. Wong, *Prog. Photovoltaics* **2019**, *27*, 264.

[136] C. Y. Tsai, Y. H. Lin, Y. M. Chang, J. C. Kao, Y. C. Liang, C. C. Liu, J. Qiu, L. X. Wu, C. Y. Liao, H. S. Tan, Y. C. Chao, S. F. Horng, H. W. Zan, H. F. Meng, F. H. Li, *Sol. Energy Mater. Sol. Cells* **2020**, *218*, 110762.

[137] S.-H. Chen, C. H. Liao, C. Y. Chang, K. M. Huang, J. Y. Chen, C. H. Chen, H.-F. Meng, H.-W. Zan, S.-F. Horng, Y.-C. Lin, M.-H. Yeh, *Org. Electron.* **2019**, *75*, 105376.

[138] K. Zhang, Z. Chen, A. Armin, S. Dong, R. Xia, H.-L. Yip, S. Shoaee, F. Huang, Y. Cao, *Sol. RRL* **2018**, *2*, 1700169.

[139] S.-L. Lim, K.-H. Ong, J. Li, L. Yang, Y.-F. Chang, H.-F. Meng, X. Wang, Z.-K. Chen, *Org. Electron.* **2017**, *43*, 55.

[140] W. C. Zhao, Y. Zhang, S. Q. Zhang, S. S. Li, C. He, J. H. Hou, *J. Mater. Chem. C* **2019**, *7*, 3206.

[141] J. Hanisch, T. Wahl, C. D. Wessendorf, E. Ahlswede, *J. Mater. Chem. A* **2016**, *4*, 4771.

[142] D. I. Kutsarov, E. New, F. Bausi, A. Zoladek-Lemanczyk, F. A. Castro, S. R. P. Silva, *Sol. Energy Mater. Sol. Cells* **2017**, *161*, 388.

[143] Y. J. Heo, Y. S. Jung, K. Hwang, J. E. Kim, J. S. Yeo, S. Lee, Y. J. Jeon, D. Lee, D. Y. Kim, *ACS Appl. Mater. Interfaces* **2017**, *9*, 39519.

[144] Y. J. Heo, B. Lim, Y. S. Jung, K. Hwang, J. E. Kim, D. Lee, D. H. Lim, J. M. Park, D. Y. Kim, *ACS Appl. Energy Mater.* **2019**, *2*, 8885.

[145] Y.-M. Chang, C.-Y. Liao, C.-C. Lee, S.-Y. Lin, N.-W. Teng, P. H.-S. Tan, *Sol. Energy Mater. Sol. Cells* **2019**, *202*, 110064.

[146] J. Lee, Y. H. Seo, S. N. Kwon, D. H. Kim, S. Jang, H. Jung, Y. Lee, H. Weerasinghe, T. Kim, J. Y. Kim, D. Vak, S. I. Na, *Adv. Energy Mater.* **2019**, *9*, 1901805.

[147] D. Vak, H. Weerasinghe, J. Ramamurthy, J. Subbiah, M. Brown, D. J. Jones, *Sol. Energy Mater. Sol. Cells* **2016**, *149*, 154.

[148] L. Mao, B. Luo, L. Sun, S. Xiong, J. Fan, F. Qin, L. Hu, Y. Jiang, Z. Li, Y. Zhou, *Mater. Horiz.* **2018**, *5*, 123.

[149] L. L. Sun, X. S. Jiang, Y. H. Zhou, *J. Energy Chem.* **2019**, *37*, 220.

[150] S. Badgujar, G. Y. Lee, T. Park, C. E. Song, S. Park, S. Oh, W. S. Shin, S. J. Moon, J. C. Lee, S. K. Lee, *Adv. Energy Mater.* **2016**, *6*, 1600228.

[151] S. Rasool, D. V. Vu, C. E. Song, H. K. Lee, S. K. Lee, J. C. Lee, S. J. Moon, W. S. Shin, *Adv. Energy Mater.* **2019**, *9*, 1900168.

[152] C.-Y. Liao, Y. Chen, C.-C. Lee, G. Wang, N.-W. Teng, C.-H. Lee, W.-L. Li, Y.-K. Chen, C.-H. Li, H.-L. Ho, P. H.-S. Tan, B. Wang, Y.-C. Huang, R. M. Young, M. R. Wasielewski, T. J. Marks, Y.-M. Chang, A. Facchetti, *Joule* **2020**, *4*, 189.

[153] T. Lee, S. Oh, S. Rasool, C. E. Song, D. Kim, S. K. Lee, W. S. Shin, E. Lim, *J. Mater. Chem. A* **2020**, *8*, 10318.

[154] S. Dong, T. Jia, K. Zhang, J. H. Jing, F. Huang, *Joule* **2020**, *4*, 2004.

[155] T. Zhang, G. Zeng, F. Ye, X. Zhao, X. Yang, *Adv. Energy Mater.* **2018**, *8*, 1801387.

[156] K. M. Huang, C. M. Lin, S. H. Chen, C. S. Li, C. H. Hu, Y. Zhang, H. F. Meng, C. Y. Chang, Y. C. Chao, H. W. Zan, L. J. Huo, P. C. Yu, *Sol. RRL* **2019**, *3*, 1900071.

[157] H. K. H. Lee, Z. Li, J. R. Durrant, W. C. Tsoi, *Appl. Phys. Lett.* **2016**, *108*, 253301.

[158] Y. Aoki, *Org. Electron.* **2017**, *48*, 194.

[159] R. Arai, S. Furukawa, Y. Hidaka, H. Komiyama, T. Yasuda, *ACS Appl. Mater. Interfaces* **2019**, *11*, 9259.

[160] R. Arai, S. Furukawa, N. Sato, T. Yasuda, *J. Mater. Chem. A* **2019**, *7*, 20187.

[161] S. Park, H. Ahn, J.-y. Kim, J. B. Park, J. Kim, S. H. Im, H. J. Son, *ACS Energy Lett.* **2020**, *5*, 170.

[162] F. C. Krebs, *Sol. Energy Mater. Sol. Cells* **2009**, *93*, 465.

[163] F. C. Krebs, S. A. Gevorgyan, J. Alstrup, *J. Mater. Chem.* **2009**, *19*, 5442.

[164] F. C. Krebs, S. A. Gevorgyan, B. Gholamkhass, S. Holdcroft, C. Schlenker, M. E. Thompson, B. C. Thompson, D. Olson, D. S. Ginley, S. E. Shaheen, H. N. Alshareef, J. W. Murphy, W. J. Youngblood, N. C. Heston, J. R. Reynolds, S. Jia, D. Laird, S. M. Tuladhar, J. G. A. Dane, P. Atienzar, J. Nelson, J. M. Kroon, M. M. Wienk, R. A. J. Janssen, K. Tvingstedt, F. Zhang, M. Andersson, O. Inganäs, M. Lira-Cantu, R. de Bettignies, et al., *Sol. Energy Mater. Sol. Cells* **2009**, *93*, 1968.

[165] J. E. Lewis, E. Lafalce, P. Toglia, X. Jiang, *Sol. Energy Mater. Sol. Cells* **2011**, *95*, 2816.

[166] Y. Galagan, H. Fledderus, H. Gorter, H. H. Mannetje, S. Shanmugam, R. Mandamparambil, J. Bosman, J. Rubingh, J. P. Teunissen, A. Salem, I. G. de Vries, R. Andriessen, W. A. Groen, *Energy Technol.* **2015**, *3*, 834.

[167] F. Guo, P. Kubis, T. Przybilla, E. Spiecker, A. Hollmann, S. Langner, K. Forberich, C. J. Brabec, *Adv. Energy Mater.* **2015**, *5*, 1401779.

[168] C. Kapnopoulos, E. D. Mekeridis, L. Tzounis, C. Polyzoidis, A. Zachariadis, C. Tsimikli, C. Gravalidis, A. Laskarakis, N. Vouroutzis, S. Logothetidis, *Sol. Energy Mater. Sol. Cells* **2016**, *144*, 724.

[169] S.-H. Park, S.-J. Lee, J. H. Lee, J. Kal, J. Hahn, H.-K. Kim, *Org. Electron.* **2016**, *30*, 112.

[170] H. C. Weerasinghe, N. Rolston, D. Vak, A. D. Scully, R. H. Dauskardt, *Sol. Energy Mater. Sol. Cells* **2016**, *152*, 133.

[171] L. Lucera, F. Machui, H. D. Schmidt, T. Ahmad, P. Kubis, S. Strohm, J. Hepp, A. Vetter, H. J. Egelhaaf, C. J. Brabec, *Org. Electron.* **2017**, *45*, 209.

[172] Y. C. Huang, C. W. Chou, D. H. Lu, C. Y. Chen, C. S. Tsao, *IEEE J. Photovoltaics* **2018**, *8*, 144.

[173] P. Maisch, K. C. Tam, P. Schilinsky, H.-J. Egelhaaf, C. J. Brabec, *Sol. RRL* **2018**, *2*, 1800005.

[174] P. Apilo, M. Välimäki, R. Po, K.-L. Väisänen, H. Richter, M. Ylikunnari, A. Vilkman, A. Bernardi, G. Corso, H. Hoppe, R. Roesch, R. Meitzner, U. S. Schubert, J. Hast, *Sol. RRL* **2018**, *2*, 1700160.

[175] S. Strohm, F. Machui, S. Langner, P. Kubis, N. Gasparini, M. Salvador, I. McCulloch, H. J. Egelhaaf, C. J. Brabec, *Energy Environ. Sci.* **2018**, *11*, 2225.

[176] Y. W. Han, S. J. Jeon, H. S. Lee, H. Park, K. S. Kim, H.-W. Lee, D. K. Moon, *Adv. Energy Mater.* **2019**, *9*, 1902065.

[177] P. Kubis, J. Winter, A. Gavrilova, M. Hennel, S. Schlosser, I. Richter, A. Distler, M. Heyder, S. Kery, P. Lenk, S. Geiger, C. J. Brabec, H. P. Huber, H. J. Egelhaaf, *Prog. Photovoltaics* **2019**, *27*, 479.

[178] N. Espinosa, R. García-Valverde, A. Urbina, F. C. Krebs, *Sol. Energy Mater. Sol. Cells* **2011**, *95*, 1293.

[179] C. J. M. Emmott, A. Urbina, J. Nelson, *Sol. Energy Mater. Sol. Cells* **2012**, *97*, 14.

[180] N. Espinosa, R. Garcia-Valverde, F. C. Krebs, *Energy Environ. Sci.* **2011**, *4*, 1547.

**ADVANCED
SCIENCE NEWS**

www.advancedsciencenews.com

**ADVANCED
ENERGY
MATERIALS**

www.advenergymat.de

[181] N. Espinosa, R. Garcia-Valverde, A. Urbina, F. Lenzmann, M. Manceau, D. Angmo, F. C. Krebs, *Sol. Energy Mater. Sol. Cells* **2012**, *97*, 3.

[182] B. Azzopardi, C. J. M. Emmott, A. Urbina, F. C. Krebs, J. Mutale, J. Nelson, *Energy Environ. Sci.* **2011**, *4*, 3741.

[183] O. Inganas, *Nat. Photonics* **2011**, *5*, 201.

[184] M. Hösel, D. Angmo, R. R. Søndergaard, G. A. d. R. Benatto, J. E. Carlé, M. Jørgensen, F. C. Krebs, *Adv. Sci.* **2014**, *1*, 1400002.

[185] G. U. Kulkarni, S. Kiruthika, R. Gupta, K. D. M. Rao, *Curr. Opin. Chem. Eng.* **2015**, *8*, 60.

[186] S. D. Lu, Y. Sun, K. K. Ren, K. Liu, Z. J. Wang, S. C. Qu, *Polymers* **2018**, *10*, 5.

[187] W. Guo, Z. Xu, F. Zhang, S. Xie, H. Xu, X. Y. Liu, *Adv. Funct. Mater.* **2016**, *26*, 8855.

[188] Y. K. Zhang, S. W. Ng, X. Lu, Z. J. Zheng, *Chem. Rev.* **2020**, *120*, 2049.

[189] Y. W. Li, G. Y. Xu, C. H. Cui, Y. F. Li, *Adv. Energy Mater.* **2018**, *8*, 1701791.

[190] M. R. Azani, A. Hassanpour, T. Torres, *Adv. Energy Mater.* **2020**, *10*, 2002536.

[191] K. Zilberberg, T. Riedl, *J. Mater. Chem. A* **2016**, *4*, 14481.

[192] J. Yun, *Adv. Funct. Mater.* **2017**, *27*, 1606641.

[193] A. Cheknane, B. Benyoucef, J. P. Charles, R. Zerdoum, M. Trari, *Sol. Energy Mater. Sol. Cells* **2005**, *87*, 557.

[194] A. Cheknane, *Prog. Photovoltaics* **2011**, *19*, 155.

[195] K. Tvingstedt, O. Inganäs, *Adv. Mater.* **2007**, *19*, 2893.

[196] Y. Galagan, B. Zimmermann, E. W. C. Coenen, M. Jorgensen, D. M. Tanenbaum, F. C. Krebs, H. Gorter, S. Sabik, L. H. Slooff, S. C. Veenstra, J. M. Kroon, R. Andriessen, *Adv. Energy Mater.* **2012**, *2*, 103.

[197] M.-G. Kang, M.-S. Kim, J. Kim, L. J. Guo, *Adv. Mater.* **2008**, *20*, 4408.

[198] J.-S. Yu, I. Kim, J.-S. Kim, J. Jo, T. T. Larsen-Olsen, R. R. Søndergaard, M. Hösel, D. Angmo, M. Jørgensen, F. C. Krebs, *Nanoscale* **2012**, *4*, 6032.

[199] D. Angmo, T. T. Larsen-Olsen, M. Jørgensen, R. R. Søndergaard, F. C. Krebs, *Adv. Energy Mater.* **2013**, *3*, 172.

[200] R. Gupta, S. Walia, M. Hosel, J. Jensen, D. Angmo, F. C. Krebs, G. U. Kulkarni, *J. Mater. Chem. A* **2014**, *2*, 10930.

[201] J. E. Carlé, T. R. Andersen, M. Helgesen, E. Bundgaard, M. Jørgensen, F. C. Krebs, *Sol. Energy Mater. Sol. Cells* **2013**, *108*, 126.

[202] M. Hösel, R. R. Søndergaard, D. Angmo, F. C. Krebs, *Adv. Eng. Mater.* **2013**, *15*, 1068.

[203] H. F. Dam, T. R. Andersen, M. V. Madsen, T. K. Mortensen, M. F. Pedersen, U. Nielsen, F. C. Krebs, *Sol. Energy Mater. Sol. Cells* **2015**, *140*, 187.

[204] T. R. Andersen, H. F. Dam, B. Andreasen, M. Hösel, M. V. Madsen, S. A. Gevorgyan, R. R. Søndergaard, M. Jørgensen, F. C. Krebs, *Sol. Energy Mater. Sol. Cells* **2014**, *120*, 735.

[205] N. K. Zawacka, T. R. Andersen, J. W. Andreasen, L. H. Rossander, H. F. Dam, M. Jørgensen, F. C. Krebs, *J. Mater. Chem. A* **2014**, *2*, 18644.

[206] T. T. Larsen-Olsen, S. A. Gevorgyan, R. R. Søndergaard, M. Hösel, Z. Gu, H. Chen, Y. Liu, P. Cheng, Y. Jing, H. Li, J. Wang, J. Hou, Y. Li, X. Zhan, J. Wu, J. Liu, Z. Xie, X. Du, L. Ding, C. Xie, R. Zeng, Y. Chen, W. Li, T. Xiao, N. Zhao, F. Chen, L. Chen, J. Peng, W. Ma, B. Xiao, et al., *Sol. Energy Mater. Sol. Cells* **2013**, *117*, 382.

[207] D. Angmo, S. A. Gevorgyan, T. T. Larsen-Olsen, R. R. Søndergaard, M. Hösel, M. Jørgensen, R. Gupta, G. U. Kulkarni, F. C. Krebs, *Org. Electron.* **2013**, *14*, 984.

[208] M. Hösel, R. R. Søndergaard, M. Jørgensen, F. C. Krebs, *Energy Technol.* **2013**, *1*, 102.

[209] J. E. Carle, M. Helgesen, M. V. Madsen, E. Bundgaard, F. C. Krebs, *J. Mater. Chem. C* **2014**, *2*, 1290.

[210] Y. Kato, M.-C. Jung, M. V. Lee, Y. Qi, *Org. Electron.* **2014**, *15*, 721.

[211] InfinityPV—Flextrodes, https://infinitypv.com/products/materials/flextrode (accessed: March 2021).

[212] J. E. Carle, M. Helgesen, N. K. Zawacka, M. V. Madsen, E. Bundgaard, F. C. Krebs, *J. Polym. Sci., Part B: Polym. Phys.* **2014**, *52*, 893.

[213] M.-R. Chen, C.-C. Fan, T. R. Andersen, H. F. Dam, W.-F. Fu, Y.-Z. Lin, E. Bundgaard, F. C. Krebs, X.-W. Zhan, H.-Z. Chen, *Synth. Met.* **2014**, *195*, 299.

[214] T. R. Andersen, H. F. Dam, B. Burkhart, D. Angmo, M. Corazza, B. C. Thompson, F. C. Krebs, *J. Mater. Chem. C* **2014**, *2*, 9412.

[215] R. G. Brandt, W. Yue, T. R. Andersen, T. T. Larsen-Olsen, M. Hinge, E. Bundgaard, F. C. Krebs, D. Yu, *J. Mater. Chem. C* **2015**, *3*, 1633.

[216] M. Helgesen, J. E. Carlé, F. C. Krebs, *Adv. Energy Mater.* **2013**, *3*, 1664.

[217] W. Q. Liu, S. Y. Liu, N. K. Zawacka, T. R. Andersen, P. Cheng, L. Fu, M. R. Chen, W. F. Fu, E. Bundgaard, M. Jorgensen, X. W. Zhan, F. C. Krebs, H. Z. Chen, *J. Mater. Chem. A* **2014**, *2*, 19809.

[218] P. Cheng, H. T. Bai, N. K. Zawacka, T. R. Andersen, W. Q. Liu, E. Bundgaard, M. Jorgensen, H. Chen, F. C. Krebs, X. W. Zhan, *Adv. Sci.* **2015**, *2*, 1500096.

[219] K. Liu, T. T. Larsen-Olsen, Y. Lin, M. Beliatis, E. Bundgaard, M. Jørgensen, F. C. Krebs, X. Zhan, *J. Mater. Chem. A* **2016**, *4*, 1044.

[220] P. Cheng, Y. Z. Lin, N. K. Zawacka, T. R. Andersen, W. Q. Liu, E. Bundgaard, M. Jorgensen, H. Z. Chen, F. C. Krebs, X. W. Zhan, *J. Mater. Chem. A* **2014**, *2*, 19542.

[221] T. R. Andersen, H. F. Dam, M. Hosel, M. Helgesen, J. E. Carle, T. T. Larsen-Olsen, S. A. Gevorgyan, J. W. Andreasen, J. Adams, N. Li, F. Machui, G. D. Spyropoulos, T. Ameri, N. Lemaitre, M. Legros, A. Scheel, D. Gaiser, K. Kreul, S. Berny, O. R. Lozman, S. Nordman, M. Valimaki, M. Vilkman, R. R. Sondergaard, M. Jorgensen, C. J. Brabec, F. C. Krebs, *Energy Environ. Sci.* **2014**, *7*, 2925.

[222] Y. Galagan, J.-E. J. M. Rubingh, R. Andriessen, C.-C. Fan, P. W. M. Blom, S. C. Veenstra, J. M. Kroon, *Sol. Energy Mater. Sol. Cells* **2011**, *95*, 1339.

[223] Y. Galagan, E. W. C. Coenen, S. Sabik, H. H. Gorter, M. Barink, S. C. Veenstra, J. M. Kroon, R. Andriessen, P. W. M. Blom, *Sol. Energy Mater. Sol. Cells* **2012**, *104*, 32.

[224] Y. Li, L. Mao, F. Tang, Q. Chen, Y. Wang, F. Ye, L. Chen, Y. Li, D. Wu, Z. Cui, J. Cai, L. Chen, *Sol. Energy Mater. Sol. Cells* **2015**, *143*, 354.

[225] L. Mao, Q. Chen, Y. Li, Y. Li, J. Cai, W. Su, S. Bai, Y. Jin, C.-Q. Ma, Z. Cui, L. Chen, *Nano Energy* **2014**, *10*, 259.

[226] Y. Li, L. Mao, Y. Gao, P. Zhang, C. Li, C. Ma, Y. Tu, Z. Cui, L. Chen, *Sol. Energy Mater. Sol. Cells* **2013**, *113*, 85.

[227] T. R. Andersen, N. A. Cooling, F. Almyahi, A. S. Hart, N. C. Nicolaidis, K. Feron, M. Noori, B. Vaughan, M. J. Griffith, W. J. Belcher, P. C. Dastoor, *Sol. Energy Mater. Sol. Cells* **2016**, *149*, 103.

[228] W. Y. Jin, R. T. Ginting, K. J. Ko, J. W. Kang, *Sci. Rep.* **2016**, *6*, 36475.

[229] S. Lu, J. Lin, K. Liu, S. Yue, K. Ren, F. Tan, Z. Wang, P. Jin, S. Qu, Z. Wang, *Acta Mater.* **2017**, *130*, 208.

[230] M. Helgesen, J. E. Carlé, G. A. d. R. Benatto, R. R. Søndergaard, M. Jørgensen, E. Bundgaard, F. C. Krebs, *Adv. Energy Mater.* **2015**, *5*, 1401996.

[231] Q. P. Fan, Y. Wang, M. J. Zhang, B. Wu, X. Guo, Y. F. Jiang, W. B. Li, B. Guo, C. N. Ye, W. Y. Su, J. Fang, X. M. Ou, F. Liu, Z. X. Wei, T. C. Sum, T. P. Russell, Y. F. Li, *Adv. Mater.* **2018**, *30*, 1704546.

[232] M. G. Kang, H. J. Park, S. H. Ahn, L. J. Guo, *Sol. Energy Mater. Sol. Cells* **2010**, *94*, 1179.

[233] W. X. Zhou, J. Chen, Y. Li, D. B. Wang, J. Y. Chen, X. M. Feng, Z. D. Huang, R. Q. Liu, X. J. Lin, H. M. Zhang, B. X. Mi, Y. W. Ma, *ACS Appl. Mater. Interfaces* **2016**, *8*, 11122.

[234] E. Georgiou, S. A. Choulis, F. Hermerschmidt, S. M. Pozov, I. Burgues-Ceballos, C. Christodoulou, G. Schider, S. Kreissl, R. Ward, E. J. W. List-Kratochvil, C. Boeffel, *Sol. RRL* **2018**, *2*, 1700192.

[235] S. Choi, Y. Zhou, W. Haske, J. W. Shim, C. Fuentes-Hernandez, B. Kippelen, *Org. Electron.* **2015**, *17*, 349.

ADVANCED
SCIENCE NEWS

www.advancedsciencenews.com

ADVANCED
ENERGY
MATERIALS

www.advenergymat.de

[236] Y. Galagan, E. W. C. Coenen, B. Zimmermann, L. H. Slooff, W. J. H. Verhees, S. C. Veenstra, J. M. Kroon, M. Jørgensen, F. C. Krebs, R. Andriessen, *Adv. Energy Mater.* **2014**, *4*, 1300498.

[237] T. M. Eggenhuisen, Y. Galagan, E. W. C. Coenen, W. P. Voorthuijzen, M. W. L. Slaats, S. A. Kommeren, S. Shanmuganam, M. J. J. Coenen, R. Andriessen, W. A. Groen, *Sol. Energy Mater. Sol. Cells* **2015**, *134*, 364.

[238] Y. F. Han, X. L. Chen, J. F. Wei, G. Q. Ji, C. Wang, W. C. Zhao, J. Q. Lai, W. S. Zha, Z. R. Li, L. P. Yan, H. M. Gu, Q. Luo, Q. Chen, L. W. Chen, J. H. Hou, W. M. Su, C. Q. Ma, *Adv. Sci.* **2019**, *6*, 1901490.

[239] J. Y. Lee, S. T. Connor, Y. Cui, P. Peumans, *Nano Lett.* **2008**, *8*, 689.

[240] L. Hu, H. S. Kim, J.-Y. Lee, P. Peumans, Y. Cui, *ACS Nano* **2010**, *4*, 2955.

[241] W. Gaynor, G. F. Burkhard, M. D. McGehee, P. Peumans, *Adv. Mater.* **2011**, *23*, 2905.

[242] D.-S. Leem, A. Edwards, M. Faist, J. Nelson, D. D. C. Bradley, J. C. de Mello, *Adv. Mater.* **2011**, *23*, 4371.

[243] L. Yang, T. Zhang, H. Zhou, S. C. Price, B. J. Wiley, W. You, *ACS Appl. Mater. Interfaces* **2011**, *3*, 4075.

[244] Z. B. Yu, L. Li, Q. W. Zhang, W. L. Hu, Q. B. Pei, *Adv. Mater.* **2011**, *23*, 4453.

[245] M. Song, D. S. You, K. Lim, S. Park, S. Jung, C. S. Kim, D.-H. Kim, D.-G. Kim, J.-K. Kim, J. Park, Y.-C. Kang, J. Heo, S.-H. Jin, J. H. Park, J.-W. Kang, *Adv. Funct. Mater.* **2013**, *23*, 4177.

[246] J. Krantz, M. Richter, S. Spallek, E. Spiecker, C. J. Brabec, *Adv. Funct. Mater.* **2011**, *21*, 4784.

[247] F. Basarir, F. S. Irani, A. Kosemen, B. T. Camic, F. Oytun, B. Tunaboylu, H. J. Shin, K. Y. Nam, H. Choi, *Mater. Today Chem.* **2017**, *3*, 60.

[248] D. Langley, G. Giusti, C. Mayousse, C. Celle, D. Bellet, J. P. Simonato, *Nanotechnology* **2013**, *24*, 452001.

[249] D. Angmo, T. R. Andersen, J. J. Bentzen, M. Helgesen, R. R. Søndergaard, M. Jørgensen, J. E. Carlé, E. Bundgaard, F. C. Krebs, *Adv. Funct. Mater.* **2015**, *25*, 4539.

[250] P. Maisch, K. C. Tam, L. Lucera, H.-J. Egelhaaf, H. Scheiber, E. Maier, C. J. Brabec, *Org. Electron.* **2016**, *38*, 139.

[251] G. A. D. Benatto, B. Roth, M. Corazza, R. R. Sondergaard, S. A. Gevorgyan, M. Jorgensen, F. C. Krebs, *Nanoscale* **2016**, *8*, 318.

[252] L. L. Sun, W. W. Zeng, C. Xie, L. Hu, X. Y. Dong, F. Qin, W. Wang, T. F. Liu, X. S. Jiang, Y. Y. Jiang, Y. H. Zhou, *Adv. Mater.* **2020**, *32*, 1907840.

[253] C. Mayousse, C. Celle, A. Fraczkiewicz, J. P. Simonato, *Nanoscale* **2015**, *7*, 2107.

[254] H. H. Khaligh, I. A. Goldthorpe, *Nanoscale Res. Lett.* **2013**, *8*, 235.

[255] C. C. Lin, D. X. Lin, S. H. Lin, *Nanotechnology* **2020**, *31*, 215705.

[256] A. R. Rathmell, B. J. Wiley, *Adv. Mater.* **2011**, *23*, 4798.

[257] H. Z. Guo, N. Lin, Y. Z. Chen, Z. W. Wang, Q. S. Xie, T. C. Zheng, N. Gao, S. P. Li, J. Y. Kang, D. J. Cai, D. L. Peng, *Sci. Rep.* **2013**, *3*, 2323.

[258] C. Sachse, N. Weiss, N. Gaponik, L. Muller-Meskamp, A. Eychmuller, K. Leo, *Adv. Energy Mater.* **2014**, *4*, 1300737.

[259] J. Y. Chen, W. X. Zhou, J. Chen, Y. Fan, Z. Q. Zhang, Z. D. Huang, X. M. Feng, B. X. Mi, Y. W. Ma, W. Huang, *Nano Res.* **2015**, *8*, 1017.

[260] Y. G. Bi, Y. F. Liu, X. L. Zhang, D. Yin, W. Q. Wang, J. Feng, H. B. Sun, *Adv. Opt. Mater.* **2019**, *7*, 1800778.

[261] D. Angmo, M. Hösel, F. C. Krebs, *Sol. Energy Mater. Sol. Cells* **2012**, *107*, 329.

[262] H. M. Stec, R. A. Hatton, *ACS Appl. Mater. Interfaces* **2012**, *4*, 6013.

[263] A. Du Pasquier, H. E. Unalan, A. Kanwal, S. Miller, M. Chhowalla, *Appl. Phys. Lett.* **2005**, *87*, 203511.

[264] I. Jeon, R. Xiang, A. Shawky, Y. Matsuo, S. Maruyama, *Adv. Energy Mater.* **2019**, *9*, 1801312.

[265] D. Khan, Z. A. Tan, I. Khan, M. K. Panjwani, *Sci. Adv. Mater.* **2018**, *10*, 747.

[266] M. Obaidullah, V. Esat, C. Sabah, *Int. J. Mod. Phys. B* **2018**, *32*, 1830007.

[267] I. Jeon, Y. Matsuo, S. Maruyama, *Top. Curr. Chem.* **2018**, *376*, 4.

[268] L. P. Yu, C. Shearer, J. Shapter, *Chem. Rev.* **2016**, *116*, 13413.

[269] Y. Zhou, R. Azumi, *Sci. Technol. Adv. Mater.* **2016**, *17*, 493.

[270] J. H. Du, S. F. Pei, L. P. Ma, H. M. Cheng, *Adv. Mater.* **2014**, *26*, 1958.

[271] K. T. Lee, D. H. Park, H. W. Baac, S. Han, *Materials* **2018**, *11*, 1503.

[272] T. A. Shastry, M. C. Hersam, *Adv. Energy Mater.* **2017**, *7*, 1601205.

[273] R. C. Tenent, T. M. Barnes, J. D. Bergeson, A. J. Ferguson, B. To, L. M. Gedvilas, M. J. Heben, J. L. Blackburn, *Adv. Mater.* **2009**, *21*, 3210.

[274] Z. Y. Yin, J. X. Zhu, Q. Y. He, X. H. Cao, C. L. Tan, H. Y. Chen, Q. Y. Yan, H. Zhang, *Adv. Energy Mater.* **2014**, *4*, 1300574.

[275] P. Mustonen, D. M. A. Mackenzie, H. Lipsanen, *Front. Optoelectron.* **2020**, *13*, 91.

[276] J. Wu, H. A. Becerril, Z. Bao, Z. Liu, Y. Chen, P. Peumans, *Appl. Phys. Lett.* **2008**, *92*, 263302.

[277] S. Tiwari, A. Purabgola, B. Kandasubramanian, *J. Alloys Compd.* **2020**, *825*, 153954.

[278] Y. Chen, Y.-Y. Yue, S.-R. Wang, N. Zhang, J. Feng, H.-B. Sun, *Adv. Electron. Mater.* **2019**, *5*, 1900247.

[279] R. K. L. Tan, S. P. Reeves, N. Hashemi, D. G. Thomas, E. Kavak, R. Montazami, N. N. Hashemi, *J. Mater. Chem. A* **2017**, *5*, 17777.

[280] R. Garg, S. Elmas, T. Nann, M. R. Andersson, *Adv. Energy Mater.* **2017**, *7*, 1601393.

[281] J. W. Jo, J. U. Lee, W. H. Jo, *Polym. Int.* **2015**, *64*, 1676.

[282] A. Manzano-Ramirez, E. J. Lopez-Naranjo, W. Soboyejo, Y. Meas-Vong, B. Vilquin, *J. Nanomater.* **2015**, *2015*, 406597.

[283] X. Huang, Z. Y. Zeng, Z. X. Fan, J. Q. Liu, H. Zhang, *Adv. Mater.* **2012**, *24*, 5979.

[284] M. He, J. H. Jung, F. Qiu, Z. Q. Lin, *J. Mater. Chem.* **2012**, *22*, 24254.

[285] L. G. De Arco, Y. Zhang, C. W. Schlenker, K. Ryu, M. E. Thompson, C. W. Zhou, *ACS Nano* **2010**, *4*, 2865.

[286] C. Backes, A. M. Abdelkader, C. Alonso, A. Andrieux-Ledier, R. Arenal, J. Azpeitia, N. Balakrishnan, L. Banszerus, J. Barjon, R. Bartali, S. Bellani, C. Berger, R. Berger, M. M. B. Ortega, C. Bernard, P. H. Beton, A. Beyer, A. Bianco, P. Boggild, F. Bonaccorso, G. B. Barin, C. Botas, R. A. Bueno, D. Carriazo, A. Castellanos-Gomez, M. Christian, A. Ciesielski, T. Ciuk, M. T. Cole, J. Coleman, et al., *2D Mater.* **2020**, *7*, 022001.

[287] Y. Wang, S. W. Tong, X. F. Xu, B. Ozyilmaz, K. P. Loh, *Adv. Mater.* **2011**, *23*, 1514.

[288] H. Park, S. Chang, X. Zhou, J. Kong, T. Palacios, S. Gradečak, *Nano Lett.* **2014**, *14*, 5148.

[289] Y. Song, S. Chang, S. Gradecak, J. Kong, *Adv. Energy Mater.* **2016**, *6*, 1600847.

[290] Z. Liu, P. You, S. Liu, F. Yan, *ACS Nano* **2015**, *9*, 12026.

[291] D. Konios, C. Petridis, G. Kakavelakis, M. Sygletou, K. Savva, E. Stratakis, E. Kymakis, *Adv. Funct. Mater.* **2015**, *25*, 2213.

[292] L. L. Notte, G. V. Bianco, A. L. Palma, A. Di Carlo, G. Bruno, A. Reale, *Carbon* **2018**, *129*, 878.

[293] Y. Jiang, T. Liu, Y. Zhou, *Adv. Funct. Mater.* **2020**, *30*, 2006213.

[294] L. Hu, J. X. Song, X. X. Yin, Z. Su, Z. F. Li, *Polymers* **2020**, *12*, 145.

[295] T. Aernouts, P. Vanlaeke, W. Geens, J. Poortmans, P. Heremans, S. Borghs, R. Mertens, R. Andriessen, L. Leenders, *Thin Solid Films* **2004**, *451*, 22.

[296] Y. M. Chang, L. Wang, W. F. Su, *Org. Electron.* **2008**, *9*, 968.

[297] S. K. Hau, H.-L. Yip, J. Zou, A. K. Y. Jen, *Org. Electron.* **2009**, *10*, 1401.

[298] Y. H. Kim, C. Sachse, M. L. Machala, C. May, L. Muller-Meskamp, K. Leo, *Adv. Funct. Mater.* **2011**, *21*, 1076.

[299] S. Jung, A. Sou, K. Banger, D. H. Ko, P. C. Y. Chow, C. R. McNeill, H. Sirringhaus, *Adv. Energy Mater.* **2014**, *4*, 1400432.

[300] L. C. Tan, H. Y. Zhou, T. Ji, L. Q. Huang, Y. W. Chen, *Org. Electron.* **2016**, *33*, 316.

[301] X. Wang, H. Jin, R. C. R. Nagiri, B. Z. L. Poliquit, J. Subbiah, D. J. Jones, N. Kopidakis, P. L. Burn, J. Yu, *Sol. RRL* **2019**, *3*, 1800286.

[302] F. C. Krebs, *Sol. Energy Mater. Sol. Cells* **2009**, *93*, 1636.

[303] D. Angmo, H. F. Dam, T. R. Andersen, N. K. Zawacka, M. V. Madsen, J. Stubager, F. Livi, R. Gupta, M. Helgesen, J. E. Carle, T. T. Larsen-Olsen, G. U. Kulkarni, E. Bundgaard, F. C. Krebs, *Energy Technol.* **2014**, *2*, 651.

[304] L. J. Zuo, S. H. Zhang, H. Y. Li, H. Z. Chen, *Adv. Mater.* **2015**, *27*, 6983.

[305] L. Zuo, S. Zhang, M. Shi, H. Li, H. Chen, *Mater. Chem. Front.* **2017**, *1*, 304.

[306] M. Koppitz, N. Hesse, D. Landerer, L. G. von Reventlow, E. Wegner, J. Czolk, A. Colsmann, *Energy Technol.* **2017**, *5*, 1105.

[307] Y. Lin, Y. Jin, S. Dong, W. Zheng, J. Yang, A. Liu, F. Liu, Y. Jiang, T. P. Russell, F. Zhang, F. Huang, L. Hou, *Adv. Energy Mater.* **2018**, *8*, 1701942.

[308] Y. Lin, S. Dong, Z. Li, W. Zheng, J. Yang, A. Liu, W. Cai, F. Liu, Y. Jiang, T. P. Russell, F. Huang, E. Wang, L. Hou, *Nano Energy* **2018**, *46*, 428.

[309] A. Liu, W. Zheng, X. Yin, J. Yang, Y. Lin, W. Cai, X. Yu, Q. Liang, Z. He, H. Wu, Y. Li, F. Zhang, L. Hou, *ACS Appl. Mater. Interfaces* **2019**, *11*, 10777.

[310] X. Jiang, L. Sun, W. Wang, F. Qin, C. Xie, L. Hu, Y. Zhou, *J. Mater. Chem. A* **2020**, *8*, 69.

[311] H. Jin, C. Tao, M. Velusamy, M. Aljada, Y. Zhang, M. Hambsch, P. L. Burn, P. Meredith, *Adv. Mater.* **2012**, *24*, 2572.

[312] M. Hambsch, H. Jin, A. J. Clulow, A. Nelson, N. L. Yamada, M. Velusamy, Q. Y. Yang, F. R. Zhu, P. L. Burn, I. R. Gentle, P. Meredith, *Sol. Energy Mater. Sol. Cells* **2014**, *130*, 182.

[313] O. A. Ibraikulov, J. Wang, N. Kamatham, B. Heinrich, S. Mery, M. Kohlstadt, U. Wurfel, S. Ferry, N. Leclerc, T. Heiser, P. Leveque, *Sol. RRL* **2019**, *3*, 1900273.

[314] M. Manceau, D. Angmo, M. Jørgensen, F. C. Krebs, *Org. Electron.* **2011**, *12*, 566.

[315] Y. Galagan, D. J. D. Moet, D. C. Hermes, P. W. M. Blom, R. Andriessen, *Org. Electron.* **2012**, *13*, 3310.

[316] S. B. Sapkota, A. Spies, B. Zimmermann, I. Dürr, U. Würfel, *Sol. Energy Mater. Sol. Cells* **2014**, *130*, 144.

[317] Movie of sunlight powering a toy electric car with OPV, http://www.rsc.org/suppdata/c6/ta/c6ta10106b/c6ta10106b2.mp4 (accessed: April 2021).

[318] X. Du, T. Heumueller, W. Gruber, A. Classen, T. Unruh, N. Li, C. J. Brabec, *Joule* **2019**, *3*, 215.

[319] X. Xu, J. Y. Xiao, G. C. Zhang, L. Wei, X. C. Jiao, H. L. Yip, Y. Cao, *Sci. Bull.* **2020**, *65*, 208.

[320] N. Grossiord, J. M. Kroon, R. Andriessen, P. W. M. Blom, *Org. Electron.* **2012**, *13*, 432.

[321] P. Cheng, X. Zhan, *Chem. Soc. Rev.* **2016**, *45*, 2544.

[322] M. Jørgensen, K. Norrman, F. C. Krebs, *Sol. Energy Mater. Sol. Cells* **2008**, *92*, 686.

[323] S. Rafique, S. M. Abdullah, K. Sulaiman, M. Iwamoto, *Renewable Sustainable Energy Rev.* **2018**, *84*, 43.

[324] H. Q. Cao, W. D. He, Y. W. Mao, X. Lin, K. Ishikawa, J. H. Dickerson, W. P. Hess, *J. Power Sources* **2014**, *264*, 168.

[325] I. F. Domínguez, A. Distler, L. Lüer, *Adv. Energy Mater.* **2017**, *7*, 1601320.

[326] E. M. Speller, A. J. Clarke, J. Luke, H. K. H. Lee, J. R. Durrant, N. Li, T. Wang, H. C. Wong, J.-S. Kim, W. C. Tsoi, Z. Li, *J. Mater. Chem. A* **2019**, *7*, 23361.

[327] E. K. Lee, M. Y. Lee, C. H. Park, H. R. Lee, J. H. Oh, *Adv. Mater.* **2017**, *29*, 1703638.

[328] L. P. Duan, A. Uddin, *Adv. Sci.* **2020**, *7*, 1903259.

[329] M. Jorgensen, K. Norrman, S. A. Gevorgyan, T. Tromholt, B. Andreasen, F. C. Krebs, *Adv. Mater.* **2012**, *24*, 580.

[330] Y. W. Wang, J. Y. Han, L. F. Cai, N. Li, Z. Li, F. R. Zhu, *J. Mater. Chem. A* **2020**, *8*, 21255.

[331] Y. M. Wang, M. J. Jafari, N. N. Wang, D. P. Qian, F. L. Zhang, T. Ederth, E. Moons, J. P. Wang, O. Inganas, W. Huang, F. Gao, *J. Mater. Chem. A* **2018**, *6*, 11884.

[332] H. K. H. Lee, A. M. Telford, J. A. Röhr, M. F. Wyatt, B. Rice, J. Wu, A. d. C. Maciel, S. M. Tuladhar, E. Speller, J. McGettrick, J. R. Searle, S. Pont, T. Watson, T. Kirchartz, J. R. Durrant, W. C. Tsoi, J. Nelson, Z. Li, *Energy Environ. Sci.* **2018**, *11*, 417.

[333] Y.-C. Huang, W.-S. Liu, C.-S. Tsao, L. Wang, *ACS Appl. Mater. Interfaces* **2019**, *11*, 40310.

[334] C. J. Schaffer, C. M. Palumbiny, M. A. Niedermeier, C. Jendrzejewski, G. Santoro, S. V. Roth, P. Muller-Buschbaum, *Adv. Mater.* **2013**, *25*, 6760.

[335] P. Boldrighini, A. Fauveau, S. Thérias, J. L. Gardette, M. Hidalgo, S. Cros, *Rev. Sci. Instrum.* **2019**, *90*, 014710.

[336] X. Z. Wang, C. X. Zhao, G. Xu, Z. K. Chen, F. R. Zhu, *Sol. Energy Mater. Sol. Cells* **2012**, *104*, 1.

[337] V. M. Drakonakis, A. Savva, M. Kokonou, S. A. Choulis, *Sol. Energy Mater. Sol. Cells* **2014**, *130*, 544.

[338] M. Hösel, R. R. Søndergaard, M. Jørgensen, F. C. Krebs, *Adv. Energy Mater.* **2014**, *4*, 1301625.

[339] S. A. Gevorgyan, I. M. Heckler, E. Bundgaard, M. Corazza, M. Hosel, R. R. Sondergaard, G. A. D. Benatto, M. Jorgensen, F. C. Krebs, *J. Phys. D: Appl. Phys.* **2017**, *50*, 103001.

[340] N. Y. Doumon, G. Wang, R. C. Chiechi, L. J. A. Koster, *J. Mater. Chem. C* **2017**, *5*, 6611.

[341] J. Kong, S. Song, M. Yoo, G. Y. Lee, O. Kwon, J. K. Park, H. Back, G. Kim, S. H. Lee, H. Suh, K. Lee, *Nat. Commun.* **2014**, *5*, 5688.

[342] Z. Li, W. Zhong, L. Ying, F. Liu, N. Li, F. Huang, Y. Cao, *Nano Energy* **2019**, *64*, 103931.

[343] M. M. Shi, T. Wang, Y. Wu, R. Sun, W. Wang, J. Guo, Q. Wu, W. Y. Yang, J. Min, *Adv. Energy Mater.* **2021**, *11*, 2002709.

[344] S. X. Li, L. L. Zhan, F. Liu, J. Ren, M. M. Shi, C. Z. Li, T. P. Russell, H. Z. Chen, *Adv. Mater.* **2018**, *30*, 1705208.

[345] S. Li, W. Liu, M. Shi, J. Mai, T.-K. Lau, J. Wan, X. Lu, C.-Z. Li, H. Chen, *Energy Environ. Sci.* **2016**, *9*, 604.

[346] S. Holliday, R. S. Ashraf, A. Wadsworth, D. Baran, S. A. Yousaf, C. B. Nielsen, C.-H. Tan, S. D. Dimitrov, Z. Shang, N. Gasparini, M. Alamoudi, F. Laquai, C. J. Brabec, A. Salleo, J. R. Durrant, I. McCulloch, *Nat. Commun.* **2016**, *7*, 11585.

[347] H. J. Cha, J. Y. Wu, A. Wadsworth, J. Nagitta, S. Limbu, S. Pont, Z. Li, J. Searle, M. F. Wyatt, D. Baran, J. S. Kim, I. McCulloch, J. R. Durrant, *Adv. Mater.* **2017**, *29*, 1701156.

[348] G.-U. Kim, Y. W. Lee, B. S. Ma, J. Kim, J. S. Park, S. Lee, T. L. Nguyen, M. Song, T.-S. Kim, H. Y. Woo, B. J. Kim, *J. Mater. Chem. A* **2020**, *8*, 13522.

[349] P. Yin, L. Wang, J. Liang, Y. Yu, L. Chen, C. Weng, C. Cui, P. Shen, *J. Mater. Chem. C* **2020**, *8*, 11223.

[350] H. Gu, L. Yan, Z. Li, J. Zhang, Q. Luo, Y. Yang, X. Liu, Z. Wei, C.-Q. Ma, *Sol. RRL* **2020**, *4*, 2000374.

[351] D. Luo, W. Zhang, J.-B. Li, Z. Xiao, F. Liu, L. Ding, X.-H. Zhu, *J. Mater. Chem. C* **2020**, *8*, 6196.

[352] A. Garg, S. K. Gupta, J. J. Jasieniak, T. B. Singh, S. E. Watkins, *Prog. Photovoltaics* **2015**, *23*, 989.

[353] F. A. S. Lima, M. J. Beliatis, B. Roth, T. R. Andersen, A. Bortoti, Y. Reyna, E. Castro, I. F. Vasconcelos, S. A. Gevorgyan, F. C. Krebs, M. Lira-Cantu, *APL Mater.* **2016**, *4*, 026104.

[354] M. Vilkman, K. L. Vaaisaanen, P. Apilo, R. Po, M. Vaalimaaki, M. Ylikunnari, A. Bernardi, T. Pernu, G. Corso, J. Seitsonen, S. Heinilehto, J. Ruokolainen, J. Hast, *ACS Appl. Energy Mater.* **2018**, *1*, 5977.

[355] B. Roth, G. A. d. R. Benatto, M. Corazza, J. E. Carlé, M. Helgesen, S. A. Gevorgyan, M. Jørgensen, R. R. Søndergaard, F. C. Krebs, *Adv. Eng. Mater.* **2016**, *18*, 511.

[356] B. Zimmermann, U. Wurfel, M. Niggemann, *Sol. Energy Mater. Sol. Cells* **2009**, *93*, 491.

[357] D. Angmo, I. Gonzalez-Valls, S. Veenstra, W. Verhees, S. Sapkota, S. Schiefer, B. Zimmermann, Y. Galagan, J. Sweelssen, M. Lira-Cantu, R. Andriessen, J. M. Kroon, F. C. Krebs, *J. Appl. Polym. Sci.* **2013**, *130*, 944.

[358] M. Corazza, F. C. Krebs, S. A. Gevorgyan, *Sol. Energy Mater. Sol. Cells* **2014**, *130*, 99.

[359] J. Jeong, J. Seo, S. Nam, H. Han, H. Kim, T. D. Anthopoulos, D. D. C. Bradley, Y. Kim, *Adv. Sci.* **2016**, *3*, 1500269.

[360] A. Uddin, M. B. Upama, H. M. Yi, L. P. Duan, *Coatings* **2019**, *9*, 65.

[361] V. Steinmann, L. Moro, *J. Mater. Res.* **2018**, *33*, 1925.

[362] M. Giannouli, V. M. Drakonakis, A. Savva, P. Eleftheriou, G. Florides, S. A. Choulis, *ChemPhysChem* **2015**, *16*, 1134.

[363] J. Ahmad, K. Bazaka, L. J. Anderson, R. D. White, M. V. Jacob, *Renewable Sustainable Energy Rev.* **2013**, *27*, 104.

[364] S. Cros, R. de Bettignies, S. Berson, S. Bailly, P. Maisse, N. Lemaitre, S. Guillerez, *Sol. Energy Mater. Sol. Cells* **2011**, *95*, S65.

[365] D. Yu, Y.-Q. Yang, Z. Chen, Y. Tao, Y.-F. Liu, *Opt. Commun.* **2016**, *362*, 43.

[366] M. Corazza, F. C. Krebs, S. A. Gevorgyan, *Sol. Energy Mater. Sol. Cells* **2015**, *143*, 467.

[367] P. R. Berger, M. Kim, *J. Renewable Sustainable Energy* **2018**, *10*, 013508.

[368] Y. Zhang, I. D. W. Samuel, T. Wang, D. G. Lidzey, *Adv. Sci.* **2018**, *5*, 1800434.

[369] S. A. Gevorgyan, N. Espinosa, L. Ciammaruchi, B. Roth, F. Livi, S. Tsopanidis, S. Züfle, S. Queirós, A. Gregori, G. A. d. R. Benatto, M. Corazza, M. V. Madsen, M. Hösel, M. J. Beliatis, T. T. Larsen-Olsen, F. Pastorelli, A. Castro, A. Mingorance, V. Lenzi, D. Fluhr, R. Roesch, M. M. D. Ramos, A. Savva, H. Hoppe, L. S. A. Marques, I. Burgués, E. Georgiou, L. Serrano-Luján, F. C. Krebs, *Adv. Energy Mater.* **2016**, *6*, 1600910.

[370] M. O. Reese, S. A. Gevorgyan, M. Jorgensen, E. Bundgaard, S. R. Kurtz, D. S. Ginley, D. C. Olson, M. T. Lloyd, P. Moryillo, E. A. Katz, A. Elschner, O. Haillant, T. R. Currier, V. Shrotriya, M. Hermenau, M. Riede, K. R. Kirov, G. Trimmel, T. Rath, O. Inganas, F. L. Zhang, M. Andersson, K. Tvingstedt, M. Lira-Cantu, D. Laird, C. McGuiness, S. Gowrisanker, M. Pannone, M. Xiao, J. Hauch, et al., *Sol. Energy Mater. Sol. Cells* **2011**, *95*, 1253.

[371] S. A. Gevorgyan, M. Corazza, M. V. Madsen, G. Bardizza, A. Pozza, H. Mullejans, J. C. Blakesley, G. F. A. Dibb, F. A. Castro, J. F. Trigo, C. M. Guillen, J. R. Herrero, P. Morvillo, M. G. Maglione, C. Minarini, F. Roca, S. Cros, C. Seraine, C. H. Law, P. S. Tuladhar, J. R. Durrant, F. C. Krebs, *Polym. Degrad. Stab.* **2014**, *109*, 162.

[372] D. Angmo, F. C. Krebs, *Energy Technol.* **2015**, *3*, 774.

[373] M. Hosel, R. R. Sondergaard, M. Jorgensen, F. C. Krebs, *Adv. Eng. Mater.* **2013**, *15*, 1068.

[374] F. Yan, J. Noble, J. Peltola, S. Wicks, S. Balasubramanian, *Sol. Energy Mater. Sol. Cells* **2013**, *114*, 214.

[375] The world's largest BiOPV installation completed in France using Heliatek's Solar Film Solution, HeliaSol. **2020**, https://www.heli-atek.com/en/news/detail/the-worlds-largest-biopv-installation-completed-in-france-using-heliateks-solar-film-solution-heliasolr/ (accessed: April 2021).

[376] S. Roberts, N. Guariento, *Building Integrated Photovoltaics/A Handbook*, Springer Science & Business Media, Basel, Boston, Berlin **2009**.

[377] F. Ribeiro, J. Maçaira, R. Cruz, J. Gabriel, L. Andrade, A. Mendes, *Sol. Energy Mater. Sol. Cells* **2012**, *96*, 43.

[378] S. Emami, J. Martins, R. Madureira, D. Hernandez, G. Bernardo, J. Mendes, A. Mendes, *J. Phys. D: Appl. Phys.* **2018**, *52*, 074005.

[379] N. Formica, P. Mantilla-Perez, D. S. Ghosh, D. Janner, T. L. Chen, M. H. Huang, S. Garner, J. Martorell, V. Pruneri, *ACS Appl. Mater. Interfaces* **2015**, *7*, 4541.

[380] K. Fukuda, K. Yu, T. Someya, *Adv. Energy Mater.* **2020**, *10*, 2000765.

[381] E. Planes, S. Juillard, M. Matheron, N. Charvin, S. Cros, D. P. Qian, F. L. Zhang, S. Berson, L. Flandin, *Adv. Mater. Interfaces* **2020**, *7*, 2000293.

[382] S. A. Gevorgyan, M. V. Madsen, B. Roth, M. Corazza, M. Hösel, R. R. Søndergaard, M. Jørgensen, F. C. Krebs, *Adv. Energy Mater.* **2016**, *6*, 1501208.

[383] D. M. Tanenbaum, H. F. Dam, R. Rösch, M. Jørgensen, H. Hoppe, F. C. Krebs, *Sol. Energy Mater. Sol. Cells* **2012**, *97*, 157.

[384] T. Kim, J. H. Kang, S. J. Yang, S. J. Sung, Y. S. Kim, C. R. Park, *Energy Environ. Sci.* **2014**, *7*, 3403.

[385] M. D. Clark, M. L. Jespersen, R. J. Patel, B. J. Leever, *Org. Electron.* **2014**, *15*, 1.

[386] P. Romero-Gomez, R. Betancur, A. Martinez-Otero, X. Elias, M. Mariano, B. Romero, B. Arredondo, R. Vergaz, J. Martorell, *Sol. Energy Mater. Sol. Cells* **2015**, *137*, 44.

[387] H. J. Lee, H. P. Kim, H. M. Kim, J. H. Youn, D. H. Nam, Y. G. Lee, J. G. Lee, A. B. Yusoff, J. Jang, *Sol. Energy Mater. Sol. Cells* **2013**, *111*, 97.

[388] F. C. Krebs, J. Alstrup, H. Spanggaard, K. Larsen, E. Kold, *Sol. Energy Mater. Sol. Cells* **2004**, *83*, 293.

[389] F. C. Krebs, *Sol. Energy Mater. Sol. Cells* **2006**, *90*, 3633.

[390] J. A. Hauch, P. Schilinsky, S. A. Choulis, R. Childers, M. Biele, C. J. Brabec, *Sol. Energy Mater. Sol. Cells* **2008**, *92*, 727.

[391] S. A. Gevorgyan, M. V. Madsen, H. F. Dam, M. Jørgensen, C. J. Fell, K. F. Anderson, B. C. Duck, A. Mescheloff, E. A. Katz, A. Elschner, R. Roesch, H. Hoppe, M. Hermenau, M. Riede, F. C. Krebs, *Sol. Energy Mater. Sol. Cells* **2013**, *116*, 187.

[392] D. Angmo, P. M. Sommeling, R. Gupta, M. Hösel, S. A. Gevorgyan, J. M. Kroon, G. U. Kulkarni, F. C. Krebs, *Adv. Eng. Mater.* **2014**, *16*, 976.

[393] H. C. Weerasinghe, D. Vak, B. Robotham, C. J. Fell, D. Jones, A. D. Scully, *Sol. Energy Mater. Sol. Cells* **2016**, *155*, 108.

[394] F. Livi, R. R. Søndergaard, T. R. Andersen, B. Roth, S. Gevorgyan, H. F. Dam, J. E. Carlé, M. Helgesen, G. D. Spyropoulos, J. Adams, T. Ameri, C. J. Brabec, M. Legros, N. Lemaitre, S. Berny, O. R. Lozman, S. Schumann, A. Scheel, P. Apilo, M. Vilkman, E. Bundgaard, F. C. Krebs, *Energy Technol.* **2015**, *3*, 423.

[395] M. Corazza, N. Rolston, R. H. Dauskardt, M. Beliatis, F. C. Krebs, S. A. Gevorgyan, *Adv. Energy Mater.* **2016**, *6*, 1501927.

Gabriel Bernardo received his Ph.D. degree in Materials Science from the University of Oxford in 2005. He worked as postdoctoral fellow at the University of Lisbon (2006–2009) and as assistant researcher at the University of Minho (2009–2015). In the period 2015–2017 he was a Marie Sklodowska-Curie individual fellow at the University of Sheffield (Physics department). After returning to Portugal, he joined the group of Prof Adélio Mendes at LEPABE (Laboratory for Process Engineering, Environment, Biotechnology and Energy). He is currently assistant researcher at LEPABE—Faculty of Engineering of University of Porto.

Tânia Lopes received her Ph.D. in Chemical and Biological Engineering from the University of Porto in 2014. Currently, T. Lopes works as a postdoctoral researcher at the same institution in the research unit LEPABE (Laboratory for Process Engineering, Environment, Biotechnology and Energy). Her research activities are focused on solar energy capture, conversion, and storage; experimental and theoretical studies under steady-state and time-resolved methods. She is leading a national project on photoelectrochemical hydrogen production (2018–2022).

David G. Lidzey studied for B.Sc. and Ph.D. degrees in Physics at the University of Birmingham (1985–1988) and (1990–1994). He then moved to the University of Sheffield to undertake postdoctoral research on polymer light emitting diodes. He has subsequently held research Fellowships from both Lloyds of London and the UK EPSRC. He has a chair in physics, and is the director of the Electronic and Photonic Molecular Materials group. His current research interests include polymer and perovskite based photovoltaics and strongly-coupled organic semiconductor micro-cavity devices. He is cofounder and Chairman of the material science company Ossila Ltd.

Adélio Mendes (born 1964) received his Ph.D. degree from the University of Porto in 1993. Currently, he is a Full Professor at the Chemical Engineering Department of the Faculty of Engineering—University of Porto. He coordinates a large research team with research interests in photovoltaic cells (DSSC, PSC, and OPV), photoelectrochemical cells and electroreduction of CO_2. He authored or coauthored more than 400 articles in peer-reviewed international journals and filled more than 25 families of patents; he was the recipient of an Advanced Research Grant from the ERC.